A CFD Study on the Extraction of Geothermal Energy from Abandoned Oil and Gas Wells

A CFD STUDY ON THE EXTRACTION OF GEOTHERMAL ENERGY FROM ABANDONED OIL AND GAS WELLS

BY

BRIANNA HARRIS, B.Eng.

A THESIS

SUBMITTED TO THE DEPARTMENT OF MECHANICAL ENGINEERING

AND THE SCHOOL OF GRADUATE STUDIES

OF MCMASTER UNIVERSITY

IN PARTIAL FULFILMENT OF THE REQUIREMENTS

FOR THE DEGREE OF

MASTER OF APPLIED SCIENCE

Master of Applied Science (2017) McMaster University

(Mechanical Engineering) Hamilton, Ontario, Canada

TITLE:	A CFD Study on the Extraction of Geothermal Energy from Abandoned Oil and Gas Wells
AUTHOR:	Brianna Harris B.Eng., (Mechanical Engineering) McMaster University, Hamilton, Canada
SUPERVISOR:	Dr. Marilyn Lightstone
NUMBER OF PAGES:	xviii, 133

Abstract

This thesis investigates the feasibility of converting spent oil and gas wells for use in geothermal power generation. A novel approach to heat exchange with the ground was proposed whereby two directionally drilled (L-shaped) wells are connected to create a continuous loop. A Computational Fluid Dynamics (CFD) model was developed that simulates flow through the connected wells and the associated heat exchange with the ground. The model consisted of a coupled fluid-solid domain; 1D fluid flow was explicitly coupled to the 2D cylindrical solid domain using a convection boundary condition. Temperatures in the solid domain were resolved using an Alternating Direction Implicit (ADI) solver, which suited the largely unidirectional nature of the heat transfer problem. Fluid temperatures were solved for using a Tri-Diagonal Matrix Algorithm (TDMA). The results from a series of simulations demonstrated that geothermal power generation from abandoned wells is feasible under certain conditions. The findings of this research show that the correct selection of a well, considering geothermal gradient, well diameter, and ambient temperatures (impacting the inlet temperature), will significantly influence the level of power production. Further, the simulations show that it is necessary to optimize the flow rate for the given well conditions. The research indicates that the addition of insulation to a portion of the system can lead to modest improvements in power when the system

is operated continuously. In contrast, it was found that insulation was necessary for the viability of intermittent use, which would allow the system to meet the demand for peak power generation. The simulations demonstrated that the proposed system could produce approximately 200 kW to 300 kW of electricity.

Acknowledgements

First and foremost, I would like to thank my supervisor, Dr. Marilyn Lightstone, for her invaluable guidance and support over the course of my Master's degree. I look forward to continuing to learn under her mentorship as a PhD student. Many thanks to Dr. Stanley Reitsma for inspiring this project and providing indispensable information along the way. And thanks to Dr. Stephen Tullis and Dr. Jim Cotton for contributing their valuable time to participate in my committee.

I am immeasurably grateful to my parents, for their unwavering support of my pursuit of an education. Without their lifelong encouragement, I would not have made it nearly this far. And thank you to all of the family, friends, and colleagues who have leant a patient ear over the last two years and seven months (and who have listened to my complaints about school stretching much further back than that, as well).

And finally, I would like to express my sincerest gratitude to Salim El Bouzidi for his constant encouragement, limitless patience, and unconditional support. His accompaniment made this endeavour far more enjoyable.

Notation and abbreviations

Nomenclature

A	Area, m^2
c_p	Specific heat capacity, J/kgK
D	Well diameter, m
E	Energy, J
f	Darcy friction factor
h	Heat transfer coefficient, W/m^2K
h_l	Major heat losses, m^2/s^2
k	Thermal conductivity, W/mK
L	Length, m
$\dot{m}$	Mass flow rate, kg/s
n	Coefficient for Dittus-Boelter relationship
p	Pressure, Pa
P	Power, W
Q	Rate of heat transfer, W

r, x, θ	Cylindrical coordinates (radial, axial, and azimuthal)
R	Radius, m
s	Streamline direction
t	Time, s, hour, day, or year
T	Temperature, °C or K
u	Fluid velocity in the axial direction, m/s
v	Fluid velocity, m/s
α	Thermal diffusivity, m^2/s
η	Efficiency
ρ	Density, kg/m^3

Subscripts

0	Of the surface (e.g. A_0, surface area)
avg	Average
C	Cold Carnot cycle reservoir
Carnot	Carnot cycle
eff	Effective
ext	Extracted by the power cycle
f	Fluid
final	Final
g	Ground
H	Hot Carnot cycle reservoir
in	Inlet
initial	Initial
inner	Inner radius
insul	Insulation property
max	Maximum
min	Minimum
net	Net output
out	Outlet
outer	Outer radius
pump	Pump property
transit	Transit
wall	Property at the well wall
well	Well property

Dimensionless Groups

Fo	Fourier Number
Nu	Nusselt Number
Pr	Prandtl Number
Re	Reynolds Number

Acronyms

ADI	Alternating Direction Implicit
CFD	Computational Fluid Dynamics
EGS	Enhanced Geothermal System
HDR	Hot Dry Rock
ORC	Organic Rankine Cycle
TDMA	Tri-Diagonal Matrix Algorithm

Contents

Abstract **iii**

Acknowledgements **v**

Notation and abbreviations **vi**

1 Introduction and Problem Statement **1**

1.1 Background 1

1.2 Scope of the Work 4

1.3 Objectives 5

1.4 Thesis Organization 7

2 Literature Review **8**

2.1 Introduction 8

2.2 Approaches to Extracting Thermal Energy from the Ground 8

2.2.1 Existing Geothermal Energy Extraction Techniques 9

2.2.2 Proposed Methods for Extracting Thermal Energy from Oil and Gas Wells 12

2.3 Parameters Studied in the Literature 18

2.3.1 The Impact of the Geothermal Gradient 18
2.3.2 The Effect of Ground Properties 19
2.3.3 The Effect of Well Geometry 23
2.3.4 The Effect of Flow Rate 24
2.3.5 The Effect of Inlet Temperature 25
2.3.6 The Use of Insulation in Double Pipe Configurations 25
2.3.7 The Impact of Working Fluids 26
2.4 Approaches to Modelling Heat Transfer in a Wellbore 27
2.5 Summary 30

3 Modelling and Methodology **33**

3.1 Geometry 33
3.1.1 Modelling Simplifications 34
3.1.2 Two-Domain Model 35
3.2 Governing Equations 36
3.3 Initial and Boundary Conditions 38
3.3.1 The Fluid-Solid Boundary 39
3.4 Mesh 40
3.5 Matrix Solvers 40
3.6 Materials 41
3.7 Electricity Generation Calculations 41
3.8 Model Verification 45
3.9 Grid and Time Step Independence Testing 47
3.10 Summary 48

4 Results and Discussion **49**

4.1 Introduction 49

4.2 Base Case 50

4.3 The Effect of Flow Rate 63

4.4 The Effect of Inlet Temperature 67

4.5 The Effect of Geothermal Gradient 69

4.6 The Effect of Diameter 70

4.7 The Effect of Insulation 74

4.8 The Effects of Intermittent Heat Extraction 81

4.9 Discussion 90

4.9.1 Considerations for Well Selection 91

4.9.2 Design Considerations for Operation 92

4.9.3 Cost Analysis 94

4.10 Summary 95

5 Conclusions and Recommendations **97**

5.1 Conclusions 97

5.2 Suggestions for Future Work 100

A Energy Contained in the Ground Surrounding Oil and Gas Wells **109**

B Model Verification **111**

B.1 Steady State Verification 111

B.1.1 Fluid Analytical Verification 111

B.1.2 Solid Analytical Verification 113

B.2 Coupling Analytical Verification 116

B.2.1 $u \to \infty$: Solid Conduction with Convection at the Inner Radius 117
B.2.2 $u, h \to \infty$: Solid Conduction with a Constant Temperature at the Inner Radius 117
B.3 Transient Analytical Verification 118
B.4 Intermittent Verification 120

C Grid and Time Step Sensitivity Testing 122
C.1 Grid Independence Testing 122
C.2 Time Step Independence Testing 125

D Time Scale Analysis 132

List of Figures

1.1 Fracking operation with multiple wells and vertical/horizontal drilling, proposed continuous loop configuration shown in orange 5

2.1 Conventional geothermal extraction from an existing hydrothermal reservoir 11

2.2 Enhanced Geothermal System, geothermal extraction from a man-made reservoir 13

2.3 Linear trend in well log temperature data measured from over 2500 wells in Texas 20

2.4 Measured temperature data from NWS1 well used by Noorollahi et al., digitized 21

2.5 Impact of thermal conductivity on fluid outlet temperature, digitized 22

3.1 Layout of vertical and horizontal wells as modelled 35

3.2 Schematic of the fluid and solid domains, with the fluid domain shaded in grey and grid lines depicting grid layout. Not to scale 36

3.3 Heat transfer within fluid domain 37

3.4 Carnot cycle efficiency vs. outlet temperature 43

4.1 Layout of the well system 51

4.2 Initial temperature of the ground and the fluid 52

4.3 Fluid temperature along the length of the base case system after 10 to 50 years of continuous operation 53
4.4 Heat flux from the ground to the fluid after 20 years of operation, base case 54
4.5 Heat transfer rate to the fluid for each well, over 50 years of continuous operation, base case 56
4.6 Well outlet temperature over 50 years of continuous operation, base case 57
4.7 Contour plots of the ground in the horizontal section over 50 years of continuous operation, base case 59
4.8 Radial temperature profiles in the ground halfway down (2000 m) the downward well over 50 years 60
4.9 Radial temperature profiles in the ground halfway across (2400 m) the horizontal well over 50 years 61
4.10 Radial temperature profiles in the ground halfway up (2000 m) the upward well over 50 years 62
4.11 Heat extraction rate from the outlet fluid over 50 years, base case . . 63
4.12 Theoretical maximum power (Carnot power), and approximate power production with 6% and 10% efficient Organic Rankine cycles, base case 64
4.13 Outlet temperature and heat extraction rate vs. flow rate from a fluid after 20 years continuous operation 65
4.14 Carnot cycle power vs. flow rate after 10 and 20 years of continuous operation 66
4.15 Outlet temperature and heat extraction rate vs. inlet temperature after 20 years of continuous operation 67

4.16 Carnot cycle power vs. inlet temperature after 10 and 20 years of continuous operation 68
4.17 Carnot cycle power vs. geothermal gradient after 20 years of continuous operation 70
4.18 Axial fluid temperature profiles for different diameters after 20 years of continuous operation 71
4.19 Fluid outlet temperatures for different diameters over 20 years of continuous operation 72
4.20 Fluid outlet temperatures for different diameters over 2 days of continuous operation 74
4.21 Contour plots of ground temperature near the wall in the downward, horizontal, and upward sections after 1 day of continuous operation. r denotes distance from the well 75
4.22 Fluid temperature in the upward well with various insulation thicknesses after 20 years continuous operation 77
4.23 Heat flux from the ground to the fluid in the upward well with various insulation thicknesses after 20 years continuous operation 79
4.24 Fluid outlet temperature over 20 years of continuous operation with varying insulation thicknesses 81
4.25 Fluid outlet temperature over six hour "on" cycles during intermittent operation, summer peak hours (11am - 5pm) 83
4.26 Fluid outlet temperature over six hour "on" cycles during intermittent operation, summer peak hours (11am - 5pm) with 2 cm insulation in the upper portion of the upward well 84

4.27 Radial temperature profile in the ground, 3000 m deep in the upward well section after 10 years with detail view, inset 85
4.28 Radial temperature profile in the ground, 1000 m deep in the upward well section after 10 years with detail view, inset 86
4.29 System layout for Bernoulli equation derivation 87
4.30 Time to bring fluid from stagnant to desired flow rate of 9 kg/s . . . 89
4.31 Time to bring fluid from 9 kg/s to stagnant 90
B.1 Verification case: fluid model verification, constant uniform wall temperature, steady state 113
B.2 Verification case: fluid model verification, constant wall temperature, $T_{wall} = -132x + 153$, steady state 114
B.3 Verification case: solid model verification, radial heat transfer in a cylindrical tube with a convection boundary condition on the inner radius and a constant temperature condition on the outer radius, steady state 115
B.4 Verification case: solid model verification, heat flow in the axial direction, steady state 116
B.5 Coupling verification case: $u \to \infty$ 118
B.6 Coupling verification case: $u, h \to \infty$ 119
B.7 Verification case: Transient heat conduction in an infinite solid internally bounded by a cylinder 120
B.8 Verification case: Variation of Nusselt number for stagnant fluid, after 1 year of intermittent operation 121

C.1 Fluid temperature after 5 years operation, grid sensitivity testing in x-direction 123
C.2 Ground temperature after 1.25 years of operation, grid sensitivity testing in x-direction 124
C.3 Ground temperature after 5 years of operation, grid sensitivity testing in x-direction 125
C.4 Fluid temperature after 1.25 and 5 years of operation, grid sensitivity testing in r-direction 126
C.5 Ground temperature after 1.25 years of operation, grid sensitivity testing in r-direction 127
C.6 Ground temperature after 5 years of operation, grid sensitivity testing in r-direction 128
C.7 Fluid temperature after 1.25 and 5 years of operation, time step sensitivity testing 129
C.8 Ground temperature after 1.25 years of operation, time step sensitivity testing 130
C.9 Ground temperature after 5 years of operation, time step sensitivity testing 131
D.1 Fluid temperature over 3 hours, including respective transit distances 133

Chapter 1

Introduction and Problem Statement

1.1 Background

Worldwide, approximately 66% of electricity generation is from fossil fuel power plants [1]. This practice releases 32 billion tonnes of carbon dioxide into the atmosphere every year, damaging the environment by contributing to the greenhouse gas effect [2]. One particular challenge of electricity production is meeting peak energy demand, which can be variable and unpredictable. While there are some promising advances in electricity storage on the utility scale, they sacrifice efficiency and none are widely implemented. As such, a large amount of electricity must be produced as it is needed, and supply must exactly meet demand. Fossil fuels remain indispensable, in part, because they enable power production to be turned on and off with little delay, allowing for the expansion capacity to meet this need. Nuclear electricity production,

by comparison, cannot be readily switched on and off, and solar and wind are too intermittent to reliably meet peak electricity demand.

Geothermal energy is unique among renewable sources in that it is not intermittent. As the name suggests, geothermal energy is thermal energy found underground, which has accumulated due to radioactive decay in the Earth's core over the lifetime of the planet.[1] Most existing geothermal capacity is installed in places such as Iceland, where underground thermal activity is high; however the potential of geothermal is not limited to these locations. Current initiatives aim to extend the viability of geothermal to areas where the ground is less active, through deep underground drilling using wells with typical depths on the order of kilometres. Once the heat is extracted from the ground, it can be used directly for heating or it can be converted to electricity using a power cycle.

Replacing fossil fuel plants with geothermal could result in meaningful reductions in greenhouse gas emissions; however, geothermal currently represents a negligible source for electricity, accounting for only 0.3% of worldwide production [3]. Among the reasons for this is the steep cost of implementation, stemming from the need to drill to great depths. If geothermal is to be embraced, the cost of drilling must be mitigated.

One possible solution is to use abandoned oil and gas wells for geothermal power. These wells are good candidates for conversion to geothermal because they extend to depths where ground temperatures are high. For example, in the Gulf Coast there are thousands of wells that reach temperatures ranging from 121°C to more than 200°C [4]. Wells are frequently deserted when they become depleted of their oil or gas or

[1]It should be noted that while the term geothermal can also refer to the use of ground source heat pumps, this document will only use the term geothermal energy when referring to pre-existing energy in the ground, as described above.

when they are not viable for production; and while their operation is not profitable, there are still costs associated with maintaining and/or sealing off the wells. When left unsealed, there is the risk that the wells will pollute the environment. It is estimated that there are at least 2.3 million abandoned wells in the United States alone [5], and another 150,000 in Alberta [6]. Conversion of abandoned oil and gas wells for use in geothermal power production could reduce the cost of abandonment, eliminate the threat of unsealed wells to the environment, and introduce more renewable energy into the electricity supply mix. Therefore there is a need to study the heat transfer behaviour associated with heat extraction from them and the optimization of their operation.

A benefit of the considerable length of oil and gas wells is that they provide access to vast amounts of underground thermal energy. Due to their length, the energy required for electricity production is contained in a very small radius around the wells. For example, to provide 200 kW of power over 20 years, which would require a heat extraction rate of roughly 2 MW, the thermal energy required would be contained within a radius of approximately 15 m. See Appendix A for details on this calculation. This radius, minuscule in comparison to the length scales of oil and gas wells, justifies the notion that the required energy could be extracted from the ground. Considering that such a small volume of ground surrounding a well is disturbed by the energy extraction, there would be no need for the ground temperatures to replenish over the time scales that geothermal extraction would be applied. This is necessary, since ground temperatures would recover very slowly by natural means.

1.2 Scope of the Work

There is a limited amount of existing research investigating the possibility of converting oil and gas wells for geothermal power generation. These studies propose inserting internal piping into vertical wells to create heat exchangers that can collect heat from the ground. While the literature suggests that this approach is viable, internal pipes such as u-tube or double pipe heat exchangers present some limitations pertaining to pressure drop. Furthermore, vertical wells do not have the same exposure to high temperatures as horizontally drilled wells. As a result, an enhanced design implemented in horizontal wells could provide significant improvements in the performance of geothermal heat exchangers.

The proposed research explores the potential of retrofitting horizontal wells for geothermal heat extraction. Horizontal drilling is a common practice in fracking operations. While vertical wells in the oil and gas industry are generally lined with a steel casing, horizontal wells are left open. The fracking process generates fractures in the rock surrounding these horizontal wells to stimulate production. It is also common in fracking operations for multiple wells to be drilled relatively close together. These two features, horizontal orientation and close proximity, allow for a novel heat exchanger configuration that would connect two adjacent wells by their horizontal sections to create a continuous loop. The original drilling configuration plus the proposed modifications (highlighted in orange) are shown in Figure 1.1. This would eliminate the drawbacks associated with internal piping while also maximizing contact with the ground where the temperatures are the highest.

The performance of this configuration can be assessed with the use of Computational Fluid Dynamics (CFD). By modelling the heat transfer within the well and the

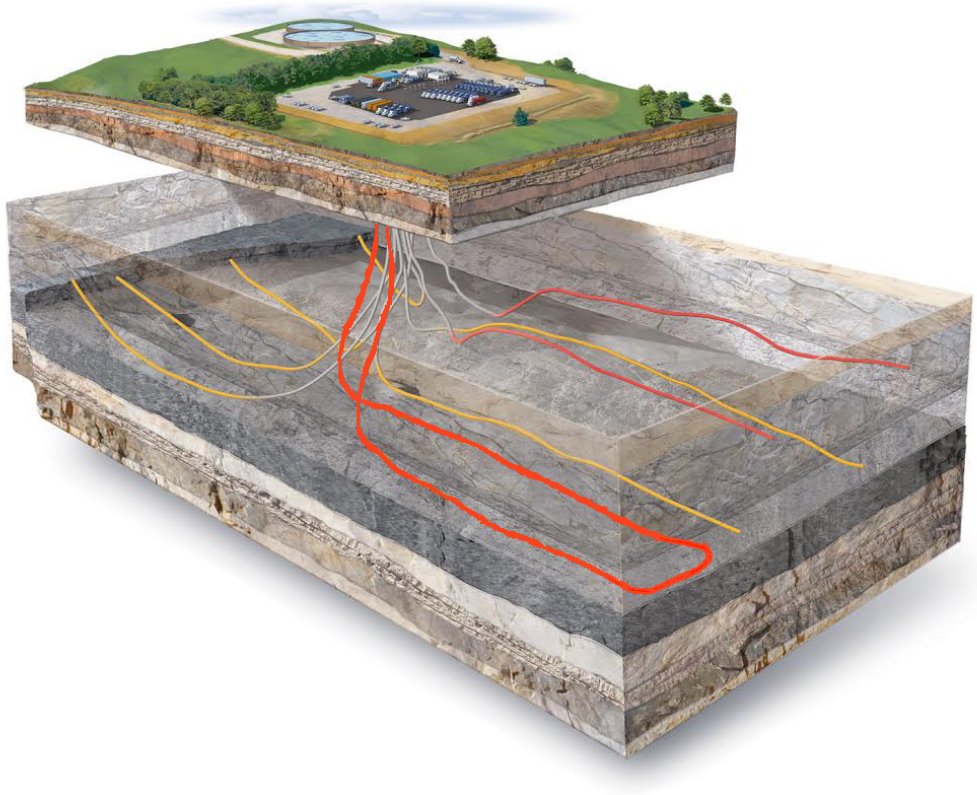

Figure 1.1: Fracking operation with multiple wells and vertical/horizontal drilling, proposed continuous loop configuration highlighted in orange. Modified from Cabot Oil & Gas Corporation [7]

surrounding ground, the parameters affecting performance can be quantified, allowing for the prediction of the power output of this type of system. The modelling is based on wells in the Haynesville shale formation, located in east Texas and northwest Louisiana, where shale gas fracking and directionally drilled wells are prevalent.

1.3 Objectives

This document details the results of CFD modelling performed with the goal of describing the performance of a continuous-loop ground heat exchanger. Performance

of the system is dictated by two main factors: the outlet temperature from the wells, and the heat extraction rate from the system to a power cycle. As there is a minimum operating temperature for the heat source to a power cycle, determining the outlet temperature will establish the viability of producing electricity from the ground heat source. Additionally, since the efficiency of a power cycle directly depends on the temperature of the heat source, the outlet temperature contributes to the quantity of power that can be produced from the system. Modelling will also allow for the determination of the rate that heat can be extracted from the system, which together with an estimate of power cycle efficiency, can be used to predict electricity production. The simulations discussed in Chapter 4 explore the different factors affecting the outlet temperature and rate of heat extraction. By investigating the impact of flow rate, inlet temperature, geothermal gradient, diameter, and the use of insulation, this research aims to establish the impact of these parameters on well selection and operation. Simulations were also carried out to explore the effects of intermittent operation, which could be used to address peak demand.

In addition to the potential power output of the system, the viability of the concept will hinge on the lifespan of the system. For this reason, long-term simulations are used to determine a reasonable estimate of the longevity of the system, given that a power cycle will only be able to operate above a certain threshold temperature. An understanding of both the transient nature of the fluid outlet temperature and the associated power generation over a long period of time can be used to establish whether the proposed configuration is a suitable alternative.

1.4 Thesis Organization

This document is divided into five chapters, describing the modelling process as well as the simulation results of this project. Chapter 2 reviews the existing literature, describing the work that has been done in modelling the existing proposed vertical well solutions. Chapter 3 outlines the CFD modelling, including geometry, simplifying assumptions, and solver algorithms. The results of the CFD simulations performed and the associated discussion can be found in Chapter 4. Finally, conclusions and recommendations for future work are discussed in Chapter 5. Additional information about the simulations and their verification can be found in the appendices.

Chapter 2

Literature Review

2.1 Introduction

This survey of the literature explores the methods of geothermal heat extraction, the parameters affecting heat extraction and power generation, and the approaches to modelling underground heat transfer.

2.2 Approaches to Extracting Thermal Energy from the Ground

All geothermal technologies require some means of transporting heat from deep underground to the surface for use in power production or heating. The primary distinction between the technologies is the method of transportation. There are three categories of heat extraction techniques that are discussed in the literature. Conventional geothermal requires the presence of an existing hydrothermal resource, such

as a geyser, to transport heat to the surface. This is a well-established means of geothermal extraction, despite the geographical limitations imposed by the need for a hydrothermal resource. Enhanced Geothermal Systems (EGS) mitigate the need for pre-existing hydrothermal resources by artificially creating reservoirs. This technique, while still developing, has been proven successful by several projects. EGS is quite costly due to the need for drilling to reach the high temperature resources. As such, a third approach has been proposed that would exploit existing wells in the form of oil and gas wells to access thermal resources deep underground. This approach is the basis for the research summarized in this thesis.

2.2.1 Existing Geothermal Energy Extraction Techniques

Conventional Geothermal

Conventional geothermal extraction relies upon two factors: high heat flow and the presence of fluid to facilitate the collection and transportation of that heat. Areas where conventional geothermal is employed generally contain features such as geysers, hot springs, or steam vents which are a consequence of close proximity to boundaries between tectonic plates, providing both the high heat flux and fluid flow that are necessary [8]. Through drilling or natural means, the underground fluid, which is commonly liquid water or steam, can be accessed and brought to the surface for use as the source for power production or heating. The temperature of this fluid can range from 100°C to 300°C [9].

Conventional geothermal extraction techniques are well established. Several countries, including Iceland, Costa Rica, El Salvador, Kenya, and the Philippines, generate

more than 10% of their required electricity using hydrothermal systems [9]. The limitation of this approach, however, is that it can only be employed where geothermal activity is unusually high and where there is a fluid available to transport the heat. Consequently, the number of possible locations in which this technology can be implemented is severely restricted.

Enhanced Geothermal Systems

An alternative developed to mitigate this limitation is Enhanced Geothermal Systems (EGS). Such systems, also known as Hot Dry Rock systems (HDR), are implemented in areas where the ground is impermeable, making it impossible for fluids to penetrate and create a hydrothermal source. Therefore, EGS relies upon the creation of artificial reservoirs. These reservoirs are produced by fracturing the rock, with the goal of generating a large heat transfer area. An enhanced system will consist of at least two wells: an injection well where a fluid is injected into the man-made reservoir, and a production well which is drilled into the fracture network so that it can transport hot fluid to the surface. The fracture network allows for high heat transfer, since there is a large contact area between the fluid and the rock. According to Potter et al. [11], EGS systems should have a contact surface area of around 16 km^2. This enormous area comes at the expense of pressure drop, as extremely high pressures will be necessary to pump fluid through the fractures and out through the production well. A high system pressure drop will have a negative impact on the amount of net power generated, as it will necessitate higher pumping power.

Breede et al. [12] documented 14 operating EGS projects as of 2013. With the oldest project established in 1963, these plants have wells ranging from 1000 m to 5093

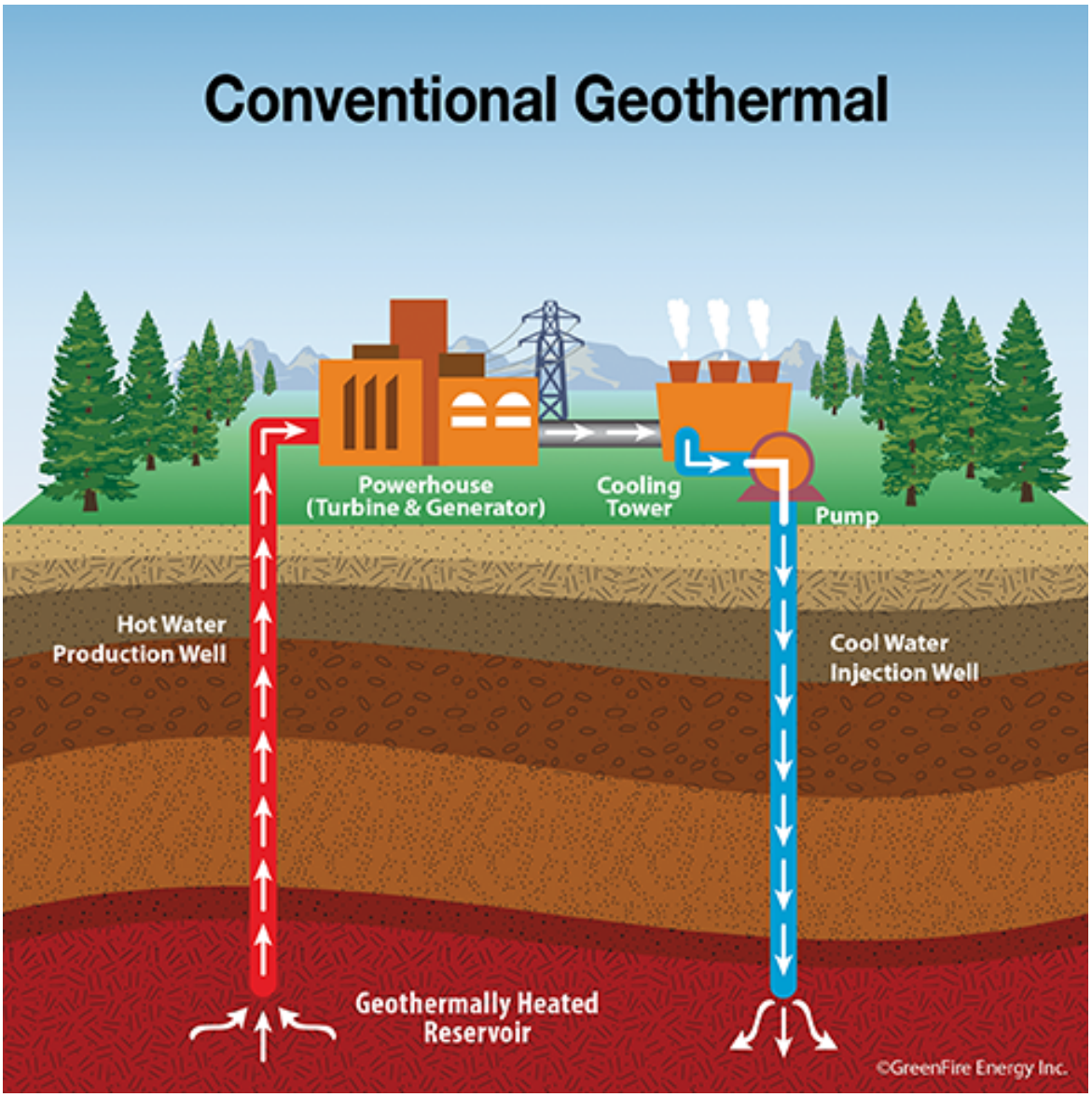

Figure 2.1: Conventional geothermal extraction from an existing hydrothermal reservoir from GreenFire Energy Inc. [10]

m in depth and have an average reservoir temperature of 189°C. The largest capacity plant produces 56 MW of electrical power, and many have additional capacity for heating.

EGS eliminates the need to produce geothermal power near an existing hydrothermal reservoir; however there are still limitations associated with this approach. There is a need for drilling, the cost of which is considerable since it is technologically challenging to drill to extreme depths. Due to the expense of drilling, EGS will be most cost effective in areas with higher than average geothermal activity, placing a restriction on the locations in which the technology will be viable. As such, both EGS and hydrothermal geothermal are subject to geographical limitations and cost constraints.

2.2.2 Proposed Methods for Extracting Thermal Energy from Oil and Gas Wells

To mitigate the cost of drilling, the use of oil and gas wells for geothermal energy extraction has been proposed. Oil and gas wells share many similarities with geothermal wells. They reach significant depths and temperatures. For example, in east and south Texas and northwest Louisiana, the area of focus for this thesis, wells can reach temperatures upwards of 150°C and typical depths of 3 km or greater [13]. As such, they may be a viable option for energy extraction and power production. One proposed approach is to exploit operational wells for their waste water, which makes up a significant portion of the fluid from hydrocarbon drilling. This concept, known as co-production, could address the energy needs of an oil and gas operation. The other

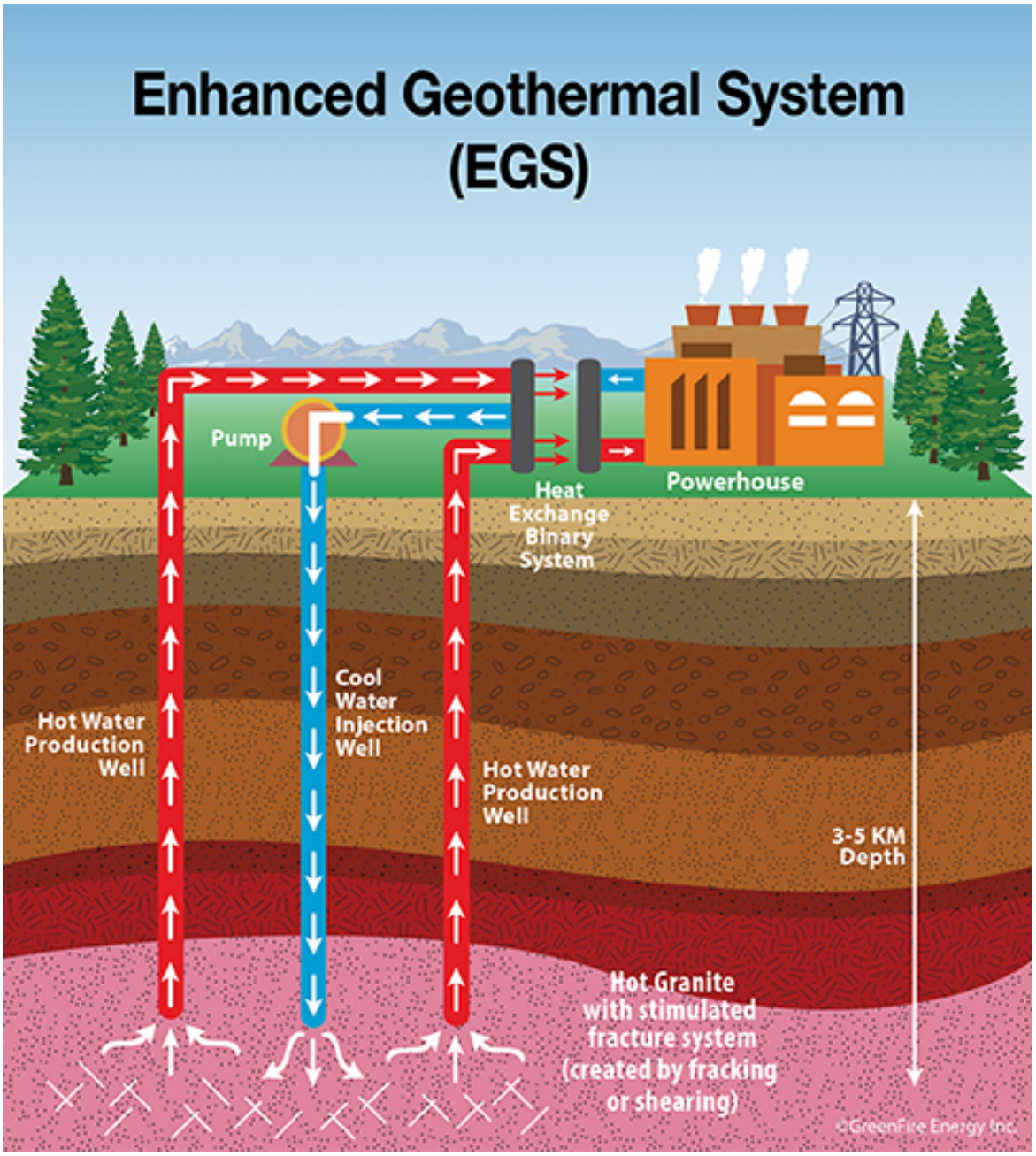

Figure 2.2: Enhanced Geothermal System, geothermal extraction from a man-made reservoir from GreenFire Energy Inc. [10]

approach is to make use of the numerous abandoned oil and gas wells for energy extraction. This allows for the collection of heat for general power production without drilling new wells.

Co-production from Operating Oil and Gas Wells

The concept of co-production involves the use of high-temperature waste water from hydrocarbon wells to produce electricity. Waste water makes up, on average, 94% of the volume from a hydrocarbon well [14]. The task of managing this waste represents a significant cost to the oil industry, accounting for roughly 5-25 billion US dollars per year in the United States [14]. The temperatures of water exiting oil wells is often below 104°C [15], which is considered low for power generation. The availability of organic working fluids that evaporate at lower temperatures, such as those found in an Organic Rankine Cycle (ORC), make it possible to produce electricity at these temperatures. Therefore, co-production provides an opportunity to provide on-site power to oil and gas operations, mitigating the cost of processing waste water.

Co-production is still developing. The National Renewable Energy Laboratory in the United States has initiated a project to test the possibility of co-production in the Williston Basin in North Dakota [16]. While there has been some publicity suggesting its success [17], there has yet to be any published data outlining its performance. A demonstration project from the Rocky Mountain Oilfield Testing Centre determined that between 80 kW to 280 kW of net power could be produced from the water collected from an operational oil well [15]. The operating conditions of the system included an inlet temperature to the Organic Rankine Cycle of 90.5°C to 92.2°C and a flow rate of 22.1 L/s to 73.6 L/s.

Abandoned Oil and Gas Wells

There are over 2.3 million spent oil and gas wells in the United States alone [5]. These wells are a liability to their owners, since correctly decommissioning a well is an expensive processes. Therefore, converting these wells for use in geothermal power production or heating would expand the availability of geothermal energy while also mitigating the cost of well abandonment.

Retrofitting an oil or gas well for geothermal power production requires adapting it into a heat exchanger, in which a heat transfer fluid can collect thermal energy and transport it to the surface. A number of researchers have approached this problem. While not explicitly for oil and gas well retrofits, Kujawa et al. [18] proposed a solution that would allow heat extraction from a single well. The proposed solution was a tube-in-tube or double pipe heat exchanger, consisting of two concentric tubes which would allow for injection into the outer annulus and extraction from the centre pipe of the heat exchanger. The cold injection fluid would collect heat from the adjacent hot rock as it travelled down on the outer annulus, and would be returned up the centre as a hot fluid. A significant issue with this design is the possibility for interaction between the inner and outer flows, which would reduce the outlet temperature of the system. This is a concern as it will reduce the efficiency of the power cycle. Furthermore, the addition of inner piping into a well reduces the cross-sectional areas of the flow, which will result in a high pressure drop and thus the need for greater pumping power. Kujawa et al. proposed the use of insulation in the form of either an air gap of 0.7 cm or 2.7 cm thick polyurethane for a portion of the well depth. The results of the study, which considered a 3950 m deep well, predicted that 140 kW of electricity could be produced by the configuration with air gap insulation.

Adding insulation further amplifies the issues with small flow areas. Another issue associated with this design is that it relies upon the assumption that the existing well is drilled completely straight, which may not be the case, particularly considering the extreme depth.

Building upon the work of Kujawa et al., Davis and Michaelides [19] proposed applying the single-well concept to an abandoned oil well. The associated numerical simulation, however, failed to account for the transient behaviour of the ground temperature, and therefore significantly overestimated the possible power production.

Following Davis and Michaelides, Bu et al. [20, 21] performed two computational studies on a tube-in-tube heat exchanger inside a well with a depth of 4000 m. The 10-year results demonstrate that an outlet temperature ranging from 120°C to 130°C can be achieved to produce a power between 53.7 kW to 59.4 kW. Cheng et al. [22, 23, 24] conducted similar studies, exploring the effects of a variety of factors such as working fluids, depth, and insulation on the performance. The numerical simulation of a 6000 m well [23] predicted that a well with a bottom hole temperature of 315°C could produce 239 kW of electricity after 300 days. This study assumed the use of refrigerant directly as the heat transfer fluid. The simulations by Noorollahi et al. [25] based on two wells in Iran demonstrated that a 4423 m deep well could produce 364 kW of power when the geothermal gradient was approximately the world average. Wight and Bennett [26] claimed that using water as a working fluid provided similar power production compared to a simulation performed by Cheng et al. that used refrigerant as the heat transfer fluid. However, the depths of the wells in both simulations were not comparable. Further, Wight and Bennett's model neglected to consider the impact of the inner tube on both flow and heat exchange. This resulted

Table 2.1: Net power predictions and associated wells in the literature

Author	Net Power	Depth	Gradient	Study Duration
Kujawa et al. [18]	140 kW	3950 m	25°C/km	1 year
Bu et al. [21]	59.4 kW	4000 m	45°C/km	10 years
Ghoreishi-Madiseh et al.* [27]	20 kW	700 m	61°C/km	10 years
Cheng et al. [23]	239 kW	6000 m	50°C/km	300 days
Noorollahi et al. [25] well AZ-II	133 kW	3861 m	29.6°C/km	Not listed
Noorollahi et al. [25] well DQ-II	364 kW	4423 m	31.2°C/km	Not listed
Wight and Bennett [26]	217 kW	6000 m	50°C/km	300 days

*Goreishi-Madiseh et al. studied a u-tube heat exchanger

in an underestimation of the system head losses and of the temperature drop the fluid would experience along the length of the centre pipe. The results of the studies are summarized in Table 2.1.

One less common approach to extraction from a single well is to employ a u-tube configuration, more commonly proposed for use in thermal storage and with ground-source heat pumps. This was suggested by Goreishi-Madiseh et al. [27] who simulated a 700 m deep well. Due to the unusually small depth of the system, there are no equivalent double pipe simulations with which to compare; however the results of the 10-year simulation suggest that the system could produce 20 kW of power. The possibility of interaction between hot and cold fluids is reduced in a u-tube configuration, but not eliminated. There is still some risk of a degradation in the temperature of the outlet fluid, which would reduce power cycle efficiency. The u-tube configuration is also associated with very small flow areas, which would result in a comparably high pressure drop over the length of a deep well.

2.3 Parameters Studied in the Literature

The research outlined in this thesis does not employ a double pipe or u-tube heat exchanger; however, it is still useful to examine the parameters explored in the studies that do employ these types of heat exchangers. The literature covers two kinds of parameters: those that cannot be easily changed once a well is selected and those that can be altered to optimize performance. Factors that cannot be changed will impact well selection and include the geothermal gradient, ground properties, and well geometry. The factors that can be altered for optimization include flow rate, inlet temperature, the application of insulation, and working fluid selection.

2.3.1 The Impact of the Geothermal Gradient

The geothermal gradient is the rate of the ground temperature increase with depth. It is a crucial factor because it determines the maximum temperature of a well. The average gradient within a few kilometers of the Earth's suface is 30°C/km, with values ranging from 10°C/km to upwards of 100°C/km, depending on the geology of the location [8]. Several authors have investigated the impacts of the geothermal gradient. Bu et al. [20, 21] used 25°C/km and 45°C/km gradients, Cheng [22] evaluated gradients from 30°C/km to 50°C/km, and Templeton [28] studied gradients from 25°C/km to 60°C/km. As expected, all of these studies concluded that a higher gradient with the same given depth resulted in higher power output.

The vast majority of the papers in this literature review employ the assumption that change in ground temperature with depth is linear. This is confirmed by Wight and Bennett [26], whose plot of well log temperature data from over 2500 wells in Texas confirmed that the temperature follows a linear trend with depth. This trend

can be seen in Figure 2.3. This is also supported by the well log data from Sanyal and Butler [29]. There are studies in which the gradient was not linear, such as the measured data used by Noorollahi et al. [30, 31]. This temperature profile shown in Figure 2.4 is closer to two piecewise linear gradients, with a steep gradient nearer to the surface and an almost flat linear profile deeper underground. Note that the depth of the well is measured in metres above sea level (m.a.s.l) on the plots. Noorollahi et al. [25, 32] have also used measured data that suggests a linear temperature profile in recent articles. The results from all of the simulations of Noorollahi et al. show that the outside annulus fluid temperature closely follows the geothermal gradient. This suggests that the gradient can have an impact on the fluid temperature, however other factors such as flow rate will control how large this effect is.

Generally, the geothermal gradient is significant because it determines the required depth of a well. In areas where the geothermal gradient is high, shorter wells can be selected for geothermal heat extraction. As a result, more wells will be viable for heat extraction, and the shallower wells will provide the benefit of reduced pressure drop, and therefore pumping power.

2.3.2 The Effect of Ground Properties

The thermophysical properties of the ground determine its temperature. According to a Massachusetts Institute of Technology led analysis on Enhanced Geothermal Systems [33], the ideal location for EGS will have high heat flow (e.g. heat flow from the core of the Earth, nearby radioactive rock, and local tectonic activity) and low thermal conductivity. This combination results in high ground temperatures, as the low conductivity will slow the rate of heat dissipation. Low thermal conductivity,

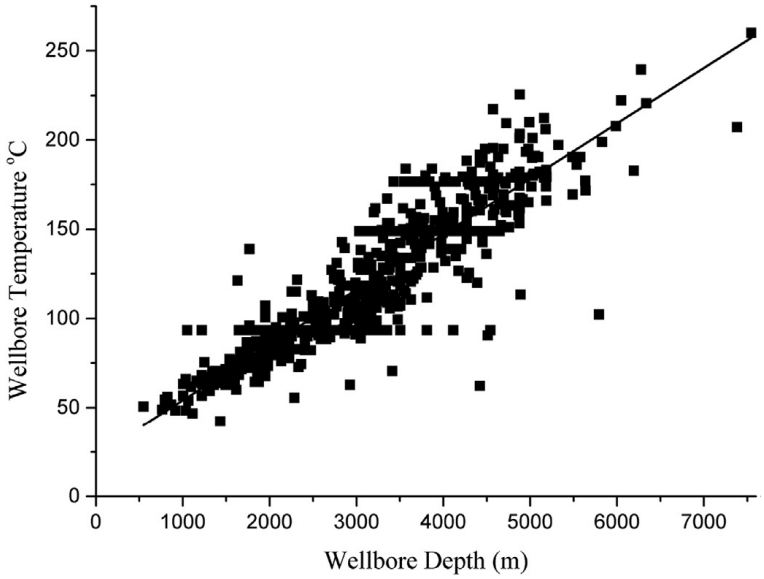

Figure 2.3: Linear trend in well log temperature data measured from over 2500 wells in Texas [26]

however, also inhibits heat transfer to the heat extraction medium. This is not prohibitive in the case of EGS, since such systems have high contact area with the rock. In applications using borehole heat exchangers, however, the benefit that low thermal conductivity provides in creating favourable initial temperature conditions must be balanced against its detriment to the heat transfer rate to the borehole. The thermal properties will depend on the lithology, the type and thickness of rock layers. Lithology will vary significantly by location. Most studies in the literature neglect to consider the lithology of the ground. Templeton et al. [28] suggested that using homogeneous thermal properties was acceptable, since petroleum deposits often exist in sedimentary basins. The one exception to this is the research by Noorollahi et al. [25], which takes into account the geological layers observed in an existing well. While this may improve the accuracy of the modelling, without a comparison to an identical well using averaged properties, the benefit of modelling lithology is unclear.

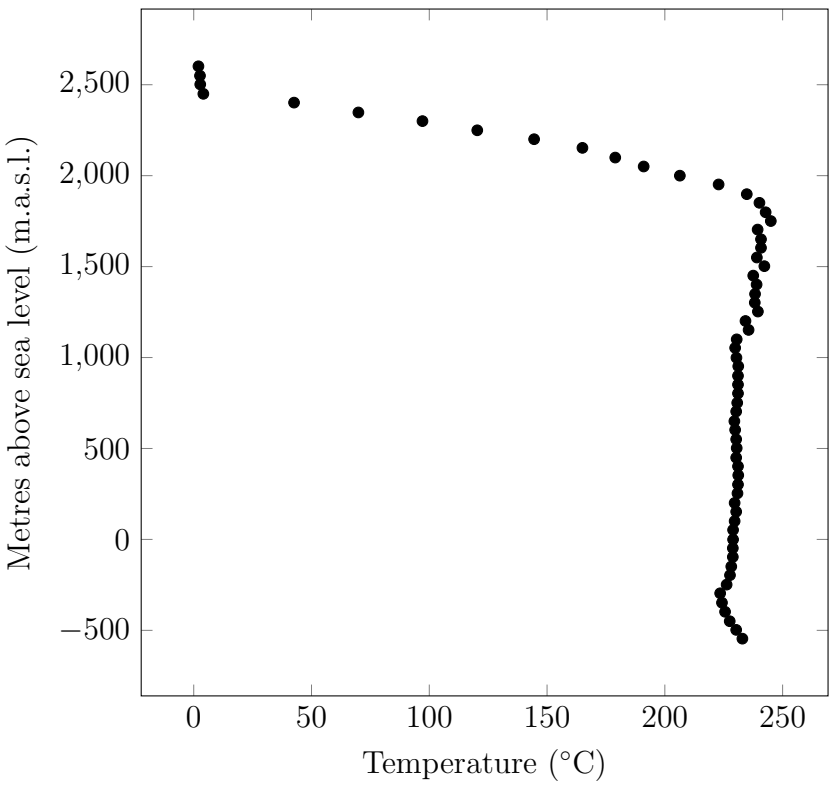

Figure 2.4: Measured temperature data from NWS1 well used by Noorollahi et al., digitized [30]

The remainder of the studies approximate the ground properties using a single material for the ground. The impact of thermal conductivity, density, and heat capacity were investigated by Cheng et al. [22]. The simulations, which tested conductivities from 1.5 W/mK to 2 W/mK, demonstrated that the outlet fluid temperature increases with a higher conductivity and that the temperature takes less time to stabilize. This is supported by the results of Goreishi-Madiseh et al. [27], which showed a temperature increase on the order of 10°C when thermal conductivity was increased from 1.5 W/mK to 3 W/mK. This is shown in Figure 2.5. This demonstrates that while low conductivity produces favourable thermal conditions for exploitation, it negatively impacts the quantity of thermal energy that can be extracted.

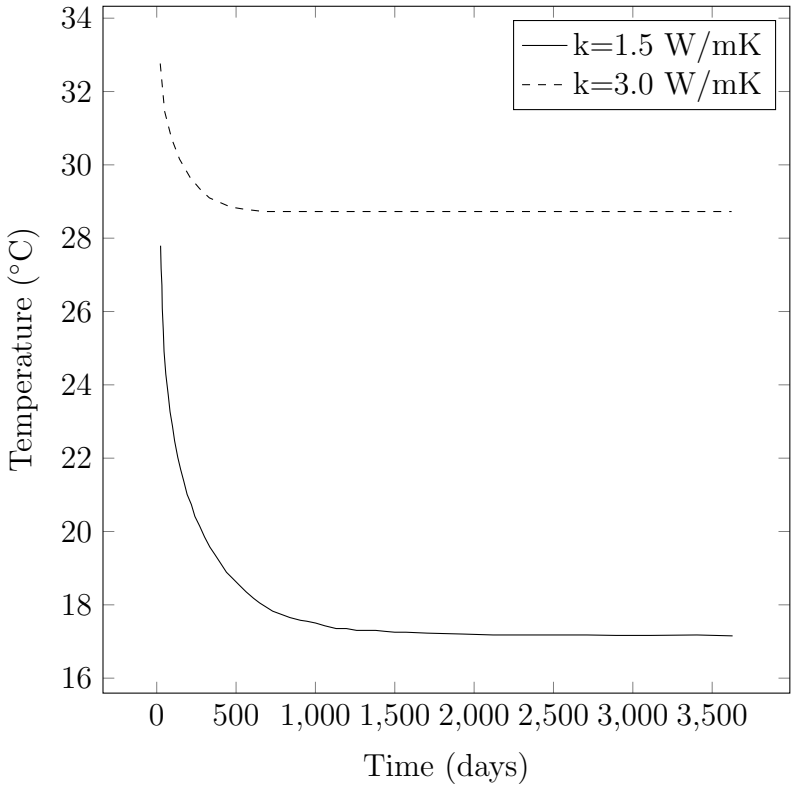

Figure 2.5: Impact of thermal conductivity on fluid outlet temperature, digitized [27]

Cheng et al. [22] found that the impact of changing heat capacity, (ρc_p), from 1.8x10^6 to 2.5x10^6 J/m^{3}K had little effect on the outlet temperatures at long times (1000 days).

Goreishi-Madiseh et al. [27] conducted a study of the importance of the ground's hydraulic conductivity. The possibility for the temperature gradients in the ground to lead to natural convection when the ground is permeable to water motivated this study. The study concluded that when the ground conductivity is less than 10^{-5} m/s, the ground conductivity can be ignored. Given that the permeability of sandstone

found in the region of east Texas and northern Louisiana is at most 280 mD (millidarcy) [34], the hydraulic conductivity is on the order of 10^{-6} m/s. As such, the impact of natural convection heat transfer is expected to be insignificant.

2.3.3 The Effect of Well Geometry

The impact of diameter on well sizing has not been discussed extensively in the literature. While diameter is a contributing factor to heat transfer, it is difficult to alter for an existing well.

Sanyal and Butler [29] discuss the impact of well diameter in the case of extraction from an existing hydrothermal resource. Their study considered extraction of existing hydrothermal resources found in an abandoned gas well. The study compared the extraction rates from small and large diameter wells. They found that water production, which they correlated positively with power production, increased dramatically with the larger tubing. While this is valuable knowledge for producing geothermal power from a hydrothermal resource, it does not demonstrate the impact of diameter for the application of wells as closed-loop heat exchangers.

Noorollahi et al. [25] considered wells of various diameters in their computational study using real well geometry. While they conclude that diameter plays an important role in heat transfer, the effect of diameter was not isolated in their simulations. Each well had different inner and outer pipe diameters, different depths, lithologies, insulation thicknesses, and casing designs. Therefore a study that isolates for the effects of these features, particularly diameter and depth, would more clearly demonstrate the impact of well geometry on heat transfer and power production.

Noorollahi et al. [25] also suggest that the decreased thermal resistance of the steel

casing plays an important role in the heat transfer of the system. Oil and gas wells are drilled with steel casings in the upper portion of the well. The purpose of the casing is to prevent contamination of ground water sources located above the petroleum source and also to provide structural support to the well. To accommodate the casings, wells are drilled in a telescoping manner, with the widest diameters drilled at the top and progressively smaller diameters drilled with increasing depth. As such, the thickness varies from thickest at the top to thinnest at the bottom of the casing. While the study by Noorollahi et al. did take into consideration the casing, it did not compare it to a well without a casing. And conversely, in a widely cited paper, Ramey [35] stated that the steel casing could be ignored when determining the heat transfer rate. Studying this would more conclusively establish the effect of steel casing on the heat transfer.

Cheng et al. [23] compared the performances of wells with depths ranging from 1000 m to 6000 m. The study, which investigated different organic heat transfer fluids, reported that wells less than or equal to 3000 m deep produced small amounts of energy, even with the presence of a relatively high 50°C/km geothermal gradient. For the range of depths and working fluids, Cheng et al. established that the net power production monotonically increased for an increase in well depth.

2.3.4 The Effect of Flow Rate

The impact of flow rate on performance was investigated by several authors in the literature. The body of research establishes that the flow rate affects two factors that determine power production. Bu et al. [20, 21] and Cheng et al. [22] found that increasing the flow rate improves the rate of heat extracted. This agrees with theory,

as heat collected is directly proportional to flow rate. However, it was also found by Bu et al. [20] and several others [22, 23, 18, 25, 32, 28], that raising the flow rate will negatively impact outlet temperature, which controls power cycle efficiency. As such, several authors, including Bu et al. [20, 21], Cheng et al. [22, 24], Noorollahi et al. [25], and Templeton et al. [28] all concluded that there is an optimal flow rate for each given well.

2.3.5 The Effect of Inlet Temperature

The inlet temperature is valuable to study, since it will affect the temperature exiting the system. The inlet temperature will be limited by the ambient temperatures surrounding the power cycle, since those temperatures will dictate the minimum cooling temperature. Varying the inlet temperature from 10°C to 25°C, Kujawa et al. [18] determined that raising the inlet temperature consistently increases the outlet temperature and decreases heat extracted. These results are supported by Templeton et al. [28], who show that, further, power production consistently decreased when the inlet temperature was raised from 10°C to 70°C.

2.3.6 The Use of Insulation in Double Pipe Configurations

As mentioned previously, insulation is used in double pipe heat exchangers to prevent losses between the hot return fluid and the cold inlet fluid. Some studies, such as those conducted by Noorollahi et al. [25] and Kujawa et al. [18], consider cases with different insulation types. They do not provide a clear comparison of insulation types, as they also include different configurations of insulation within the well, such as different lengths and varying thicknesses with depth. The study by Cheng et al.

[24] provided a more systematic analysis of the impact of insulating around the inner pipe. This was done by modelling varying thicknesses of polystyrene and a case with perfect insulation. The study concludes that 3 cm thick polystyrene is sufficient to prevent a significant temperature drop in the outlet flow, with a difference in outlet temperature of only 6°C compared to the perfectly insulated case.

Like in other studies, Templeton et al. [28] modelled insulation around the inner pipe of the tube-in-tube heat exchanger. Notably, since their study considered inlet temperatures that were greater than that of the ground near the surface, insulation on the outer casing of the well was also considered. It was determined that by adding a quantity of insulation (which is not explicitly mentioned in the article) with a thermal conductivity of 0.025 W/mK, an improvement of 4.4°C can be obtained, which corresponds to a thermal power increase of 40%. This suggests that insulating hot fluid in contact with cooler rocks could be beneficial to electrical power production.

2.3.7 The Impact of Working Fluids

While most researchers chose water as the heat transfer fluid within the well, Cheng et al. [22, 23, 24] chose to use the organic fluid from the power cycle directly in the wells. This potentially removes the need for a heat exchanger between the well and the power cycle, however Cheng et al. do not consider the possibility of contamination of the fluid inside the well. It is unlikely that fluid exiting the well can directly enter a power cycle, as it is possible the fluid was contaminated with sediment or petroleum products while underground. And while using refrigerant may provide performance benefits due to favourable thermal properties, it also presents a risk of ground contamination.

Wight and Bennett [26] explored this in their study by comparing the results of Cheng et al. [23], which used the refrigerant R245fa as the heat transfer fluid, with a simulation using water instead. Wight and Bennett suggested that there was no significant difference in performance between using R245fa compared to using water. However, the simulation used by Wight and Bennett to support this claim did not use the same well depth as that used by Cheng et al. In addition, Wight and Bennett neglected the impact of the inner tube on both heat transfer and pressure losses. It is likely that these modelling assumptions led to an overestimation in power production. Therefore further study into the performance differences associated with different heat transfer fluids is required.

2.4 Approaches to Modelling Heat Transfer in a Wellbore

The challenge of modelling heat transfer in a wellbore is relevant to the oil and gas industry as well as the geothermal community. Consequently, for decades, practitioners have relied upon Ramey's [35] analytical approximation of heat transfer between a fluid in an oil wellbore and the surrounding rock. The simplified approach was necessary at the time Ramey developed the solution, since there was not yet sufficient computing power to solve the heat transfer equations directly. Ramey's solution was developed using an effective overall heat transfer coefficient, U, which approximates the transience of the heat transfer using a time function, $f(t)$:

$$dq = U\left(T_2 - T_e\right) \tag{2.1}$$

where T_2 is the temperature at the wall and T_e is the temperature of the Earth in the far field and U is given by:

$$U = \frac{2\pi\Delta Z k}{f(t)} \tag{2.2}$$

where ΔZ is the length of an axial element and k is the ground conductivity. The value for $f(t)$, which varies based on the time scale, can be found using the figure or relationships discussed in Ramey's paper.

This eliminated the need to solve the transient portion of the thermal energy equation, simplifying the equations enough to be solved with the resources available at the time.

Ramey's approach was adapted to work with a tube-in-tube heat exchanger design by Cheng et al. [22, 23, 24], who used it to study various aspects of that design. The same approach was taken by Wight and Bennett [26], with updates to the model from Alves et al. [36].

Another semi-analytical approach to solving the well heat transfer problem is that of Kujawa et al. [18]. Kujawa's unique approach was to develop an analytical solution in the radial direction with a moving outer boundary to account for the transient nature of the problem. Kujawa et al. accomplished this by using an empirical value of Fourier number, 0.25, where the Fourier number is defined as [37]:

$$Fo = \frac{\alpha t}{r^2} \tag{2.3}$$

Defining the outer radius of the domain based on the Fourier number, R_{outer} becomes:

$$R_{outer} = 2\sqrt{\alpha t} \tag{2.4}$$

This outer radius was then applied to generate an overall heat transfer coefficient, which Kujawa et al. used to solve the radial heat transfer in cells dividing the domain in the axial direction of the well.

Since computational power is no longer scarce as it was when Ramey developed their approximations, computational methods can now be employed to determine the heat transfer, without the simplifying assumptions of the analytical model. This approach was taken by a number of researchers. Bu et al. [20, 21], Ghoreishi-Madiseh et al. [27], and Noorollahi et al. [25, 32] all developed CFD models to study their respective geometries. Templeton et al. [28] used finite element to study the heat transfer between the well and the ground.

In these studies, there were two approaches to modelling the fluid. Noorollahi [30, 25, 32, 31] and Templeton [28] chose to model the fluid directly. While this could possibly lend to greater accuracy of the model, it is computationally expensive, particularly given the considerable length of the domain. The alternative, chosen by the majority of authors in the literature, was to model the heat transfer in the fluid using a heat transfer coefficient. The most commonly chosen model was the Dittus-Boelter relationship. This was the approach taken by Bu et al. [20], Cheng et al. [22, 23, 24], and Goreishi-Madiseh et al. [27]. Templeton provided some criticism of this approach, citing the fact that the Dittus-Boelter equation is based on the assumption that the pipe is smooth and the pipe wall is isothermal [28]. Furthermore, Templeton noted that the Dittus-Boelter equation is not designed for annular flows. Kujawa et al. used a variety of relationships for the heat transfer coefficient, using those of Mikheev, Sarma, and Averin [18]; however these relationships are not commonly employed and could not be verified.

Table 2.2: Approaches to modelling the fluid inside the well

Author	Modelling Approach	Correlation
Bu et al. [20, 21]	Heat transfer coefficient	Dittus-Boelter
Cheng et al. [22, 23, 24]	Heat transfer coefficient	Dittus-Boelter
Goreishi-Madiseh et al. [27]	Heat transfer coefficient	Dittus-Boelter
Noorollahi et al. [25, 32]	Direct modelling	—
Templeton et al. [28]	Direct modelling	—

2.5 Summary

While EGS has advanced geothermal technology by allowing for thermal extraction without a hydrothermal resource, further exploration of different underground heat exchange approaches is still necessary. This research aims to do so by proposing a novel heat exchanger configuration retrofitted from directionally drilled oil and gas wells.

Tube-in-tube heat exchangers are commonly suggested to retrofit abandoned hydrocarbon wells. The primary benefit of this approach is that it only requires a single well; however, the single well configuration has several downsides. Since both inlet and outlet flows must fit within the diameter of the well, the small flow areas would result in a considerable pressure drop. Furthermore, the design of the heat exchanger leads to the risk of thermal interaction between the counter-directional flows. This is a significant drawback to the design, as it is a direct detriment to the power cycle efficiency. The challenges of pressure drop and, to a lesser extent, thermal interaction are also present in the less-commonly studied u-tube heat exchanger.

This thesis outlines a novel approach to underground heat exchange, which takes advantage of existing wells while eliminating the need for the close proximity of inlet and outlet flows. This is achieved by connecting two directionally drilled wells to

create a closed-loop heat exchanger. Fluid would flow down one vertical well and across the bottom portion of the L-shaped directionally drilled well. It would flow to the adjacent well, which is connected through some drilling, exiting out the vertical portion. This allows for a larger cross sectional area for the fluid to flow through and maintains significant separation between the cold and hot flows.

The new heat exchanger configuration requires the study of many of the same parameters that were discussed in the literature for the double pipe arrangement. Factors that impact the selection of the well, such as geothermal gradient and well geometry were explored to understand their impact on the proposed configuration. In addition, parameters related to the operation of the system, including flow rate, and inlet temperature were considered. Water was used as the heat transfer fluid throughout. Although there is no longer the issue of close proximity between hot and cold fluids, insulation was still explored for the closed-loop configuration, as it may reduce temperature losses when the fluid travels up the exit well, as was suggested by Templeton et al. [28]. Intermittent heat extraction, which could be used to address peak demand, was not explored in the literature but was considered in this thesis. The study of these factors will be discussed in Chapter 4.

The study that was undertaken makes use of CFD, rather than analytical models, as CFD does not require approximations to account for transient behaviour. The model made use of a 1D assumption in the fluid, using the Dittus-Boelter heat transfer correlation. This allows for reduced computational cost with appropriate accuracy. Since the hydraulic conductivity of rock is low in the location of concern, natural convection in the ground was ignored. In addition, as some of the studies only capture the heat transfer behaviour over short times, the study in this thesis considers a longer

time scale of 50 years. The long term study establishes the power output decay over time, and allows for a prediction of the lifespan of the system.

Chapter 3

Modelling and Methodology

This chapter outlines the approach to modelling the heat transfer in the ground. It describes the geometry, modelling assumptions, initial and boundary conditions, solver choice, and grid and time step independence testing.

3.1 Geometry

The geometry studied in this thesis is modelled after fracking wells found in the Haynesville shale formation, located in east Texas. To investigate the possibility of extracting heat from connected adjacent wells, the geometry studied consists of two vertical wells attached together at the bottom by a horizontal well. This can be seen in Figure 1.1. Haynesville fracking wells are typically drilled to depths of 3350 to 3800 m and commonly include horizontal wells, which extend 1220 to 1670 m outwards [13]. For this study, the vertical wells were chosen to be 4000 m (approximately 13,000 ft) deep and the horizontal well was set to be 4800 m (roughly 16,000 ft) long. The chosen well depth, while slightly larger than typical values in the region, is comparable to

depths studied in the literature. The length of the horizontal section accounts for the combined lengths of two horizontal wells and the additional length needed to connect them. The diameter of the wells was selected, unless otherwise specified, to be 0.1937 m (7 5/8 inches), a well diameter referred to in the literature [29, 28].

3.1.1 Modelling Simplifications

Starting with the proposed well configuration shown in Figure 1.1, the model was made simpler for the purpose of carrying out simulations. A simplified version of the well configuration can be seen in Figure 3.1a. Due to the considerable length of the wells, the effect of the heat transfer along the entire length of the wells is much more significant than the interaction between the corners where the wells meet. As a result, the corners between well sections were eliminated by straightening the domain to create a single, continuous pipe. The resulting geometry is a cylindrical domain with an inner radius representing the collection of well sections, shown in Figure 3.1b. Heat transfer is modelled in two directions, axial and radial, with the assumption that heat transfer does not vary in the azimuthal direction. As such only a portion of the angular domain was modelled. A one radian angular segment was chosen for the domain, with zero heat flux conditions set on either side. The length of the cylinder is the combined length of every well, which sums up to 12,800 m. Each section representing a well maintains the temperature conditions that would be found surrounding that well in its original arrangement. The outer radius of the cylinder represents the far field of the system. As such, it is defined such that the temperature of the ground at the outer radius is undisturbed by the heat transfer near the well.

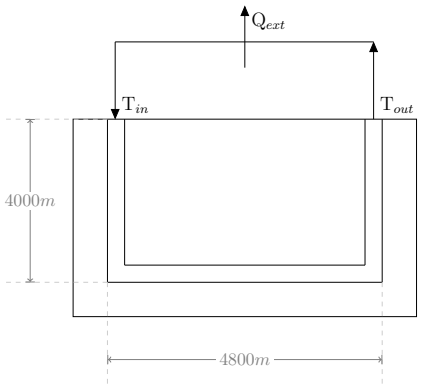

(a) Simplified layout of model domain prior to simplifications

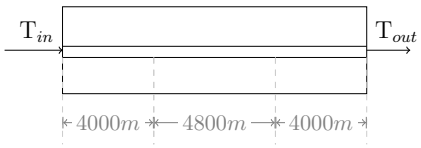

(b) Layout of domain after straightening

Figure 3.1: Layout of vertical and horizontal wells as modelled

3.1.2 Two-Domain Model

The model considers both the solid ground and the heat transfer fluid which flows through the wells to collect heat. The temperatures of these materials are coupled, however they are simulated in two distinct domains. While it is possible to develop a formulation in which the fluid and solid temperatures are solved together, implicitly, the vast difference in the magnitude of the fluid and solid coefficients proves to be a limiting factor. A fully coupled model was attempted; however it was numerically unstable. As a result, the two domains are solved for separately, explicitly connected through a boundary condition. The ground is modelled as a two dimensional solid in cylindrical coordinates and the fluid is approximated as one dimensional flow. A schematic of the two domains is shown in Figure 3.2. At each time step, the temperatures of each domain are calculated separately, with the solid computed first, followed by the fluid. The coupling between them is managed using a convection boundary condition. The scheme is highly conservative such that the energy leaving the soil exactly matches that which enters the fluid.

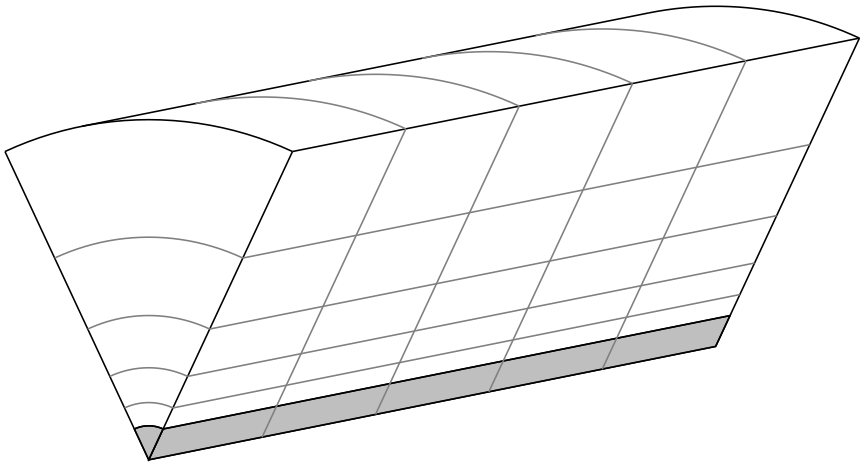

Figure 3.2: Schematic of the fluid and solid domains, with the fluid domain shaded in grey and grid lines depicting grid layout. Not to scale

3.2 Governing Equations

Heat transfer in the ground is modelled using the discretized conduction equation in cylindrical coordinates [38]:

$$\frac{1}{\alpha_g}\frac{\partial T_g}{\partial t} = \frac{1}{r}\frac{\partial}{\partial r}\left(r\frac{\partial T_g}{\partial r}\right) + \frac{\partial^2 T_g}{\partial x^2} \tag{3.1}$$

where T_g is the ground temperature and α_g is the thermal diffusivity of the ground.

The fluid is approximated as a 1D flow. It is assumed that the fluid remains liquid, which would require it to be pressurized if it reaches its saturation temperature. The fluid heat transfer equation is discretized using upwinding [39]. It is assumed that axial conduction in the fluid is insignificant in comparison to convection, and is therefore ignored. A schematic of the heat transfer in the fluid is shown in Figure 3.3. The fluid temperature advection equation is given by:

$$\rho_f c_{p,f}\left\{\frac{\partial T_f}{\partial t} + u\frac{\partial T_f}{\partial x}\right\} = \frac{4h}{D}\left(T_g - T_f\right) \tag{3.2}$$

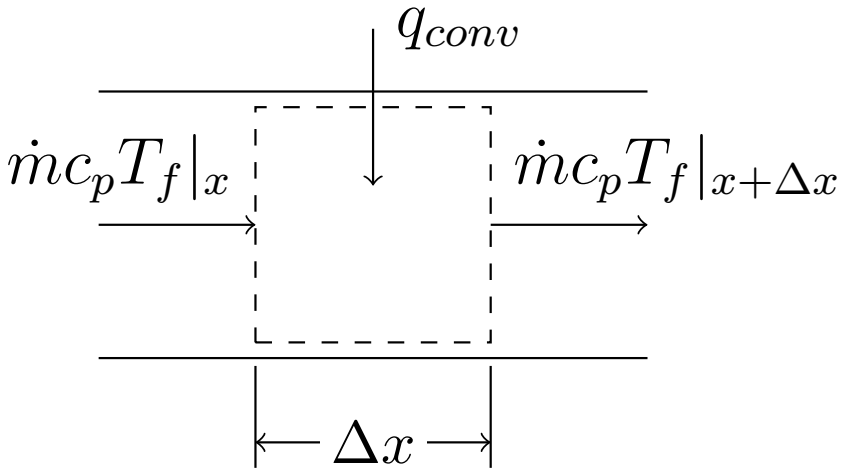

Figure 3.3: Heat transfer within fluid domain

where T_f is the fluid temperature, ρ_f and $c_{p,f}$ are the density and specific heat capacity of the fluid, u is the fluid velocity, h is the heat transfer coefficient, and D is the well diameter.

The Nusselt number for the convection heat transfer was determined using the Dittus-Boelter relationship for heating [37]:

$$Nu = 0.023 Re^{0.8} Pr^{n} \tag{3.3}$$

Re is the Reynolds number and Pr is the Prandtl number. The variable n is 0.4 when the fluid is being warmed and is 0.3 when the fluid is being cooled. The Dittus-Boelter relationship is valid for Reynolds numbers greater than 10,000 and Prandtl numbers greater than 0.7 and less than 160 [37]. Expected Reynolds numbers for this application range from 40,000 to 170,000. Since water is used as the heat transfer fluid in this study, its Prandtl number falls within the accepted range. The model takes into account the difference between the fluid and wall temperatures in order to

apply the correct exponent. The heat transfer coefficient was determined using the Nusselt number, Nu [37]:

$$h = \frac{Nuk_f}{D} \tag{3.4}$$

where k_f is the fluid conductivity.

3.3 Initial and Boundary Conditions

The temperature of the solid domain is set based on the geothermal gradient in the ground. The temperature gradient is assumed to be linear, increasing from 21°C at the ground surface to 153°C at the bottom of the wells, unless otherwise specified. In the sections representing vertical wells, the ground temperature follows this geothermal gradient. Where the domain represents the horizontal wells, the temperature is constant. Since the domain has been straightened out, there are two surfaces representing the ground surface, one at each end of the cylindrical domain. As an approximation, the heat flux was set to zero at these boundaries. Given the long length of the domain, the majority of the heat transfer will take place underground, therefore surface effects are considered negligible.

The outer radius of the domain also has a zero heat flux boundary. This boundary represents the far field, where the ground is completely undisturbed by the heat transfer occurring close to the well. To ensure the validity of this condition, it was confirmed that there was no temperature change at or near the boundary after every simulation. If this was not the case, the radial location of the boundary was expanded until this condition was met. The radius of this boundary was set to 502.5 m for all simulations.

This boundary condition assumes that there is no significant heat flux from the centre of the Earth. While there is heat generation in the Earth's core, when spread over the entire area of the Earth, the resulting flux is very small. This is even the case at the location of the horizontal well, 4000 m deep. Therefore, this flux will have a negligible effect on the temperature of the system, and need not be considered. It was only from accumulation of heat over millions of years, combined with the heat left over from the creation of the Earth, that the ground temperatures reached their current levels. However, the heat flux over the time scales discussed in this thesis will have little impact on the results.

The fluid temperature is initialized to match the solid initial temperature along the length of the axis. The inlet boundary condition is a constant temperature, and the outlet boundary condition is a zero-flux condition.

3.3.1 The Fluid-Solid Boundary

The interface boundary between the fluid and the ground must be handled carefully in order to accurately represent the coupling between the two domains. The boundary is a Robin boundary condition defined as the convection between the fluid and the wall determined using the fluid heat transfer coefficient [38]:

$$-k_g \frac{\partial T_g}{\partial r}\bigg|_{R_{in}} = h\left(T_f^{old} - T_g\right) \tag{3.5}$$

This boundary is applied to each domain. Equation 3.5 shows that the old fluid temperature, T_f^{old}, is used to define the boundary. This is done to maintain consistency. The boundary is first applied to the solid, using the fluid temperature from the previous time step. Once the solid temperatures are resolved and the heat flux is

determined, the same heat flux is applied to the fluid cells. This algorithm covers a single time step. This ensures that the heat flux across the interface remains constant over a time step and the scheme is highly conservative. Once these calculations are completed, the program progresses to the next time step and repeats the algorithm with updated values. Care was taken to ensure time step sensitivity, which is further discussed in Section C.2.

3.4 Mesh

The solid domain is divided into a mesh in two directions. Axially, the mesh is uniform, with a length of 50 m. In the radial direction, an expanding grid was chosen to minimize the total number of cells. This allows for a refined mesh near the wall, where the largest gradients occur, and a coarser mesh further away. The cells nearest to the wall have a radial thickness of 0.0488 m and the expansion factor is 1.05. The fluid mesh matches the axial mesh of the solid domain. A not-to-scale depiction of the mesh can be found in Figure 3.2. In total, the model contains 33,540 cells. This value was obtained through grid sensitivity testing, discussed in Section 3.9.

3.5 Matrix Solvers

The CFD simulations were carried out in Fortran using the GNU Fortran compiler [40]. Since the fluid heat transfer is modelled as one-dimensional, it was solved for using a Tri-Diagonal Matrix Algorithm (TDMA) [41]. The 2D solid domain is resolved using an Alternating Direction Implicit (ADI) solver [42]. ADI separates a matrix into two directions, in this case axial and radial, and solves them independently using

TDMA. ADI is well-suited to this problem since the majority of heat transfer occurs in a single direction, radially from the well.

The selected mesh is very anisotropic, with a maximum aspect ratio of approximately 1000 near the inner wall. This results in the addition of some error to the solution, which can be managed with the use of block correction. Block correction is a special form of multi-grid, which agglomerates all of the cells in one direction in order to apply a correction based on calculated residuals [43]. For these simulations, block correction was applied to cells grouped together in the radial direction to account for the relatively small order of magnitude of the axial coefficients.

3.6 Materials

The working fluid in the wells was chosen to be water. Since the temperature of the water varies significantly throughout the length of the wells, material properties were selected to represent the average temperature of the water [45]. This was determined by running a simulation where the fluid properties were those of room-temperature water. The average temperature was found, and the properties were updated based on this value. The ground properties were chosen to approximately reflect the rock found around the Haynesville shale formation [44, 49]. The material properties chosen for the rock and water are listed in Table 3.1, below.

3.7 Electricity Generation Calculations

To accurately predict the amount of electricity produced by a power cycle it is necessary to make design choices for details such as the type of power cycle, the working

Table 3.1: Properties used in CFD simulation

Property	Symbol	Value
Vertical well depth		4000 m
Horizontal section length		4800 m
Well diameter	D	0.1937 m
Surface temperature		21°C
Bottom-hole temperature [53]		153°C
Water density [37]	ρ_f	983 kg/m^3
Water specific heat capacity [37]	$c_{p,f}$	4185 J/kgK
Water thermal conductivity [37]	k_f	0.654 W/mK
Water Prandtl number [37]	Pr_f	2.99
Water viscosity [37]	μ_f	4.67×10^{-4} kg/ms
Ground density [49]	ρ_g	2500 kg/m^3
Ground specific heat capacity [49]	$c_{p,g}$	805 J/kgK
Ground thermal conductivity [49]	k_g	2.8 W/mK
Insulation conductivity [54]	k_{insul}	0.058 W/mK

fluid, and the operating conditions. Since this is beyond the scope of this project, it is necessary to employ certain approximations to characterize the potential electricity output of the system.

One approach is to use the maximum theoretical power output, calculated from the Carnot cycle efficiency. Carnot cycle efficiency is defined as [45]:

$$\eta_{Carnot} = 1 - \frac{T_C}{T_H} \tag{3.6}$$

where T_C is the temperature of the cold reservoir and T_H is the temperature of the hot reservoir in this theoretical power cycle. The temperatures in the calculation are expressed in Kelvin. For the purposes of this research, the cold reservoir temperature is the inlet temperature of the wells, and the hot source temperature is the outlet of the wells. Since the cool temperature is constrained by the temperature of the

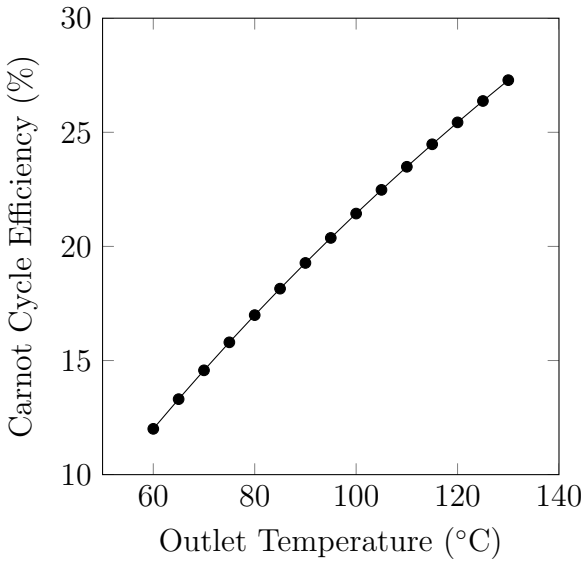

Figure 3.4: Carnot cycle efficiency vs. outlet temperature

atmosphere, in this study set to a minimum of 20°C, Carnot cycle efficiency will only improve if the well outlet temperature increases, as is shown in Figure 3.4.

The Carnot cycle power is then defined as [45]:

$$P_{Carnot} = \eta_{Carnot} Q_{ext} \tag{3.7}$$

Q_{ext} is the rate of heat extracted from the system, defined as [37]:

$$Q_{ext} = \dot{m} c_{p,f} \left(T_{f,out} - T_{f,in} \right) \tag{3.8}$$

where $\dot{m}$ is the fluid flow rate, $c_{p,f}$ is the specific heat capacity of the fluid, $T_{f,out}$ is the temperature of the fluid leaving the well system, and $T_{f,in}$ is the temperature of the fluid entering the system.

The advantage of using the Carnot cycle efficiency to approximate power production is that it accounts for the impact of the outlet temperature. This approach, as opposed to choosing a reasonable, static efficiency value, allows for a more complete understanding of how all parameters affect the system output. While the Carnot efficiency does not provide an accurate estimate of the amount of power that can be produced, it remains valuable in comparing the outputs of different systems. As such, this research employs the Carnot cycle power in parametric studies. These estimates are only useful for the purposes of comparison, rather than an accurate estimate of electricity production.

For a more reasonable estimate of power production, an efficiency of an existing power cycle can be chosen. For the purposes of approximation, the efficiency of an Organic Rankine cycle can be used, since it is a common choice for geothermal systems. According to a report on a US Department of Energy project, operating efficiencies of Organic Rankine cycle range from 6-10%, with 6% considered acceptable [16]. For this research, the efficiency range can be used to provide an prediction of possible electricity production.

In addition to considering power output, the power requirements of the system were also taken into account. The system requires a pump to operate, which will reduce the net power produced. The net power is defined as:

$$P_{net} = \eta_{Carnot} Q_{ext} - P_{pump} \tag{3.9}$$

where the pumping power, P_{pump}, is defined as [46]:

$$P_{pump} = \left(\frac{1}{\eta_{pump}}\right) f \left(\frac{L}{D}\right) \frac{u^2}{2} \dot{m} \tag{3.10}$$

where η_{pump} is the pump efficiency, f is the Darcy friction factor, L is the length of the entire system, D is the well diameter, u is the flow velocity, and $\dot{m}$ is the flow rate. The pump efficiency is assumed to be 80%, a value commonly employed in the literature [19, 23, 25]. For the pumping power calculation, the length of the system is the combined lengths of the wells, 12,800 m, plus additional length for the piping above ground. A conservative value of 500 m of above-ground piping was assumed in this research, however it is possible that the real value will be smaller. The diameter of the above-ground piping is assumed to match the well diameters. The roughness value needed to compute the friction factor was chosen to be 3 mm, corresponding to rough concrete. The Darcy friction factor was computed iteratively using the Colebrook equation [46].

3.8 Model Verification

The model was verified by comparing the model's output against analytical solutions. There is no suitable analytical solution to verify the coupled, transient behaviour that this model aims to simulate; therefore, the two domains were verified separately. The coupling of the fluid and solid domains was also verified using analytical equations for conduction heat transfer in the solid. The results of this verification and further details can be found in Appendix B.

The fluid domain was tested against steady state solutions for forced internal convection with a constant temperature wall. Two cases were analyzed. One considered a uniform wall temperature in the axial direction, which is similar to the heat transfer in the horizontal well section. The second considered a temperature which varied from hot to cold in the axial direction, which mimics the scenario where fluid travels

up a vertical well. Both simulations were found to be in good agreement with the analytical solutions.

The solid domain was also tested against steady state analytical solutions. Due to the two-dimensional nature of the solid domain, verification testing was performed by isolating for heat transfer behaviour in the radial and axial directions. In the tests, heat transfer occurred in one direction and heat flux was set to zero on the boundaries in the other direction. In the axial direction, the model was tested by applying constant temperature boundary conditions to both ends. In this case, the steady state temperature profile should be linear, which was found in the simulation results. In the radial direction, the heat transfer was verified using a convection boundary condition on the inner radius, where the fluid temperature was held constant. The outer boundary was set to have a constant temperature. In this case, the temperature profile should be logarithmic. In both cases, the solid temperature profile matched the analytical solution.

The coupling of the domains was verified by running simulations with the complete coupled model. By setting the fluid flow rate to a very large number approaching infinity, the conduction in the solid mimics the behaviour of the analytical solutions used to verify the solid domain. When u approaches infinity and the heat transfer coefficient, h, is set to a finite value, the solid behaves as if it has a conduction boundary condition at the inner radius with a constant fluid temperature. When the fluid velocity and heat transfer coefficient approach infinity, the solid behaves as if it has a constant temperature inner radius boundary condition. In both cases, testing showed that the model predicted the expected temperature profiles.

Transient verification was also performed on the solid domain using a solution

from Carslaw and Jaeger's *Conduction of Heat in Solids* [47]. Carslaw and Jaeger's solution considered the case of an infinite domain internally bounded by a cylinder at which a constant heat flux is applied. The transient results from the model agreed reasonably well with the analytical solution for the temperature of the cylinder wall.

Further verification was performed by comparing the amount of energy extracted over a 50-year base case simulation to a rough estimate of the amount of energy contained in a cylinder of rock. The findings showed a comparable magnitude of energy predicted by both the model and the rough estimate. For all details on verification, see Appendix B.

3.9 Grid and Time Step Independence Testing

Testing was performed to ensure that the simulation solutions were independent of grid and time step sizing. This was accomplished by progressively decreasing each parameter until the solution no longer changed. A separate independence study was carried out for each parameter: Δr, Δx, and Δt. The grid and time step independence were determined using a case with an inlet temperature of 20°C and a flow rate of 8 kg/s. The bottom-hole temperature was set to 171°C and the surface temperature was 18°C. All results are presented for a case where the system has been operating for five years.

The resulting grid contains 33,540 cells. The first cell in the expanding radial grid is 0.0488 m in length. The uniform cells in the axial direction measure 50 m in length. The time step was chosen to be 2700 s (or 0.75 hr). The outlet temperature of the system varied by no more than 0.18% between successive parameter size decreases

during the independence studies. Further information, including plots for the grid and time step testing, can be seen in Appendix C.

3.10 Summary

In summary, the modelling for the coupled fluid and solid domain consists of a straight, cylindrical tube with water flowing through the centre. The dimensions of the well and the initial temperature profiles were chosen based on the conditions in the Haynesville shale formation. Boundaries representing the surface of the tube were approximated with zero heat flux, as well as the far-field boundary at the outer radius of the cylinder. An algorithm was developed to accurately represent the transfer of heat between the separate, but coupled, fluid and solid domains. The grid and time step sizes were rigorously tested to ensure independence of the solution. Given this model configuration, a 20-year simulation takes just over one day of computational time to run.

Chapter 4

Results and Discussion

4.1 Introduction

This chapter explores the heat transfer behaviour within a well and its effects on power production. The analysis begins with a base case, which outlines the temperature distributions of the fluid and the ground and how they change with time. The factors affecting power production, primarily outlet temperature and heat extraction, are discussed and predictions of power output are established. A series of parameters related to well selection and operation are explored to determine their effect on the productivity of the system. Topics in this chapter include the assessment of the impact of flow rate, inlet temperature, the geothermal gradient, well diameter, and the insulation level. Finally, to address the possibility of applying this technology to alleviate peak power needs, a case involving intermittent heat extraction is examined.

4.2 Base Case

The base case consists of two 4000 m deep wells connected by a 4800 m long horizontal section. All wells have a diameter of 7 5/8 inches (19.37 cm). The fluid enters the wells at a constant 20°C and flows at 9 kg/s. All of the system's conditions can be found in Table 4.1. The 50-year simulation demonstrates the nature of the heat exchange between the fluid and the solid.

Table 4.1: Base case properties

Property	Value
Duration	50 years
Depth	4000 m
Horizontal section length	4800 m
Diameter	7 5/8 in (0.1937 m)
Domain outer radius	502.5 m
Flow rate	9 kg/s
Inlet temperature	20°C
Surface temperature	21°C
Geothermal gradient [53]	33°C/km
Ground density [49]	2500 kg/m^3
Ground specific heat capacity [49]	805 J/kgK
Ground thermal conductivity [49]	2.8 W/mK
Water density [37]	983 kg/m^3
Water specific heat capacity [37]	4185 J/kgK
Water thermal conductivity [37]	0.654 W/mK
Water Prandtl number [37]	2.99
Water viscosity [37]	4.67×10^{-4} kg/ms
Insulation	No insulation
Intermittent/continuous extraction	Continuous

The simulations model flow through a system consisting of three well sections: the downward, horizontal, and upward sections, as pictured in Figure 4.1. To simplify the model, the domain was straightened to create a single pipe, as was discussed in Chapter 3. This results in the initial temperature profile of the ground, depicted in

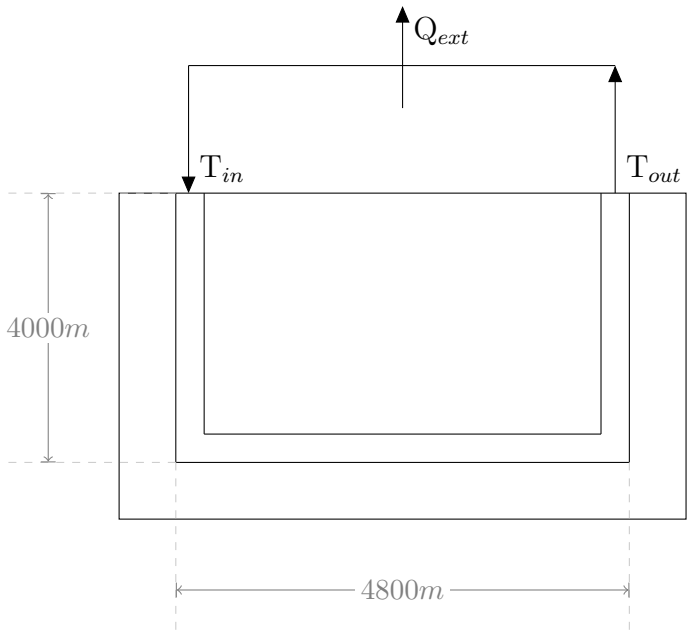

Figure 4.1: Layout of the well system

Figure 4.2, where the ground temperature is initialized to reflect the temperature of the three distinct well sections, which run along the same axis. When the fluid exits the system from the upward section, the Organic Rankine cycle extracts thermal energy from the fluid, denoted by Q_{ext}, before returning the fluid to the inlet at a constant temperature, T_{in}. In the base case, the inlet temperature is 20°C.

Figure 4.3 shows the fluid temperature along the length of the system at a range of times. The initial temperature of the fluid was set to match the initial temperature of the ground, shown in Figure 4.2. As the fluid travels down the first well, the ground temperature increases with depth, causing the fluid to gain heat. When the fluid reaches the horizontal section at 4 km, it is still cooler than the adjacent ground, which is initially at a uniform temperature. Since the horizontal segment possesses the highest ground temperature in the system, it is the section in which the fluid undergoes the largest temperature increase. Under the conditions of the base case,

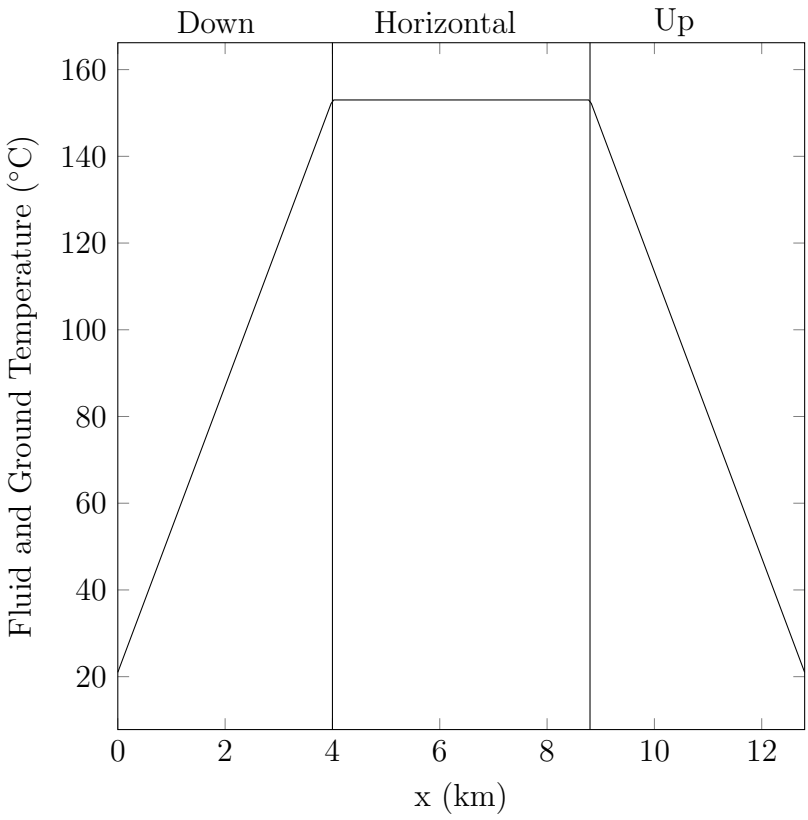

Figure 4.2: Initial temperature of the ground and the fluid

the fluid exits the horizontal section (at 8.8 km) still cooler than the ground. As such, the fluid continues to gain heat along a portion of the upward well. As the fluid travels upwards, the ground temperature will decline. At a shallow enough depth, the fluid will become hotter than the ground and begin to lose heat. This occurs on Figure 4.3 where the fluid temperature is maximized. As a consequence of this heat loss, the fluid exits the system at a cooler temperature than its maximum.

The heat flux from the ground to the fluid, shown in Figure 4.4, provides further insight into the behaviour of the fluid temperature along the axis of the well system. The heat flux reaches its peak at the bottom of the downward well. At this point, the difference between the fluid and ground temperatures is at its greatest. The heat flux

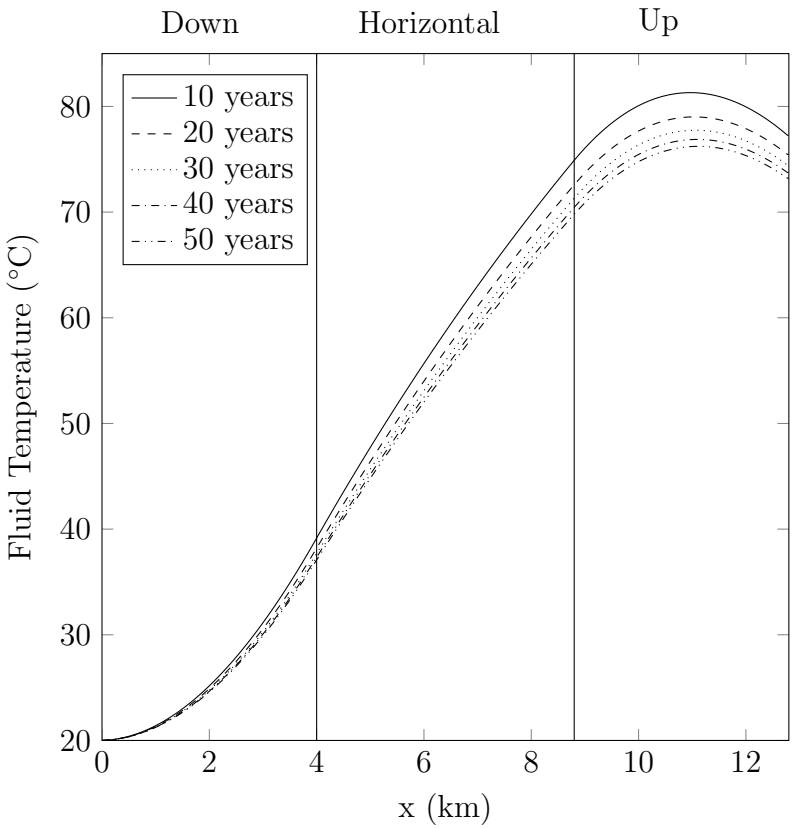

Figure 4.3: Fluid temperature along the length of the base case system after 10 to 50 years of continuous operation

begins to decrease in the horizontal section as the fluid warms up, bringing its temperature closer to the wall temperature. The fluid temperature continuously increases in the horizontal section since heat flux remains positive throughout this portion of the well. In the upward section, the heat flux decreases, since the temperature of the wall decreases as depth decreases, approaching the surface of the ground. When the fluid temperature becomes greater than the wall temperature, marked by the maximum temperature of the fluid in Figure 4.3, the heat flux becomes negative. This is the point where heat begins to flow into the ground, rather than into the fluid.

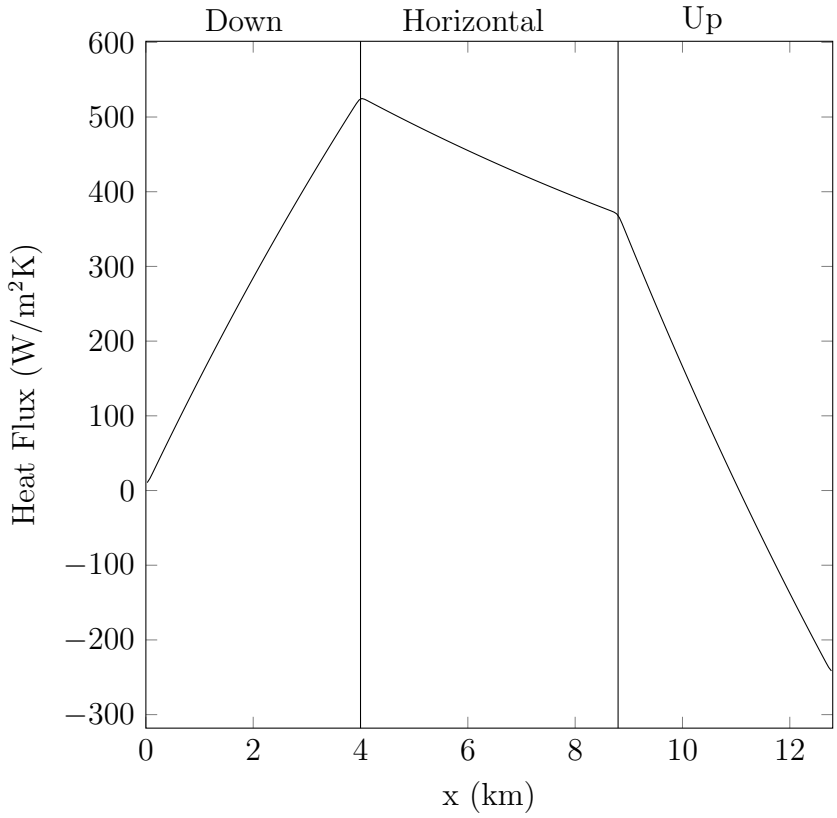

Figure 4.4: Heat flux from the ground to the fluid after 20 years of operation, base case

Figure 4.3 also depicts the fluid temperatures taken at various times in the simulation, ranging from 10 years to 50 years. The plot shows that the fluid temperature will decay over time. The effect is observed for the entire system, but particularly in the latter half of the domain. The results agree with expectation, since the ground will lose heat to the fluid, causing a decrease in the wall temperature and a smaller rate of heat transfer at later times. It is interesting to note that the rate at which the fluid temperature decreases diminishes over time. The difference between the fluid temperature is greatest between 10 and 20 years, and decreases with each successive

decade. This suggests a settling of the fluid temperature at the outlet over large time scales, which would be associated with stabilized power production.

The behaviour of the heat transfer along the length of the system can be seen in Figure 4.5, which shows the rate of heat transfer to the fluid in each section of the well. The fluid in the downward well experiences a significant addition of thermal energy over its length, averaging approximately 684 kW over 50 years. The most energy is added in the horizontal section, where nearly double the thermal energy is added compared to the downward section. In the upward well, very little energy is added to the fluid. This is because the fluid begins to lose some of the thermal energy it has collected when it reaches the cooler upper portion of this well. In fact, in the first year the fluid loses more energy than it gains in the upward well. For the remainder of the 50 years, the fluid gains a small net quantity of thermal energy; however, it is insignificant compared to the energy gained in the downward and horizontal sections of the system. Insulating the top portion of the upward well would help to increase the net thermal energy gains. This concept is explored in Section 4.7.

The settling trend of the outlet temperatures can be observed more clearly in Figure 4.6, which shows the outlet temperature over time. The fluid outlet temperature curve behaves logarithmically with time. Over the first ten years of continuous operation, the fluid temperature drops by approximately 11.1°C. The temperature drop over the following decade, however, is only 1.8°C. In fact, over the final 40 years of operation, the fluid temperature decreases by only 4.0°C. The result conforms with expectation, because as the ground near the wells cools down, it will become closer in temperature to the fluid. This will produce a lower heat transfer rate between the

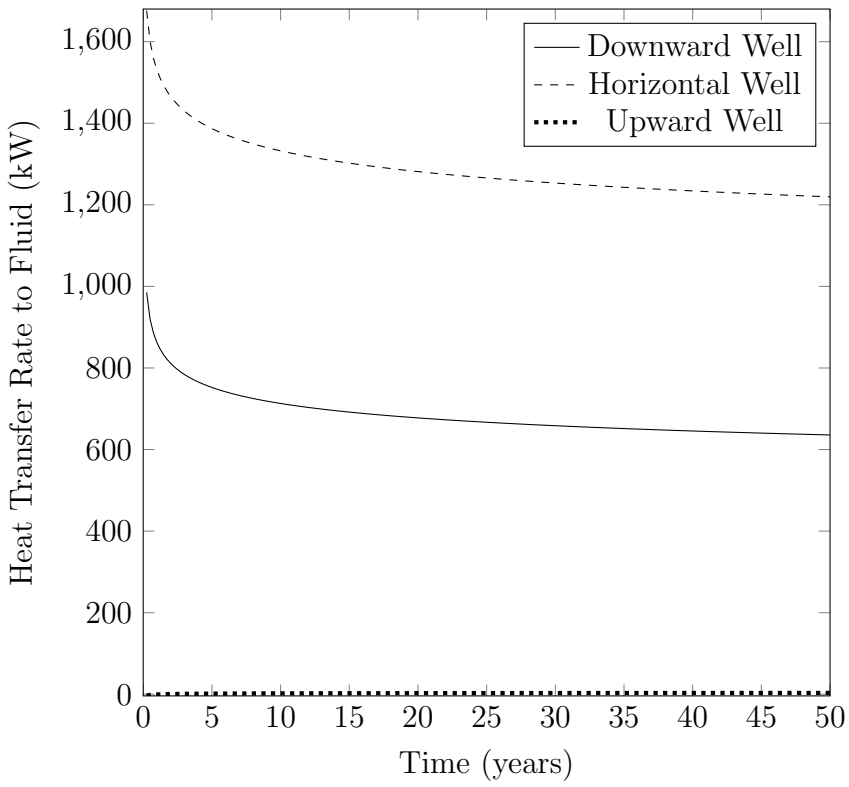

Figure 4.5: Heat transfer rate to the fluid for each well, over 50 years of continuous operation, base case

ground and the fluid, resulting in a smaller change in the fluid temperature as time progresses.

In the literature, low temperature geothermal fluid is typically classified by a minimum of 70°C or 80°C [26, 50, 51]. This corresponds to a 15-17% Carnot efficiency. Operating at temperatures lower than this will lead to an inefficient power cycle that is unlikely to be economically viable. While there are examples of systems operating below 80°C [52], favourable efficiencies will be obtained if the fluid exits the system at a higher temperature. Therefore the outlet temperatures observed in Figure 4.6 will not lead to high efficiencies and may not be hot enough for certain Organic Rankine cycle working fluids. A geothermal system should be designed to produce

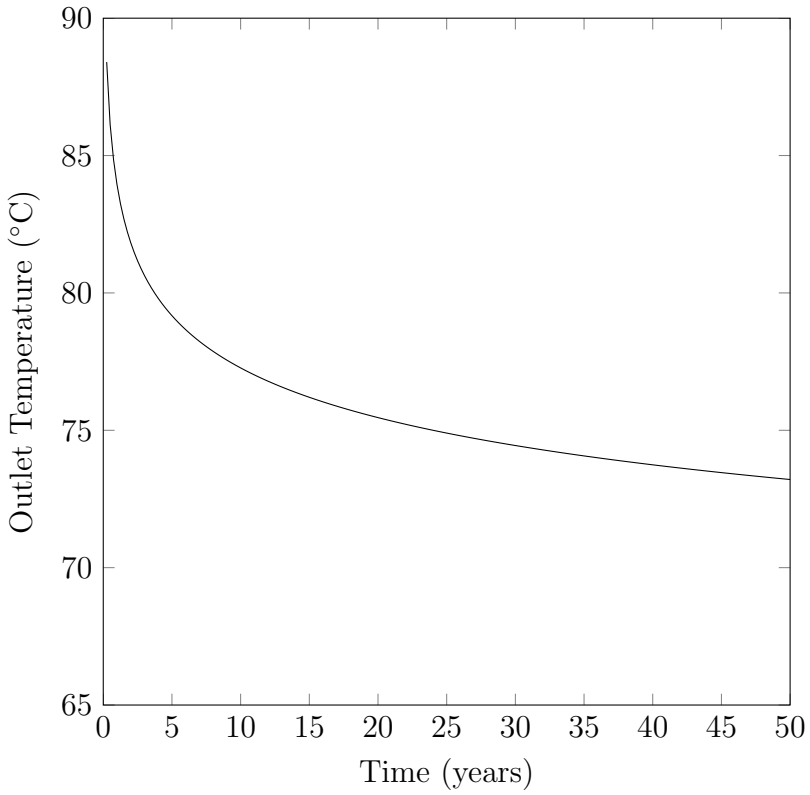

Figure 4.6: Well outlet temperature over 50 years of continuous operation, base case

higher outlet temperatures. This can be achieved by changing the system operating parameters and is explored as part of this research.

In Figure 4.7, one can observe temperature contour plots of the ground in the horizontal well. The contour plots at 10, 20, and 50 years depict thermal energy leaving the ground progressively over time. This loss of energy can be attributed to to heat transfer from the ground to the fluid. The contour plots, particularly at later times, are not uniform in the axial direction. More heat is lost at the entrance of the horizontal system than at the exit. This agrees with theory, since the cooler fluid at the start of the section will produce a higher heat transfer rate than the warmed fluid at the end of the section.

The plots in Figure 4.7 also indicate that the extent to which the heat transfer affects the ground is relatively small. The 10-year plot shows that the ground temperature is largely undisturbed beyond a radial distance of 40 m from the well. After 20 years, the cooler temperatures reach 55 m, rising to 86 m once the system has been running for 50 years. These contour plots demonstrate that the cooling effect of the fluid is restricted to a small region around the well. Considering that the length scales of the system are on the order of kilometres, a disturbance of less than 100 m around the well is insignificant in comparison. These plots also suggest that, even after 50 years, much of the initial thermal energy remains in the ground.

The temperature in the ground in the downward, horizontal, and upward sections can also be seen in Figures 4.8, 4.9, and 4.10. The plots show that beyond approximately 100 m, the ground is undisturbed by the heat transfer in the well after 50 years of operation. This represents a small fraction of the length scales of the entire well system. It is also much smaller than the size of the domain, which has an outer radius of 502.5 m. This confirms that the zero heat flux outer boundary condition is valid for the simulations in this study.

The rate of energy extracted from the fluid by the Organic Rankine cycle is shown in Figure 4.11. The rate of heat extraction, Q_{ext}, defined in Equation 3.8, is proportional to the difference in temperature between the outlet and inlet temperatures of the fluid. Since the inlet fluid temperature is constant, the heat extraction rate is proportional to the outlet temperature. As such, the heat extraction curve also behaves logarithmically with time. The change in the amount of the heat extraction rate drops quickly in the first 10 to 15 years, stabilizing at later times. After the first 3 months of operation, thermal energy can be extracted at a rate of about 2.6 MW

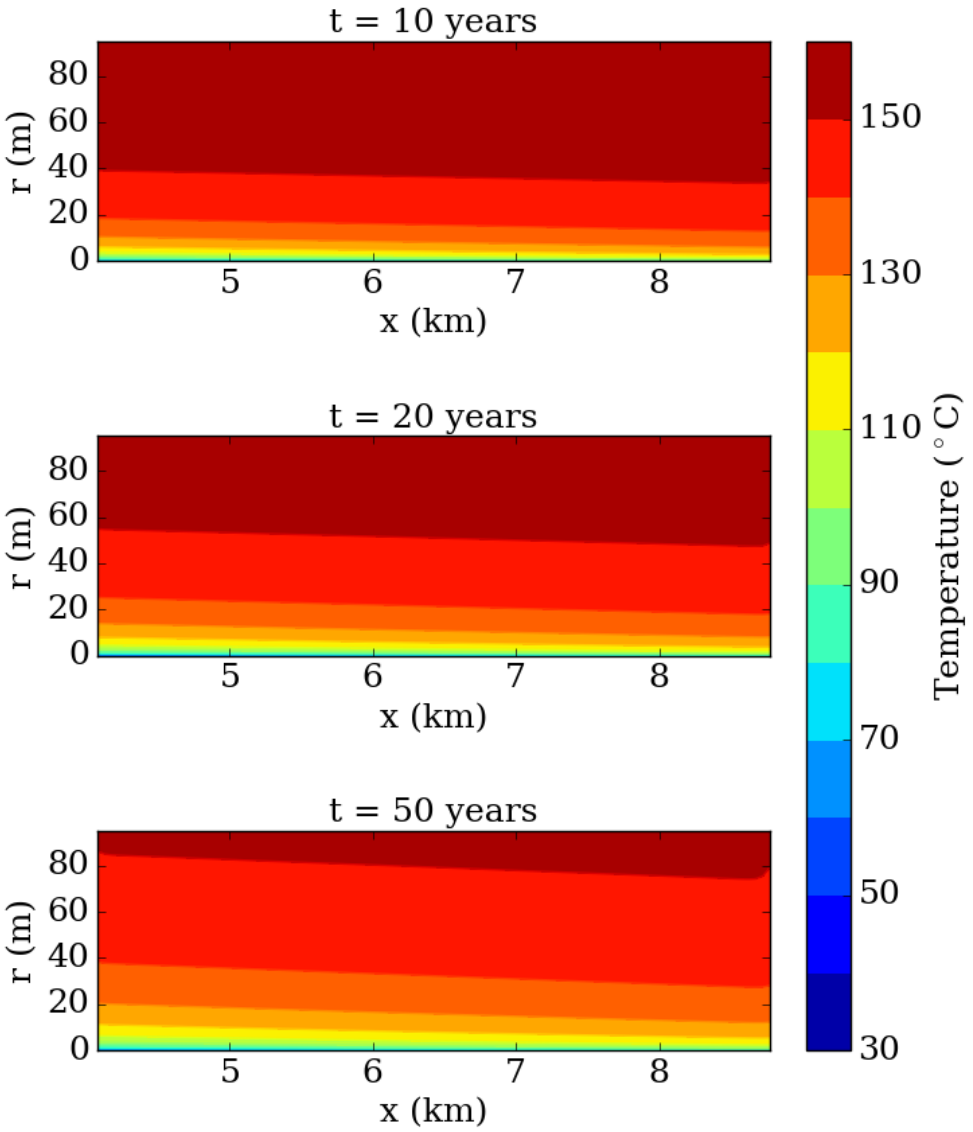

Figure 4.7: Contour plots of the ground in the horizontal section over 50 years of continuous operation, base case

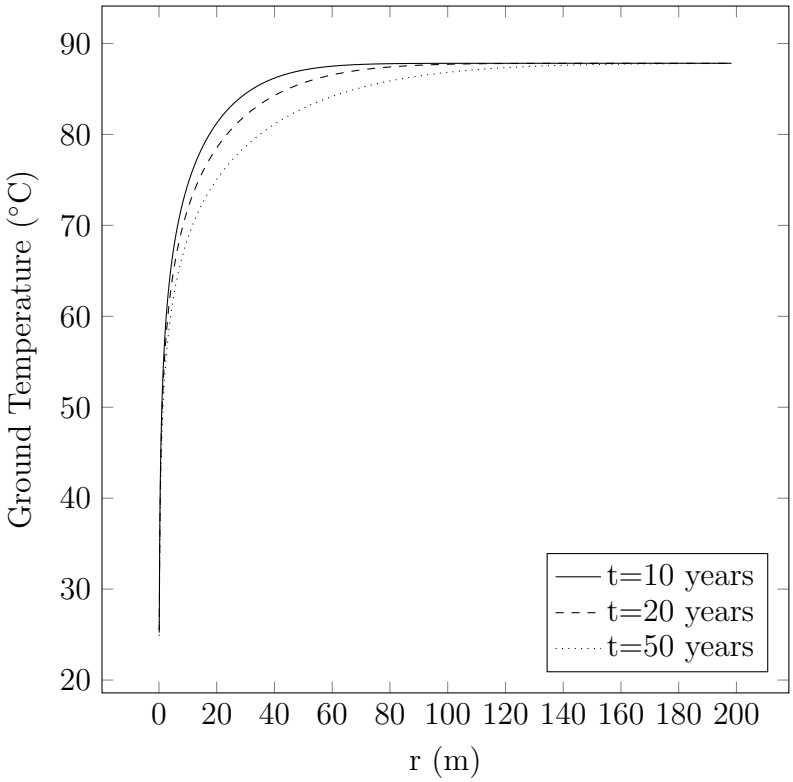

Figure 4.8: Radial temperature profiles in the ground halfway down (2000 m) the downward well over 50 years

from the system. After 10 years, the system extracts thermal energy at a rate of 2.1 MW, and by the time the system has been running continuously for 50 years, the heat extraction rate has dropped to 2.0 MW.

$$Q_{ext} = \dot{m} c_p \left(T_{out} - T_{in} \right) \tag{3.8}$$

The rate of heat extracted by the power cycle can be used to estimate electrical power production. The Carnot cycle efficiency can be used to predict the maximum theoretical power production, which changes as the fluid outlet temperature declines

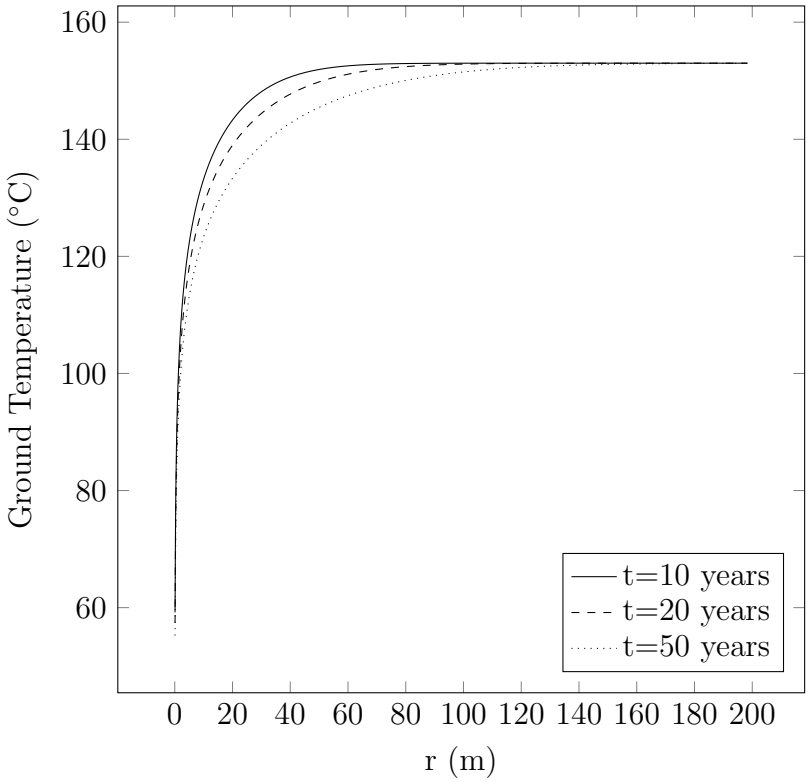

Figure 4.9: Radial temperature profiles in the ground halfway across (2400 m) the horizontal well over 50 years

with time. For a more reasonable estimate of electricity production, common efficiencies for Organic Rankine cycles, ranging from 6% to 10% can be employed. Each of these predictions over 50 years can be seen in Figure 4.12. The Carnot cycle power prediction shows a much steeper decline in early years compared to the percentage-based predictions because it reflects the large drop in the outlet temperature at early times. Therefore the Carnot cycle power curve is likely to predict the behaviour of power output over time, despite over-estimating the magnitude of power. The 6% to 10% efficiency estimates provide reasonable predictions of the power, although they do not account for the dynamic nature of the the outlet temperature. At 20 years, a 6% efficient Organic Rankine cycle will produce power at a rate of 124 kW, while

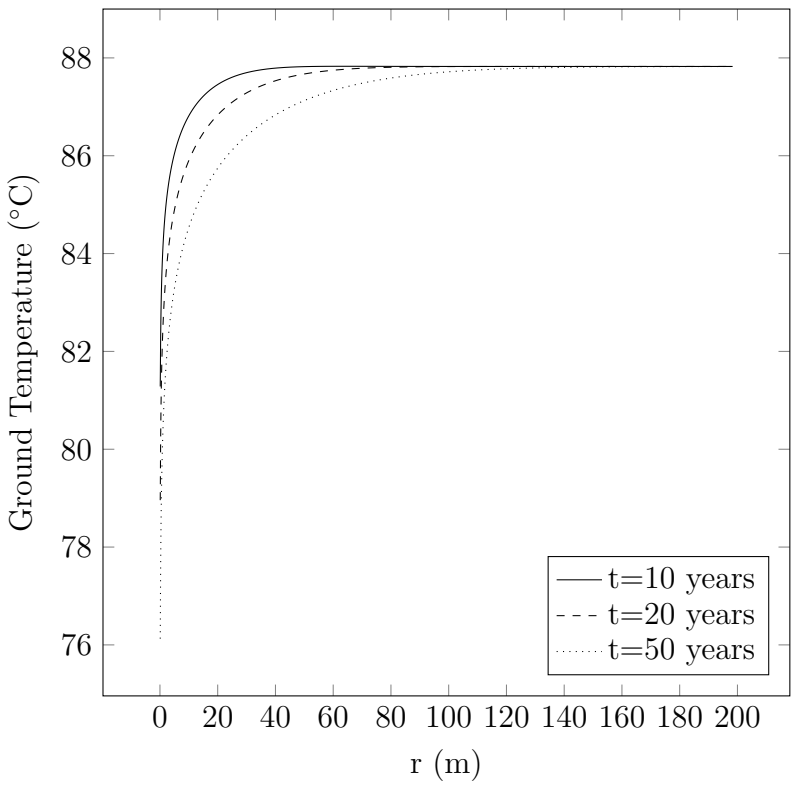

Figure 4.10: Radial temperature profiles in the ground halfway up (2000 m) the upward well over 50 years

a 10% efficient cycle will produce at a rate of 207 kW. It should be noted that since the outlet temperatures fall below 80°C in the base case, the temperatures may be below the minimum threshold for certain Organic Rankine cycles.

The power production figures speak to the potential longevity of the system. Whereas there would be a larger drop in productivity over the first 10 years, while the outlet temperatures stabilize, the remaining 40 years would experience, at most, a 10 kW drop in power output, with further stabilization expected at longer times.

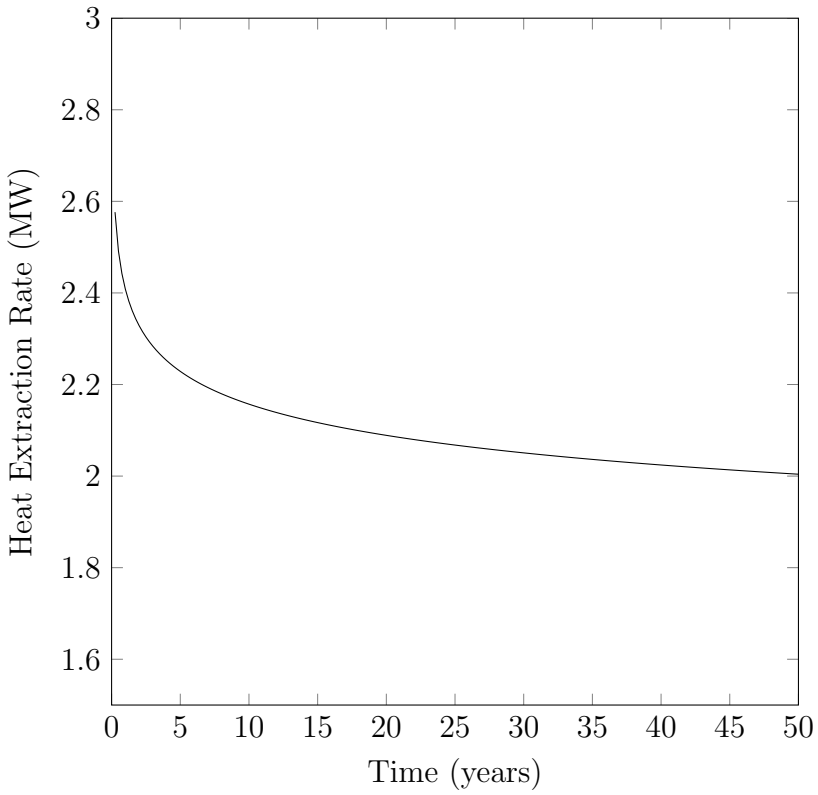

Figure 4.11: Heat extraction rate from the outlet fluid over 50 years, base case

4.3 The Effect of Flow Rate

The fluid flow rate influences two factors that directly impact power production: the heat extraction rate and the outlet temperature. A greater heat extraction rate will improve the amount of thermal energy available for conversion to electricity. Higher outlet temperatures will improve power cycle efficiency, resulting in a larger power output.

Figure 4.13 shows the results from several simulations where the flow rate was varied, while maintaining all other conditions from the base case. The plots show that increasing the system's flow rate produces two opposing effects. The heat extraction

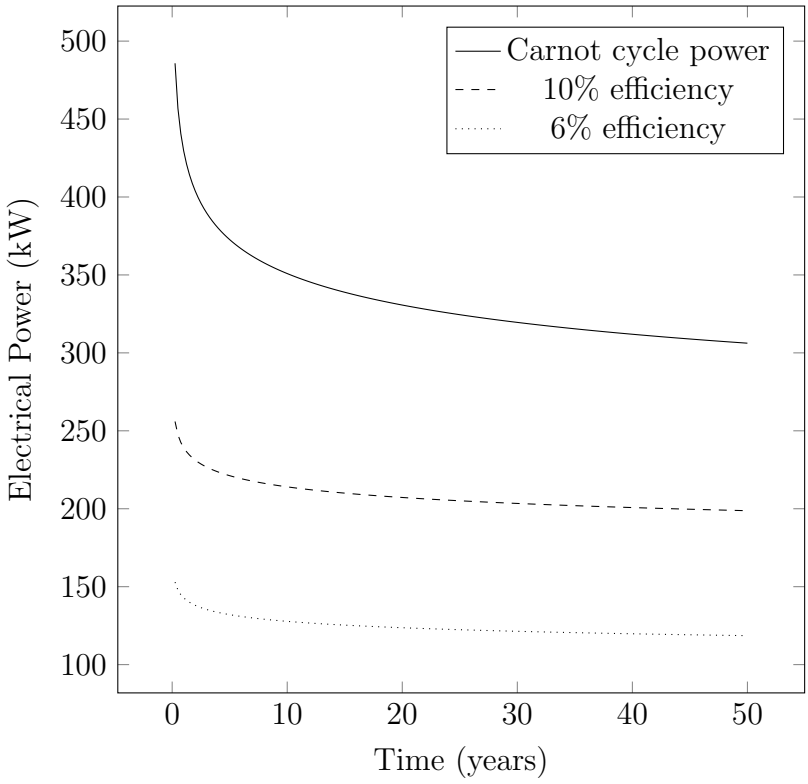

Figure 4.12: Theoretical maximum power (Carnot power), and approximate power production with 6% and 10% efficient Organic Rankine cycles, base case

rate increases, while at the same time, the outlet temperature decreases. The rate of heat extraction increases because it is directly proportional to flow rate, as shown in Equation 3.8. While an increase in flow rate improves heat extraction, it is detrimental to the outlet temperatures. When the fluid is moving faster, it has less time in contact with the hot rock, so it does not heat up as much, resulting in lower outlet temperatures. A decrease in outlet temperature results in a lower efficiency of the Organic Rankine cycle, which will diminish the net power production. Therefore it is clear from the results depicted in Figure 4.13 that there is an optimal flow rate for which the power output will be maximized. These findings are consistent with those described in the literature.

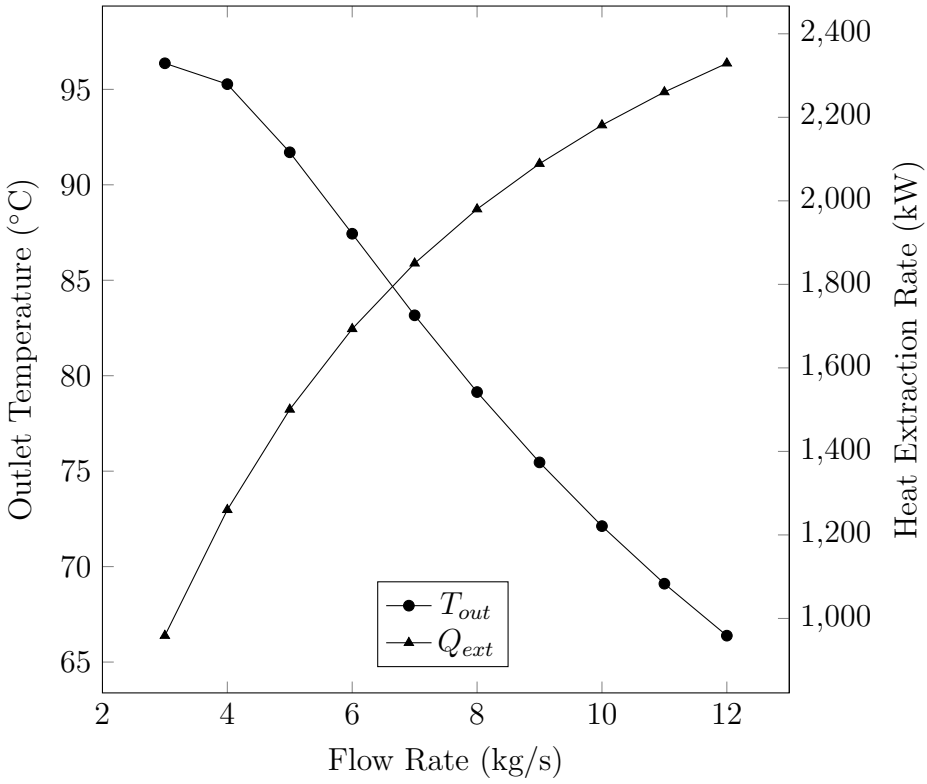

Figure 4.13: Outlet temperature and heat extraction rate vs. flow rate from a fluid after 20 years continuous operation

The combined effects of heat extraction and outlet temperature are seen in Figure 4.14, which shows the Carnot cycle power. The Carnot cycle power is the maximum theoretical power that can be produced by a power cycle. This is not a realistic value for electricity generation, but is used here for the purposes of comparison. The Carnot cycle power plotted is the net power, which accounts for the reduction in the power output due to the pump power requirements. The effect of pumping power will be highest at higher flow rates, since pressure drop is proportional to velocity squared. The plot shows a clear optimum flow rate which balances the two opposing effects. This result agrees with the findings in the literature from Bu et al. [20, 21], Cheng et al. [22, 24], Noorollahi et al. [25], and Templeton et al. [28].

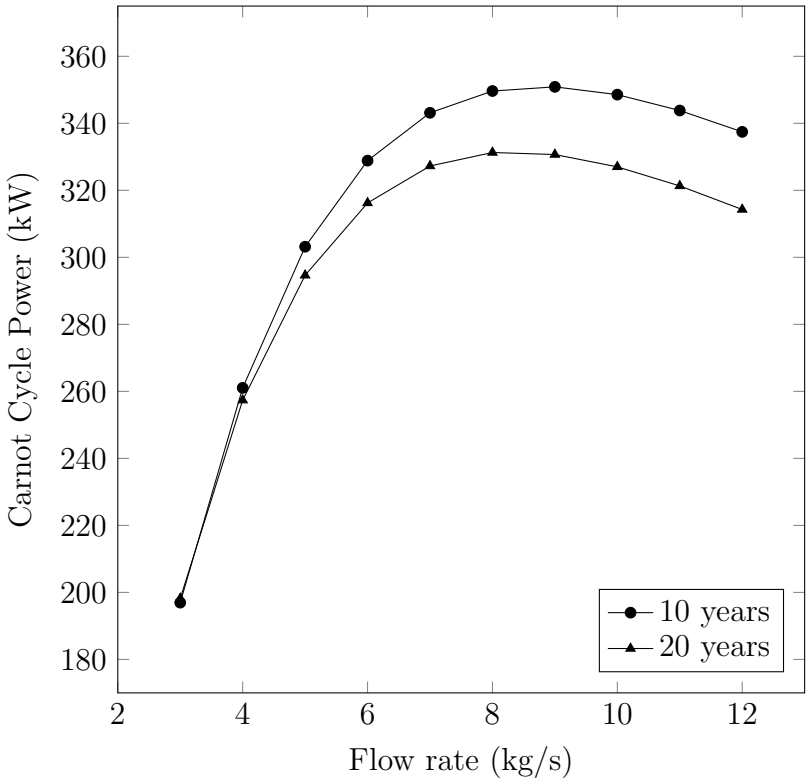

Figure 4.14: Carnot cycle power vs. flow rate after 10 and 20 years of continuous operation

For 10 years of operation the optimal flow rate is approximately 9 kg/s, while after 20 years of operation, the optimum shifts to around 8 kg/s. This highlights the impact of the flow rate on the longevity of the system. Since the cases with higher flow rates collect thermal energy more quickly, the decline in performance also occurs at a faster rate. As a result, over 10 years there is very little change in performance in the 3 kg/s case, while there is a nearly 7% decrease in performance when the flow rate is 12 kg/s. Therefore, the optimal values of the operation parameters will shift with time.

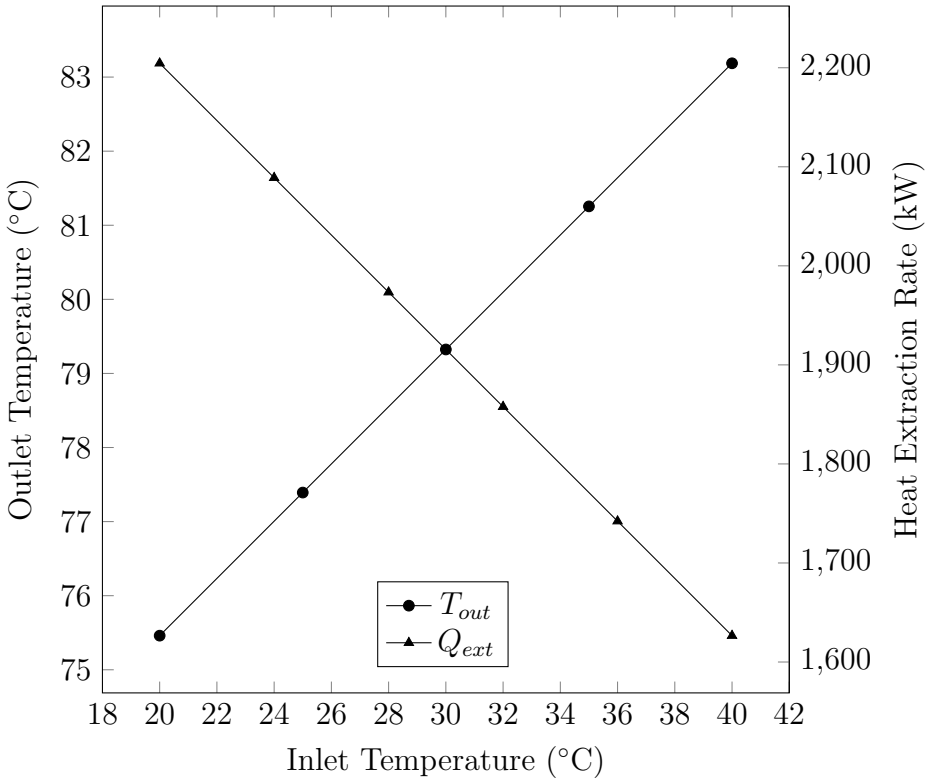

Figure 4.15: Outlet temperature and heat extraction rate vs. inlet temperature after 20 years of continuous operation

4.4 The Effect of Inlet Temperature

Figure 4.15 shows that the temperature of the fluid entering the well affects both the outlet temperature and the heat extraction rate. This result was obtained by performing multiple simulations where the inlet temperature was increased from 20°C to 40°C using the base case configuration and properties. The plot shows that the outlet temperature of the fluid increases linearly with inlet temperature. This result agrees with the findings in the literature. A one-degree increase in the inlet temperature produces a 0.39°C increase in the outlet temperature. The observed behaviour of the outlet temperature agrees with the physics of heat transfer, since less heat will flow

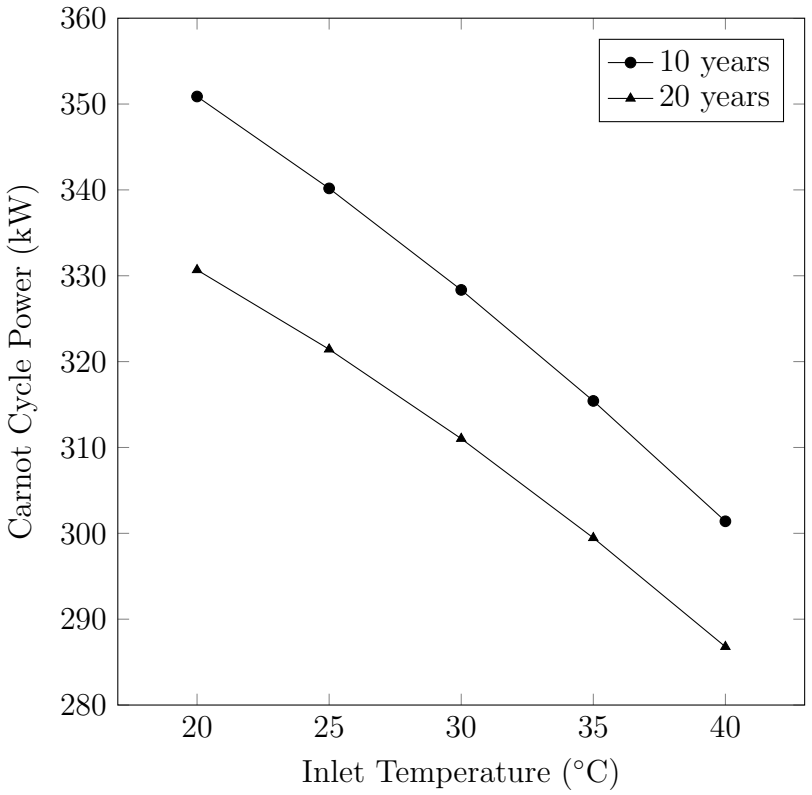

Figure 4.16: Carnot cycle power vs. inlet temperature after 10 and 20 years of continuous operation

when the temperature difference between the fluid and the ground is smaller. The information gathered from the outlet temperature behaviour lends itself to explaining the change in the rate of heat extraction with time. The heat collected from the fluid, defined using Equation 3.8, diminishes with a gain in the inlet temperature due to the reduced temperature differential between the outlet and inlet.

The impact of the decreasing heat extraction rate on power production can be seen in Figure 4.16. The plot shows that the Carnot cycle power production consistently decreases when the inlet temperature is increased. This is the case after 10 and 20 years of operation. This result was also consistent with the literature. Although the

increase in the outlet temperature helps to improve power cycle efficiency, the effect does not outweigh the detrimental effect of the reduction in heat extraction rates. This demonstrates that using the lowest temperature possible for the inlet will result in the best power production.

4.5 The Effect of Geothermal Gradient

The effect of the geothermal gradient (i.e. the rate of increase of ground temperature with depth) on power production can be seen in Figure 4.17. The data was obtained by running 20-year simulations of the system with three different gradients, each using the same geometry and surface temperature. All other parameters were consistent with the base case conditions. The gradients were selected using temperature well log data from Louisiana and Texas [53], where the Haynesville shale play is located. Three cases were simulated, modelling the mean geothermal gradient and one standard deviation above and below the mean. Wells that had at least three temperature measurements were selected from the data set in order to determine the average gradient. The plot shows that power increases with the geothermal gradient, which conforms with expectation and the findings in the literature, since a higher geothermal gradient results in higher temperatures in the well.

The Carnot cycle power for the 42.3°C/km case is 519 kW, 57% greater than that of the base case. For a rough estimate of real power production, with a power cycle efficiency of 10%, the high geothermal gradient case will produce 265 kW of power. These results suggest that selecting a well in a location with a higher than average geothermal gradient will significantly benefit power production.

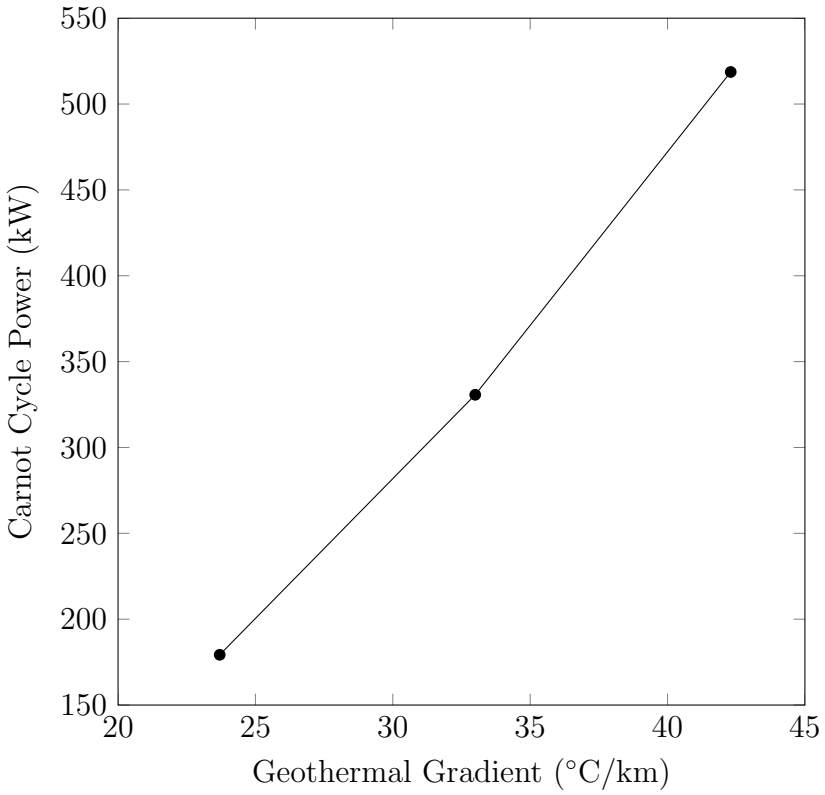

Figure 4.17: Carnot cycle power vs. geothermal gradient after 20 years of continuous operation

4.6 The Effect of Diameter

While it would not be feasible to increase the diameter of a well after it is selected, there is some variation in well diameters. Since it will have an impact on well selection, it would be valuable to explore what effect diameter has on power production. Two diameters were chosen to be studied: 6 inches (15.24 cm) and the base case, 7 5/8 inches (19.37 cm). Each case had the same flow rate, 9 kg/s. Due to the smaller diameter, the 6 inch case had a much higher velocity, 0.50 m/s. This is much greater than the 0.31 m/s velocity for the base case. In the simulations, parameters other than diameter matched those of the base case.

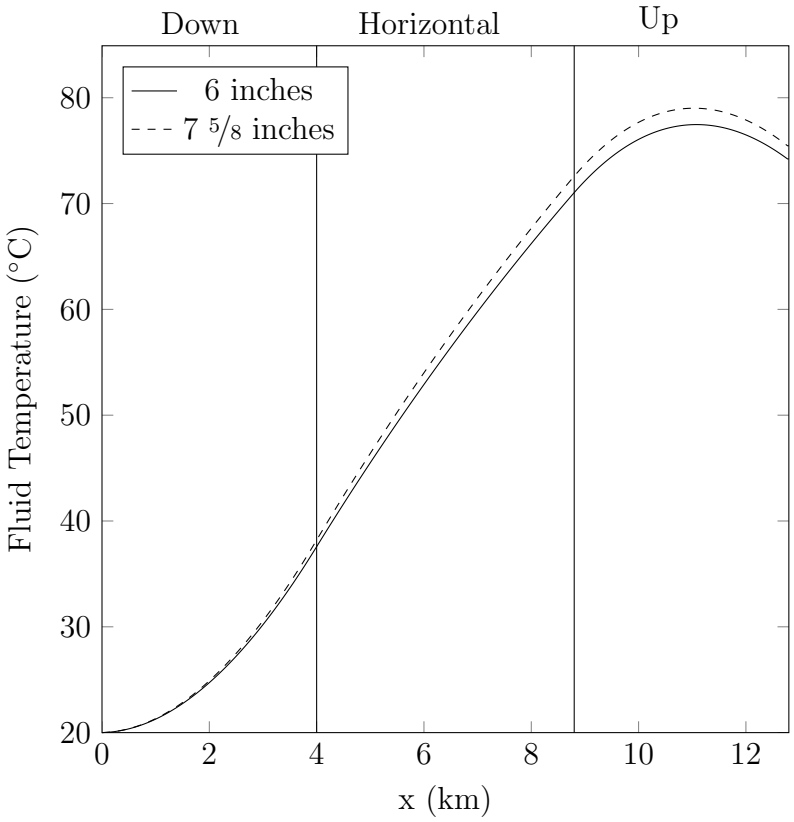

Figure 4.18: Axial fluid temperature profiles for different diameters after 20 years of continuous operation

Figure 4.18 shows the axial fluid temperature for the two diameters at 20 years of operation. It is clear from the figure that reducing the diameter resulted in lower fluid temperatures along the length of the system. The temperature of the fluid in the base case increases more in the downward and horizontal well sections in comparison with the 6 inch diameter case. In the upward well section, the fluid in the base case reaches a higher maximum than that of the smaller diameter case. The smaller diameter case has an outlet temperature of 74.2°C, which is 1.7% smaller than the base case outlet temperature of 75.5°C.

The difference in temperature between the two cases can also be seen in Figure

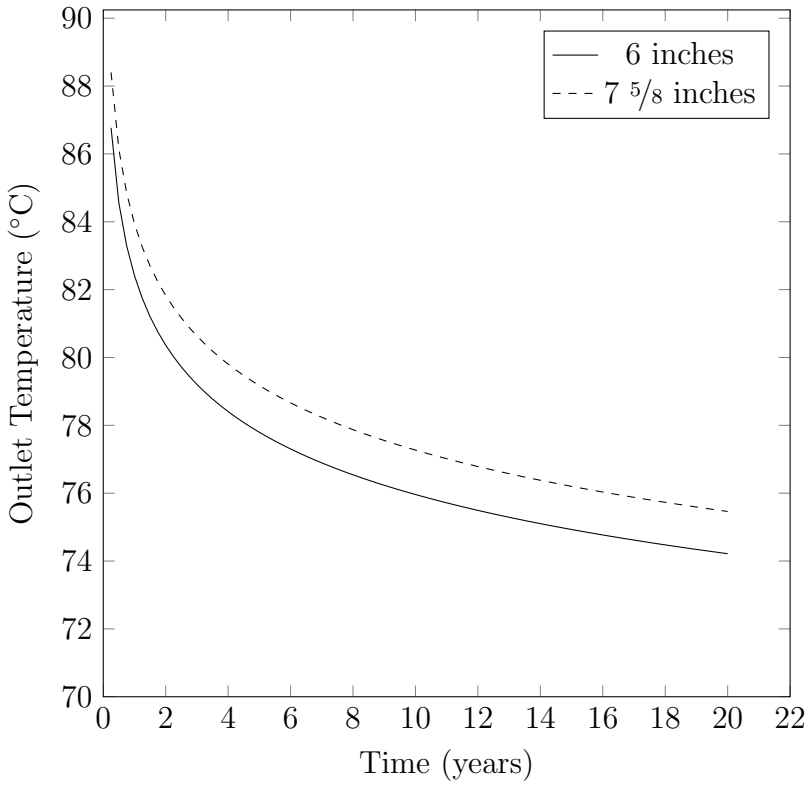

Figure 4.19: Fluid outlet temperatures for different diameters over 20 years of continuous operation

4.19, which shows the outlet temperatures over 20 years. The figure shows that, in each case, the outlet temperature drops steeply at the beginning before stabilizing with time. The results show that the difference in the outlet temperature between the base case and 6 inch diameter case is greater near the start of operation.

It was found that the larger diameter case had higher fluid temperatures even though the heat transfer coefficient is greater in the smaller diameter case. The effect of diameter on the heat transfer rate at any point along the wall can be seen in Equation 4.1, which is further expanded in Equation 4.2. In Equation 4.1, A_0 is surface area. This shows that the rate of heat transfer from the wall to the fluid is

inversely proportional to $D^{0.8}$. This relationship suggests that decreasing the diameter could help to enhance heat transfer rates and increase the fluid temperature; however, the results show the opposite in the long term.

$$Q\left(x\right) = hA_0\left(T_{wall}(x) - T_f(x)\right) \tag{4.1}$$

$$Q(x) = 0.023\left(\frac{4\dot{m}}{\pi\mu}\right)^{0.8} Pr^n \frac{k}{D^{0.8}} \pi L\left(T_{wall}(x) - T_f(x)\right) \tag{4.2}$$

If one examines the outlet temperatures at very early times, as seen in Figure 4.20, it becomes clear that the temperatures in smaller diameter case were initially higher than those of the base case. However, the base case outlet temperature quickly surpasses the 6 inch case outlet temperature after one day. This is explained by the cooling of the soil in the region near the wall. As is seen in Figure 4.21, the temperatures near the wall are warmer in the base case. If the difference between the wall temperature and the fluid temperature from Equation 4.1 is small enough in the 6 inch case, this would result in lower heat transfer rates and lower temperatures, despite the higher heat transfer coefficient. The contour plots suggest that this is what occurs, causing lower temperatures in the smaller diameter case for the remainder of the simulation.

The decrease in the outlet temperature in the small diameter case corresponds to a decrease in power output. The reduction in efficiency means that the Carnot cycle power will be 313 kW, a 5% reduction in comparison with the base case. With a 10% efficient power cycle, the smaller diameter case would produce roughly 198 kW of electricity.

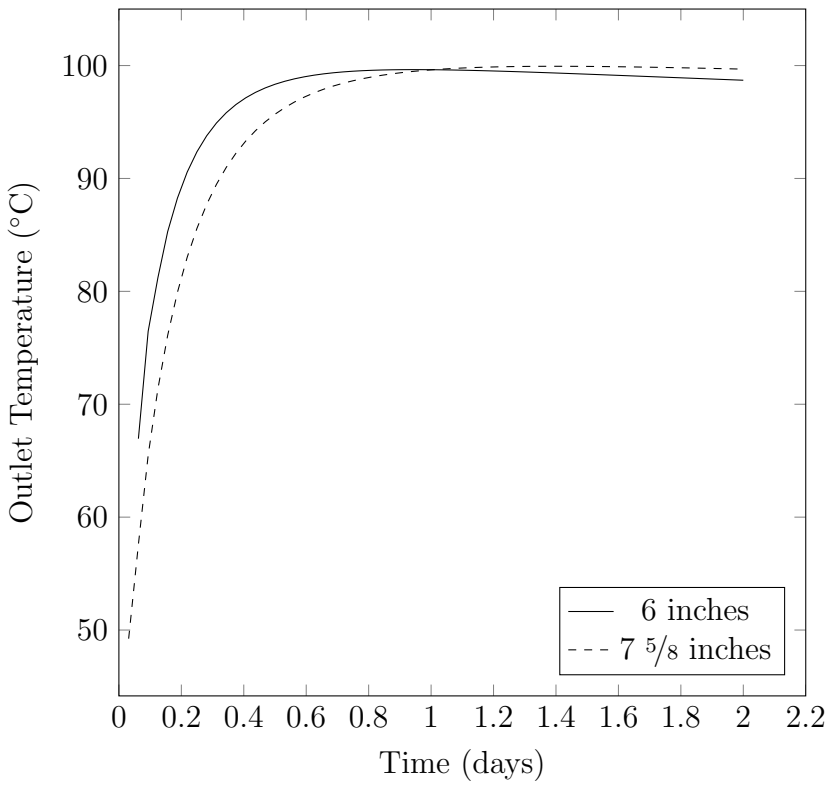

Figure 4.20: Fluid outlet temperatures for different diameters over 2 days of continuous operation

The results demonstrate that a larger diameter well produces higher outlet temperatures and thus has higher power production. Therefore, larger diameters should be favoured during the well selection process.

4.7 The Effect of Insulation

As shown in Figure 4.3, the fluid temperature begins to decrease as it travels up the exit well. This cooling can be attributed to the natural decrease in ground temperature with decreasing depth associated with the geothermal gradient. One

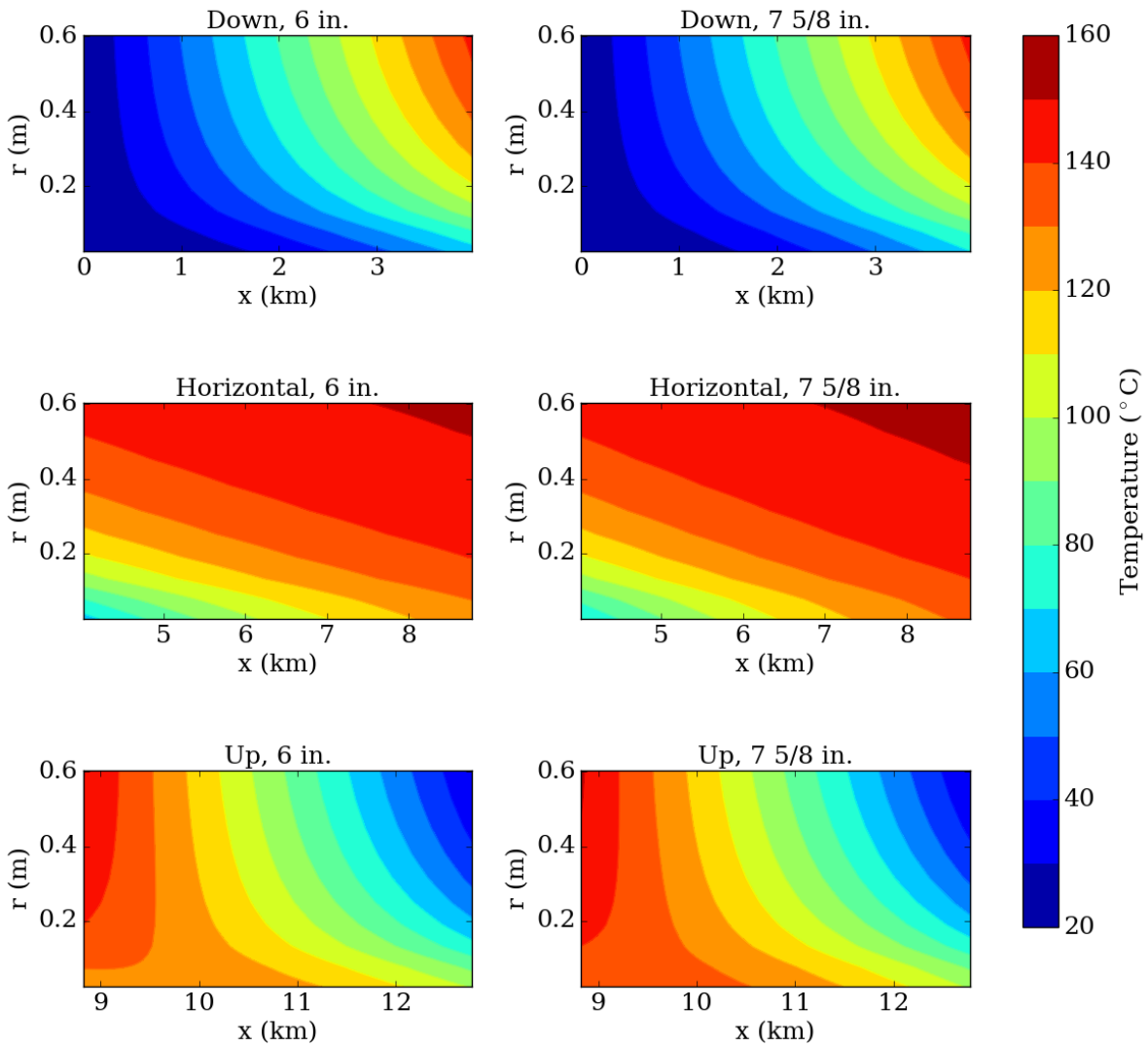

Figure 4.21: Contour plots of ground temperature near the wall in the downward, horizontal, and upward sections after 1 day of continuous operation. r denotes distance from the well

possible solution that would mitigate the loss of heat from the fluid is the addition of insulation.

To establish the length of insulation to be added, 10- and 20-year base case simulations were analyzed. The depth at which insulation is needed can be determined by identifying the location at which the fluid temperature becomes greater than the ground temperature. Since the problem is transient, this location will change. At 10 years, the fluid exceeds the ground temperature at the cell located 1775 m deep. After 20 years, this has shifted to the cell centred at 1725 m. To limit heat loss at early times, the insulation was chosen to extend to the 1775 m cell, giving a total insulation depth of 1800 m.

Figure 4.22 shows the fluid temperature in the upward well with various levels of insulation. Where perfect insulation is indicated, there is no heat transfer between the fluid and the ground over the length of the insulation. As such, the fluid exits at its maximal temperature. The remainder of cases denote varying thicknesses of insulation, from uninsulated to 3 cm thick insulation. The conductivity of the insulation was chosen to be that of cellular glass, which has a conductivity of 0.058 W/mK at 93°C [54]. This will provide a conservative estimate of the benefit of adding insulation. The insulation was represented in the model with an effective heat transfer coefficient which incorporated the resistance of the fluid and the insulation. The effective heat transfer coefficient was defined as:

$$h_{eff} = \frac{1}{\frac{1}{h_{insul}} + Res_{insul}} \tag{4.3}$$

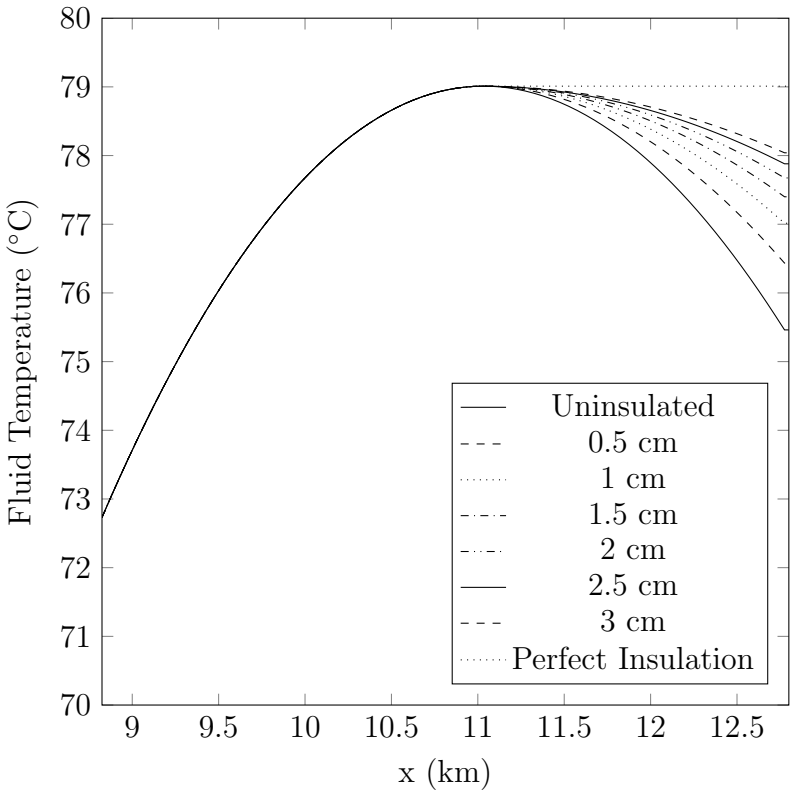

Figure 4.22: Fluid temperature in the upward well with various insulation thicknesses after 20 years continuous operation

with Res_{insul}, the thermal resistance due to the insulation, defined as:

$$Res_{insul} = \frac{\ln\left(R_{well}/\left(R_{well} - L_{insul}\right)\right) R_{well}}{k_{insul}} \tag{4.4}$$

where h_{insul} is the heat transfer coefficient, which takes into account the reduction in area due to the addition of insulation, R_{well} is the radius of the well, L_{insul} is the insulation thickness, and k_{insul} is the conductivity of the insulation.

Figure 4.22 shows that, aside from the uninsulated case, the case with the smallest thickness of insulation, 0.5 cm, corresponds to the lowest outlet temperature. From

the results, one can also observe that the outlet temperature will improve with increased insulation size. Increasing the insulation thickness by the same amount, however, does not improve the outlet temperature by a proportional increment. Raising the insulation thickness from 0.5 cm to 1.0 cm causes the temperature to rise from 76.4°C to 77.0°C, a 0.6°C increase. In comparison, changing the insulation thickness from 2.5 cm to 3.0 cm only raises the temperature by 0.1°C.

The impact of adding insulation can also be observed from the heat flux from the ground to the fluid, seen in Figure 4.23. As greater thicknesses of insulation are added to the pipe wall, the heat flux between the ground and the fluid decreases. One can observe a diminishing reduction of the absolute value of the heat flux with each successive increment of insulation thickness. In the case of perfect insulation, the heat flux is zero. It can be noted that the heat flux in the insulated cases is slightly below that of the uninsulated case at one cell, where the bottom of the insulation is located (at approximately 11 km). This is due to extraneous insulation, placed where the fluid would still be cooler than the ground. This can be avoided by choosing the optimal insulation depth for a desired time frame.

The diminishing improvement from adding insulation can be explained by analyzing the heat transfer rate. In the insulated section, an increase in heat transfer will result in a decrease in the outlet temperature, since more heat will be lost from the fluid to the ground. The heat transfer rate is defined as:

$$Q = h_{eff} P L \left(T_{wall} - T_{fluid}\right) \tag{4.5}$$

and P is the perimeter, defined as πD. If the insulation thickness is successively

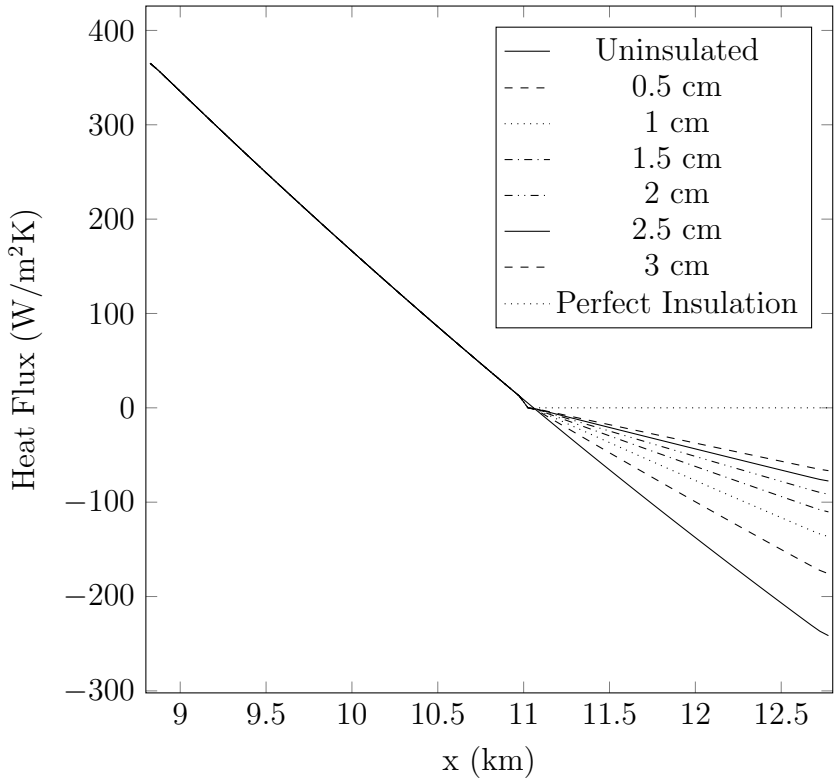

Figure 4.23: Heat flux from the ground to the fluid in the upward well with various insulation thicknesses after 20 years continuous operation

increased with equal increments, D will decrease proportionally. Therefore, the decrease in perimeter is not responsible for the diminishing improvements from the added insulation. Instead, it is the heat transfer coefficient that is responsible for the observed effect. As defined in equation 4.3, h_{eff} is dominated by the Res_{insul} term, which is much greater than $\frac{1}{h_{insul}}$. This is shown in Table 4.2. The heat transfer coefficient for the uninsulated pipe was computed using the Dittus-Boelter relationship for warming, where $n = 0.4$, defined in Equation 3.3. For the insulated pipe, the relationship for cooling fluid where $n = 0.3$ was used. As such, the change in h_{eff} is dictated by the change in Res_{insul}. Since Res_{insul} is defined in terms of a logarithm, $\ln\left(R_{well}/\left(R_{well} - L_{insul}\right)\right)$, the increase in Res_{insul} will always be less as L_{insul} gets

Table 4.2: Heat transfer coefficients and insulation resistance value for a pipe with 2 cm thick insulation

Feature	Heat Trans. Coeff.	Resistance Value
Uninsulated pipe, fluid warming ($n = 0.4$)	1454.5 (W/mK)	6.9×10^{-4} (mK/W)
Insulated pipe, fluid cooling ($n = 0.3$)	1976.9 (W/mK)	5.1×10^{-4} (mK/W)
Insulation		0.39 (mK/W)

larger. The physical reason for this is that as the insulation thickness is increased, the additional material will be added to the inner radius. With each increment of insulation thickness, the surface area that the insulation covers on the inner diameter will get smaller. As a result, the newest addition of insulation will always be less valuable for reducing heat losses than the previous one.

This effect is emphasized in Figure 4.24, which shows the outlet temperature plotted over the duration of operation for various insulation conditions. One can clearly see that increasing the insulation thickness by equal increments provides diminishing returns. Furthermore, one can observe that the perfect insulation case provides little improvement over the highest thickness simulated. The perfectly insulated case produces an outlet temperature of 79.0°C after 20 years, while the case with 3 cm of insulation has an outlet temperature of 78.0°C.

Adding insulation improves the final power output. The Carnot cycle power of the 3 cm case after 20 years is 358 kW, 8% greater than the base case. Assuming a 10% efficient power cycle, the system will produce roughly 215 kW.

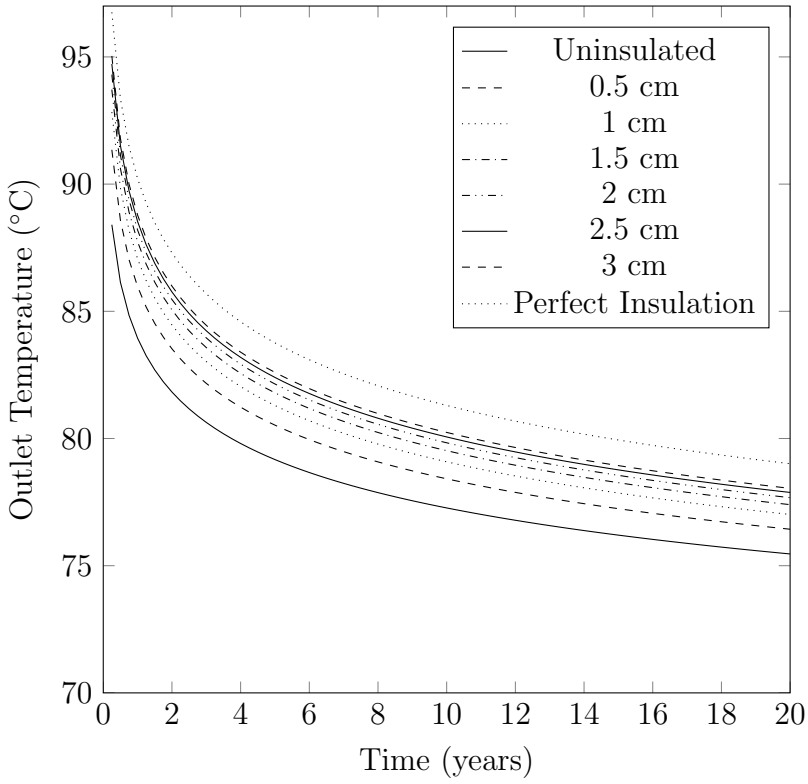

Figure 4.24: Fluid outlet temperature over 20 years of continuous operation with varying insulation thicknesses

4.8 The Effects of Intermittent Heat Extraction

One potential benefit of geothermal power generation is that it could be switched on whenever it is needed. As a result it may be worthwhile to explore geothermal as a solution to peak power production. To address peak demand, the system would be operated for short windows of time. In Ontario, peak hours are 11 am to 5 pm in the summer [55]. When demand for electricity is not high, the system could be turned off.

To investigate the possibility of intermittent operation, simulations were performed where the flow was periodically turned off. To approximate a stagnant fluid in

the model, the velocity of the fluid was set to zero and the Nusselt number was set to 1. Further analysis on the choice of Nusselt number can be found in Appendix B. For ease of modelling, the time step was reduced to one half hour (1800 s). Simulations modelled a case where the flow was turned on for 6 hours a day, representing the summer peak demand hours.

Initial simulations were based off the base case geometry with intermittent flow. The outlet temperature over a six-hour "on" cycle at different times in a 20-year simulation can be seen in Figure 4.25. The plot shows the outlet temperatures of the system while the fluid is flowing (six hours of the day). During the first cycle, which occurs on the first day, the fluid outlet temperature increases significantly, as fluid from deep in the well travels to the surface. Following peak hours, the fluid is stopped. While the flow is stopped, the fluid temperature in the upper portion of the upward well decreases, as heat dissipates outwards into the ground. As a result, the outlet temperature of the following "on" cycle starts much lower than at the end of the previous cycle. Consequently, the outlet temperatures are consistently lower than 80°C for a portion of the peak demand cycle. Outlet temperatures lower than 80°C may not be hot enough to produce electricity through some Organic Rankine cycles and will not allow for efficient production of electricity.

Examining the outlet temperatures after one year of operation, also shown in Figure 4.25, it is clear that the low outlet temperatures are not limited to the start-up phase. While the outlet temperatures are higher at later times, there are still portions of the "on" cycle where the outlet temperature is below 80°C. After 10 and 20 years, the outlet temperatures are only slightly above 80°C at the start of a cycle. With outlet temperatures below 80°C, electricity cannot be efficiently produced for

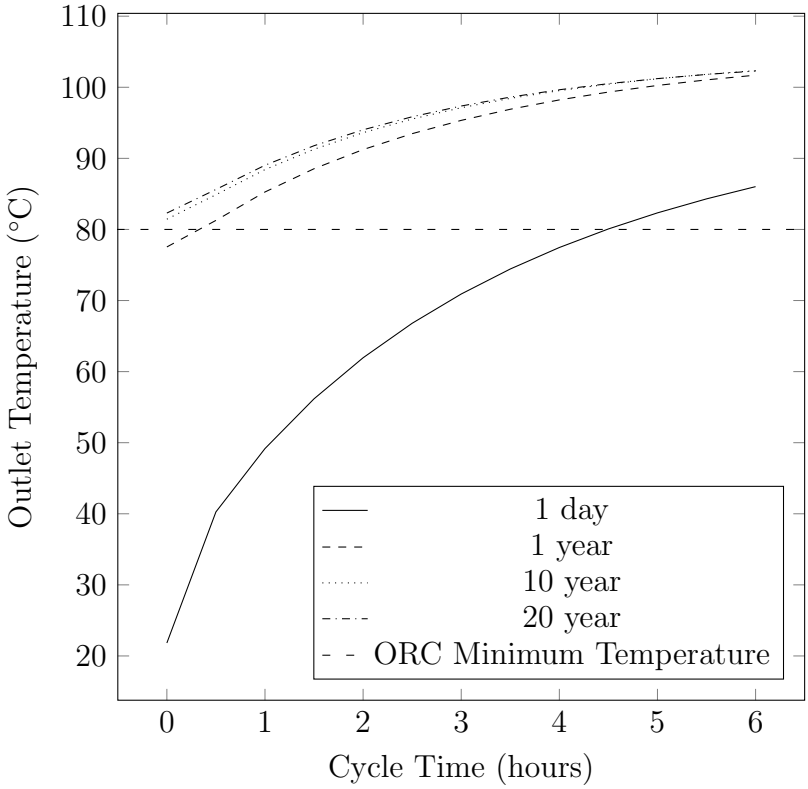

Figure 4.25: Fluid outlet temperature over six hour "on" cycles during intermittent operation, summer peak hours (11am - 5pm)

the entirety of the "on" cycle. This suggests that intermittent operation may not be viable for power production unless changes are made to the system.

Since the stagnant fluid loses heat at the top of the upward leg, a simulation was performed with insulation added to the upward well in the configuration discussed in Section 4.7. The results of the simulation showed that the addition of 2 cm of insulation significantly improved the outlet temperatures of the system. This can be seen in Figure 4.26. While without insulation, the outlet temperatures exceeded the minimum threshold for only part of the "on" cycle, with insulation, the outlet temperatures consistently exceed 80°C after the completion of the first cycle. This

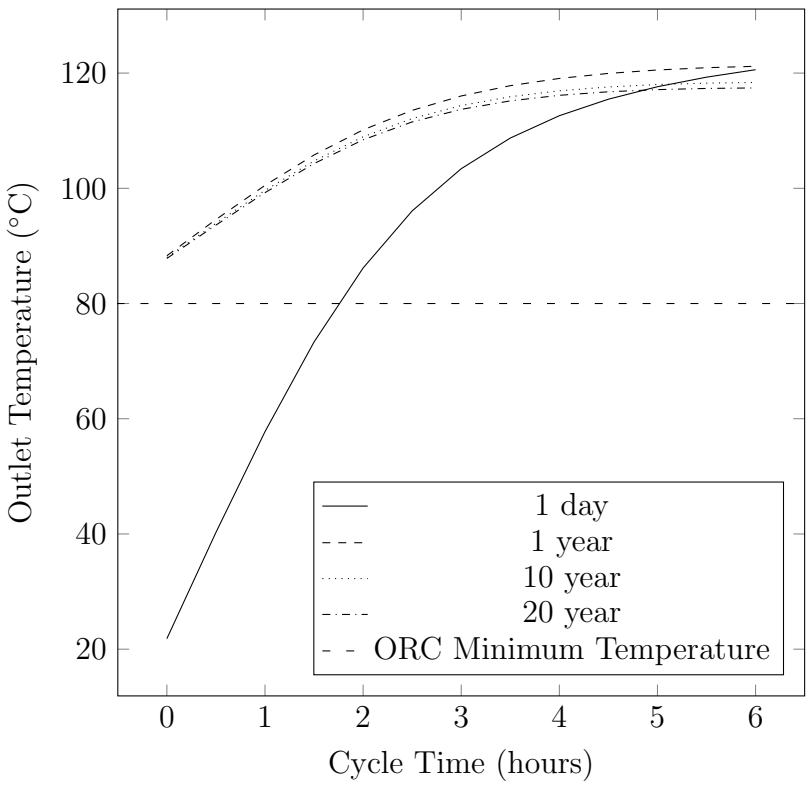

Figure 4.26: Fluid outlet temperature over six hour "on" cycles during intermittent operation, summer peak hours (11am - 5pm) with 2 cm insulation in the upper portion of the upward well

indicates that the intermittent use can be made viable with the addition of insulation to the upward well.

The impact of intermittent operation with insulation on the ground temperatures in the upward well can be seen in Figures 4.27 and 4.28. These figures show the temperatures at 3000 m and 1000 m deep in the upward well section, respectively, after 10 years of intermittent operation. Figure 4.27 shows the ground temperatures at 3000 m deep, where the fluid is still cooler than the ground. After the fluid has been stationary for 18 hours, the wall temperature in the region very close to the well has cooled off, as shown in the inset figure. After the following six hours, where

the fluid was flowing again, warmer fluid from the horizontal well has warmed up the ground immediately surrounding the well, resulting in the warmer wall temperature, particularly visible in the inset plot. The difference in the wall temperature between on and off cycles is approximately 2.3°C. The inset also shows that the radial temperature profiles also converge after 0.6 m. Beyond this point, the ground temperature remains unchanged by the cycling of the flow. The main plot shows that the ground temperature remains unchanged by the heat transfer beyond approximately 100 m away from the wall.

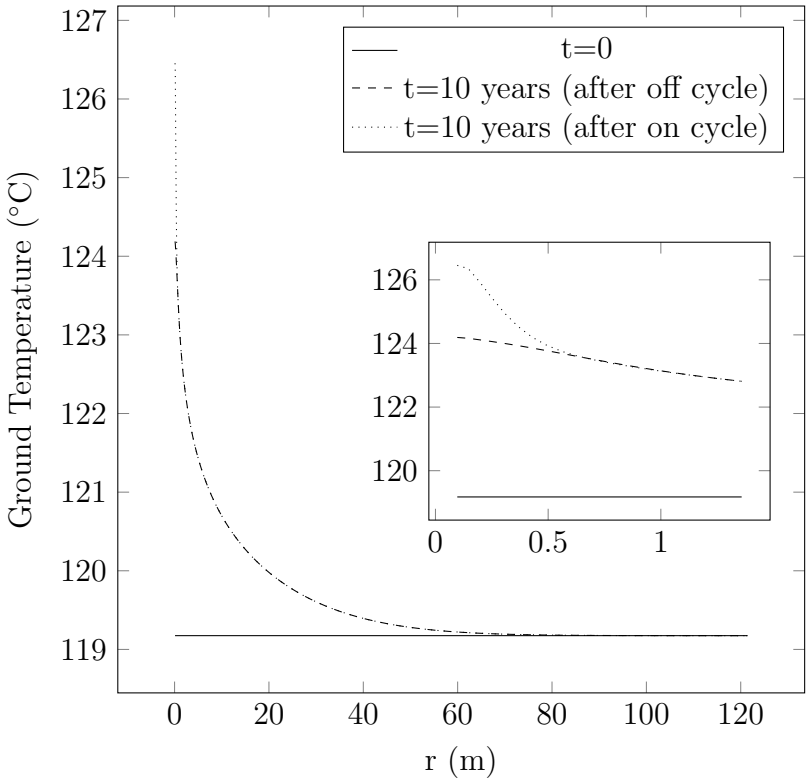

Figure 4.27: Radial temperature profile in the ground, 3000 m deep in the upward well section after 10 years with detail view, inset

Figure 4.28 shows the ground temperature at 1000 m deep around the upward well. As with the temperature profiles 3000 m deep, cycling of the fluid flow impacts

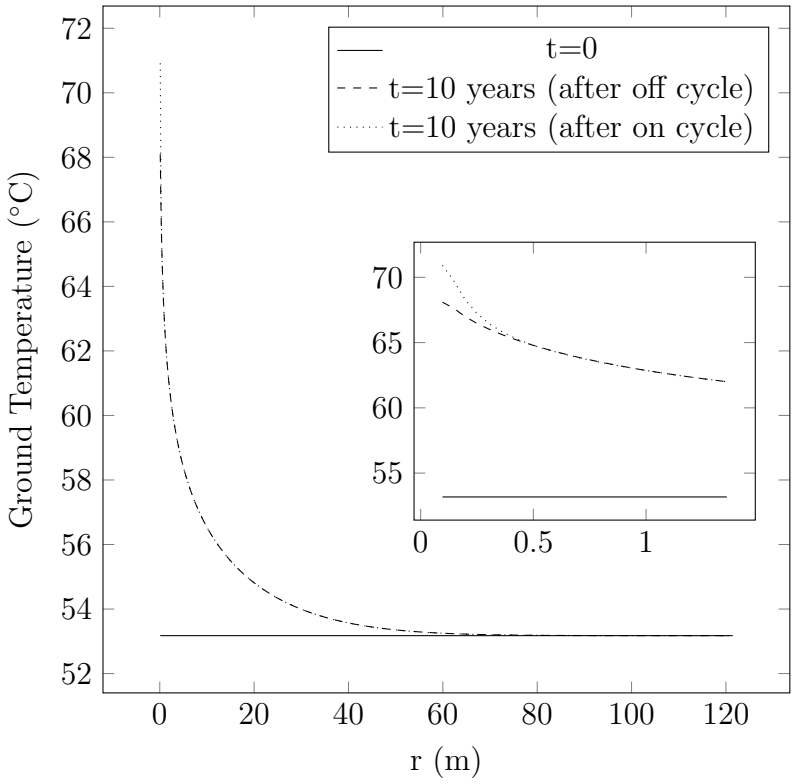

Figure 4.28: Radial temperature profile in the ground, 1000 m deep in the upward well section after 10 years with detail view, inset

the ground temperature in the region very near the wall. After the "on" cycle, the wall temperature is 2.8°C higher than it was after the previous "off" cycle. Beyond 0.5 m, the ground temperature is unaffected by the intermittent flow, and beyond approximately 105 m, the ground is unaffected by any heat transfer to the well. The plot shows that some warming of the top half of the ground occurs even with the presence of insulation.

One potential issue associated with running the system intermittently is that it might take considerable energy and time to bring the large volume of fluid in the well to the desired flow rate, once the pump is started. To quantify this, the unsteady Bernoulli equation was solved. This can be derived from the Euler equation

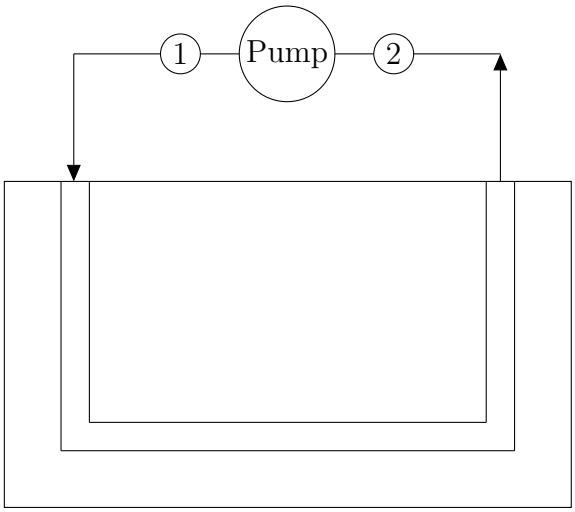

Figure 4.29: System layout for Bernoulli equation derivation

of momentum for inviscid, incompressible flow along the direction of a streamline, s [46]:

$$\frac{\partial v_s}{\partial t} + v_s \frac{\partial v_s}{\partial s} = -\frac{1}{\rho}\frac{\partial p}{\partial s} - g\frac{\partial z}{\partial s} \tag{4.6}$$

where v_s is the velocity along the streamline, p is the pressure, ρ is the fluid density, g is acceleration due to gravity, and the z coordinate is the height. Integrating along the streamline from points (1) to (2), shown in Figure 4.29 and incorporating a head loss term, h_l, to account for the pressure losses gives the following unsteady Bernoulli equation:

$$\frac{p_1}{\rho} + \frac{v_1^2}{2} = \frac{p_2}{\rho} + \frac{v_2^2}{2} + h_l + L\frac{dv}{dt} \tag{4.7}$$

where p is the pressure of the fluid at a given point, L is the total length of the piping (the sum of the well lengths, plus 500 m external piping), and v is the velocity of the flow.

From Figure 4.29, the body force term can be eliminated, since the points are at

an equal height. Using the assumption that the area of the pipe remains constant, the velocity terms will also cancel out. Rearranging and expanding the head loss term gives the ordinary differential equation:

$$\frac{dv}{dt} = \frac{1}{L}\left\{\frac{\Delta p}{\rho} - f\frac{L}{D}\frac{v^2}{2}\right\} \tag{4.8}$$

where f is the Darcy friction factor and D is the pipe diameter.

Solving this with a fourth-order Runge-Kutta scheme gives the solution pictured in Figure 4.30. The plot shows that the time for the fluid to reach the desired flow rate is short; it takes approximately 1.2 minutes for the fluid to go from 0 kg/s to 99% of 9 kg/s, assuming the pump runs at full speed immediately after being switched on. This means that the additional energy required to bring the fluid to the correct velocity is small in comparison to the energy used during the operational period, since start up represents about 0.3% of the runtime.

Conversely, when the pump is stopped, it will take longer for the flow to slow down. Figure 4.31 shows that the flow has slowed down significantly after one hour, and continues to decrease in velocity afterwards. Considering that the "off" cycle takes 18 hours, a one hour time scale for the fluid to slow down is reasonable for the purposes of these intermittent simulations.

The fluid outlet temperatures at the end of one year of operation with insulation are shown in Figure 4.26. The outlet temperatures are significantly higher than those of the uninsulated case. Furthermore, the outlet temperatures are also higher than the continuously operating case. After a one-year simulation of continuous operation with 2 cm thick insulation, the fluid outlet temperature was 88°C. In comparison, the outlet temperature over an intermittent cycle ranges from 88°C to 121°C, with an

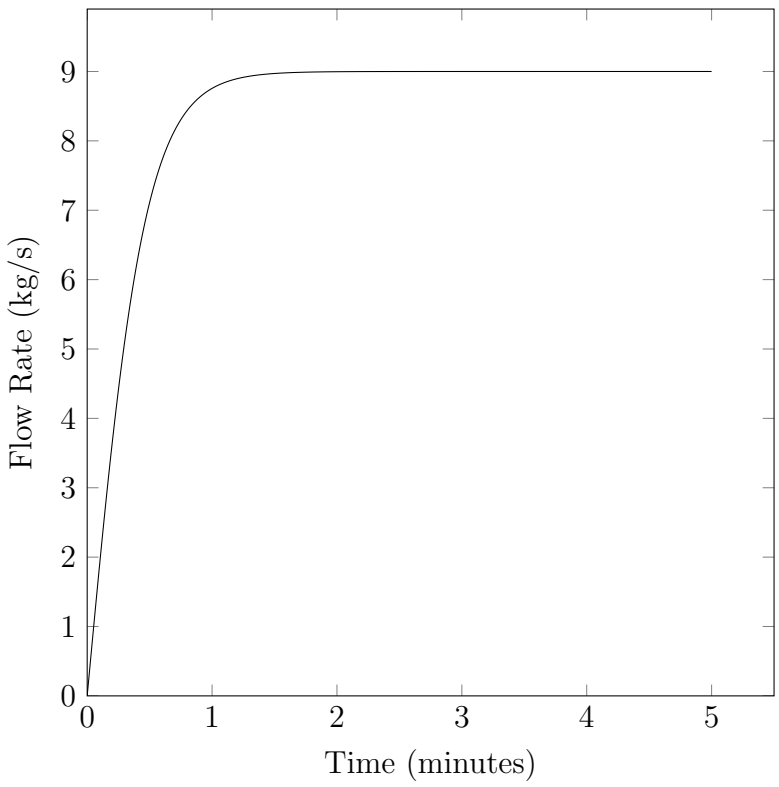

Figure 4.30: Time to bring fluid from stagnant to desired flow rate of 9 kg/s

average of 104.5°C. This average temperature would produce a Carnot cycle power of 714 kW, which represents a 66% improvement over the continuous case after one year.

After 20 years of operation, the fluid outlet temperatures remain high, as is shown in Figure 4.26. Both the maximal and minimal outlet temperature values are well above 80°C. The Carnot cycle power, determined from the average outlet temperature over a cycle, is 683 kW. With a 10% efficient Organic Rankine cycle, this would correspond to 310 kW of power. This confirms the longevity of an intermittently operated, insulated system.

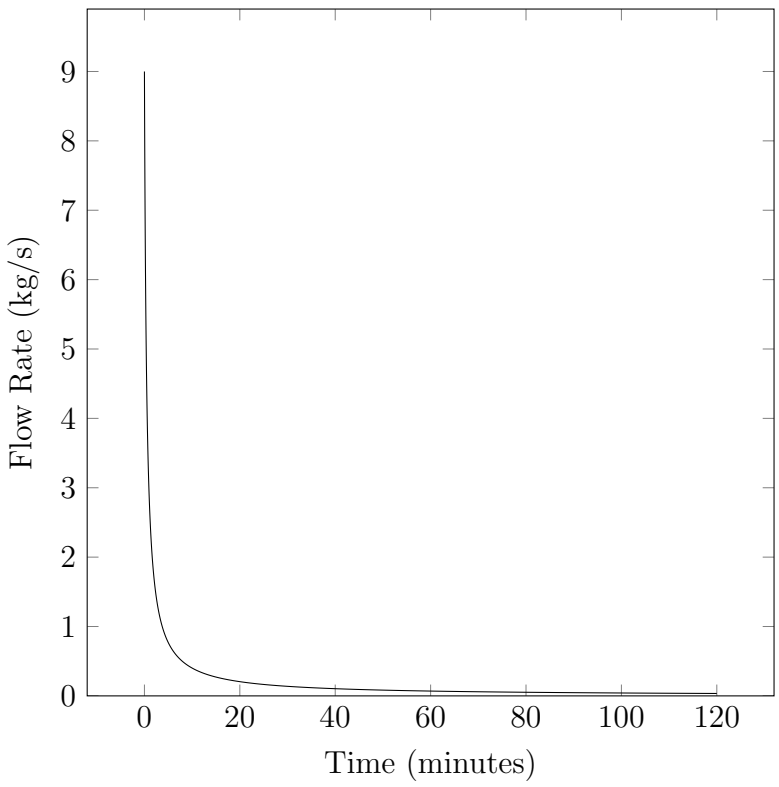

Figure 4.31: Time to bring fluid from 9 kg/s to stagnant

4.9 Discussion

The results of this study clearly establish that modelling and designing for a well for the purposes of geothermal electricity production is a complex, multivariable problem. Developing a successful geothermal project requires balancing and optimizing for a multitude of parameters. However, there are some general points that can be made on the subject. The variables affecting performance can be divided in to two main categories: those that impact well selection and those that impact operation.

4.9.1 Considerations for Well Selection

There are three properties of a well that will direct selection: diameter, depth, and geothermal gradient. This study focussed on the impact of diameter. It was discovered that decreasing the well diameter had a detrimental effect on the outlet temperature and power production. This was a result of initial high heat transfer rates in the small diameter well, which depleted the thermal energy in the near wall region of the ground, causing lower fluid temperatures in the long term. A decrease in diameter of 1.625 inches resulted in a small decrease in Carnot cycle power of approximately 5%. While diameter cannot be easily changed, there is some variation in well sizing in the oil and gas industry so this may be a factor in decision-making. In addition, the well depth will factor heavily into selecting a well. While this was not investigated in this thesis, the literature demonstrated a clear relationship between increased depth and increased power output due to higher well bottom temperatures. Further, a well should be chosen to maximize geothermal gradient, as the results in Section 4.5 demonstrate that a high gradient will significantly improve results.

While the inlet temperature can be controlled to some degree, the results show that that minimizing the inlet temperature provides the best results for electricity production. This variable, however, is constrained by ambient conditions, which dictate the temperature of atmospheric cooling. While this research employed the assumption that the inlet temperature was constant, it will in fact be determined by the climate of the well location. As a result, locations with a high ambient temperatures for a portion or the entirety of the year will be at a disadvantage for electricity production. As such, the inlet temperature and weather conditions should be factored into the selection of a well and any predictions of a system's performance.

An additional consideration that should be made during selection is the spacing between the two vertical wells. The results show that after 50 years, the ground has been disturbed out to approximately 100 m. Should the selected wells be closer together, thermal interference could diminish performance and limit the longevity of the system. A study to optimize the flow rate should be undertaken before selecting wells that have the potential to interfere. In addition, the option of reducing the diameter by employing smaller tubing and grout should be explored to determine if it may reduce the radius over which the ground is thermally affected.

4.9.2 Design Considerations for Operation

The considerations for the operation of the system centre around factors that can be changed with some ease. The results clearly show that changing the operating conditions of the system can have a profound effect on the output of the system. Furthermore, the optimal conditions must be tailored to the geometry and initial conditions of a given well.

Optimization was shown to be necessary in Section 4.3, which explored the effect of changing the flow rate. For the geometry investigated in this study, it was shown that the optimal flow rate was approximately 9 kg/s. It was also shown that this has a tendency to shift lower with time, since the higher flow rate cases depleted the heat in the ground faster. This effect was small, however, with the optimal flow rate dropping to between 8 kg/s and 9 kg/s over the course of 20 years. The results showed a more dramatic decrease in power output when flow rate was dropped, as it reduced the amount of heat that could be extracted by the power cycle without adequately improving the outlet temperature. For any change in geometry, initial conditions, or

material properties, it will be necessary to determine the optimal flow rate for those specific conditions.

The possibility of adding insulation was also explored in this research. The findings show that adding insulation over the portion of the well that is cooler than the fluid will improve outlet temperatures. Determining the point at which the ground is cooler than the fluid required simulations and was found to change with time. It would likely be necessary to perform simulations on a system to determine the correct insulation depth for the given well conditions and desired longevity. Further, it may not be necessary to insulate as far as the depth where the fluid is hotter than the ground. A study of what is economically optimal, balancing the cost of insulation with the energy loss would be valuable. It was also found that increasing the thickness of the insulation provided diminishing returns, since any additional insulation would be added to an increasingly small surface area on the inner radius. This effect was found to be more significant than the resulting increase in flow velocity due to the reduction in area caused by adding thicker insulation.

This research also explored the idea of using the system intermittently. A major challenge associated with electricity production is addressing peak demand. Therefore, it would be significantly beneficial to provide a means to meet this need. The simulations performed demonstrated that intermittent operation is not viable in the base case configuration. Without constant heating of the upward well, the heat from the fluid in that well will dissipate outwards. This will cause a decrease in the outlet temperature, resulting in a drop below power production thresholds. By adding insulation, however, heat losses to the upper part of the exit well can be reduced. This resulted in outlet temperatures averaging 104.5°C after one year, considerably higher

than the continuously operated outlet temperature of 88°C. Consideration must be given to the amount of time that the fluid will take to be brought from stagnant to the desired flow rate and the time for the fluid to slow down again. If, for the given conditions, the slow down and start up times are a significant fraction of the "on" and "off" cycles, this will impact the system performance and the pump power requirements. It should be considered when carrying out modelling for the design of the intermittent system. The transit time for the fluid to travel from the bottom of the upward well to the exit should also be considered. If the "on" cycle is less than this transit time, the hottest fluid will not be available to the power cycle. Running the insulated system intermittently improved the Carnot cycle power by 66% compared to the case where the system was run continuously. A proportional increase in the real power production would amount to an output of 344 kW.

4.9.3 Cost Analysis

While a complete financial analysis is beyond the scope of this project, it is useful to examine the potential revenue of the system. Assuming a power cycle efficiency of 10%, the power output of the base case is 214 kW at 10 years of operation. If the electricity could be sold for 15 cents per kilowatt hour, a rough estimate, the resulting annual income would be $281,000. This would drop with time, reaching $261,000 by 50 years of operation. The base case represents the case with the optimal flow rate at 10 years. The results of the simulations can be used to quantify the benefit of changing the parameters explored in this research. Locating the system in an area with a geothermal gradient one standard deviation higher than average would improve the Carnot cycle power by 57%. Therefore, a proportional increase in real power

production would result in an increase in income of $160,000 at 10 years. Operating using a well 1.625 inches smaller than the base case would decrease Carnot power production to 313 kW, reducing income to $267,000. Adding 3 cm of insulation to a depth of 1800 m would provide a modest benefit, increasing Carnot power by 8% and income to $304,000. Running the system intermittently improves efficiency but reduces runtime; however, electricity during peak periods commands a higher value. Therefore, assuming that peak demand electricity is worth 25 cents, and knowing that running the system for six hours a day improves the Carnot cycle power by 66%, the income earned by the system would be $195,000. Therefore, running the system for a third of the day still creates earnings of roughly 69% of the continuous system. This also provides the benefit of limiting wear on the machinery, reducing maintenance costs and extending the lifespan of the system.

4.10 Summary

Simulations were performed to determine the temperature of the fluid flowing through a system of connected wells. These results were used to make predictions of power production, using a theoretical Carnot cycle power for the purposes of comparison and an Organic Rankine cycle efficiency from the literature for a more realistic estimate. A base case was established with a diameter of 7 5/8 inches, and a geothermal gradient was assigned based on the average for the region surrounding the Haynesville shale play. The vertical wells had a depth of 4000 m, and the flow conditions included a flow rate of 9 kg/s and an inlet temperature of 20°C. The simulations predicted an outlet temperature of 75.5°C after 20 years, which is lower than the desired outlet temperature of 80°C. Varying the flow rate demonstrated that the Carnot cycle power

must be optimized to balance the effects of the outlet temperature on efficiency and the flow rate on heat extraction. By varying the inlet temperature, it was established that the inlet temperature should be minimized to produce the largest rate of power. However, this will be complicated by ambient conditions, which will determine the temperature for cooling in the power cycle. The testing showed that increasing the geothermal gradient improves power production, as would be expected, suggesting that it would be advantageous to select a well in an area with a high geothermal gradient. The impact of diameter was investigated to determine that decreasing the well diameter is detrimental to the power production of the system. It was found that adding insulation to the top half of the upward well provides a modest improvement to power production, although increasing the insulation thickness provides diminishing returns. This was found to be related to the decrease in inner surface area as the insulation thickness was increased. And while adding insulation did not considerably benefit power production in the cases where flow was continuous, it was necessary to make intermittent operation viable. Simulations demonstrated that cooling in the top of the upward well reduced the outlet temperatures and thus the efficiency of the system when the fluid was left stagnant. Therefore adding insulation prevented this cooling, creating significant improvements to the outlet temperature when the system was run for 6 hours each day. Intermittent operation was shown to provide high outlet temperatures and, therefore, better efficiencies, when paired with insulation, compared to the base case.

Chapter 5

Conclusions and Recommendations

5.1 Conclusions

The goal of this research was to explore the feasibility of converting spent oil and gas wells for the purposes of geothermal power generation. A novel approach of connecting two directionally drilled wells to create a continuous loop was proposed that would eliminate some of the drawbacks associated with the tube-in-tube approaches previously suggested. CFD simulations were carried out to understand the heat transfer behaviour inside the wells, which allowed for predictions to be made about the power production of such a system.

The model developed consisted of two coupled domains: the 2D cylindrical domain representing the ground, and the 1D fluid, flowing through the centre of the solid domain. The modelling employed the assumption that the three perpendicular wells could be straightened to create one long pipe, rather than a 3D well configuration. The fluid and solid domains were coupled using a convection heat transfer boundary condition. The simulations determined the temperatures throughout the fluid and

solid domains. Approaches to predicting power production were developed using the outlet temperatures of the system. A theoretical maximum Carnot cycle power was used for the purposes of comparison, while an Organic Rankine cycle efficiency was used for more a more realistic estimation of power.

A base case was established with a depth of 4000 m and a diameter of 7 5/8 inches. With an inlet temperature of 20°C and a flow rate of 9 kg/s, the simulations predicted that the outlet temperature would be 75.5°C after 20 years of continuous operation. The literature suggests that the source temperature for an Organic Rankine cycle must be at least 70°C to 80°C. Therefore the outlet temperature of the fluid in the base case may meet the minimum threshold for certain organic working fluids; however, to ensure viability and efficiency the outlet temperature should be higher. To ensure the outlet temperature of the system is high enough, several parameters discussed in this thesis can be optimized.

Parametric studies were performed to understand the effect of inlet temperature and flow rate. The results suggested that minimizing the inlet temperature will produce the best power output; however, the inlet temperature will be limited by the ambient cooling temperature of the power cycle. It was found that the flow rate can be optimized. For the base case, the optimal flow rate was approximately 9 kg/s, although this shifted slightly lower as time progressed. Customizing these parameters for the conditions of a given well will ensure that the system performs to its maximum potential.

The simulations exploring the impact of the geothermal gradient demonstrated that it can have a significant effect on power production. Testing was performed using the average gradient and one standard deviation above and below that in the

area surrounding the Haynesville shale play. It was found that increasing the geothermal gradient by one standard deviation could improve Carnot cycle power by 57%. Therefore, it is crucial to consider the geothermal gradient when selecting a well.

Diameter was also studied to determine its effect on power generation. It was found that decreasing diameter decreased the power production to a small extent. A 1.625 inch decrease in diameter from the base case dimension was found to reduce Carnot cycle power by 5%. Therefore, if possible, it is beneficial to select a well with a larger diameter.

One measure to increase production after well selection is the addition of insulation. Adding insulation to the top half of the upward well, where the ground is cooler than the fluid, improves outlet temperatures by reducing heat losses in that segment of the system. It was found that adding 3 cm of insulation to a portion of the upward well improved power production by 8%. It was also found that increasing the thickness of insulation provided diminishing returns, since the inner radius surface area decreased. The improvement to production from adding insulation was modest in comparison to changing parameters associated with well selection. The cost of adding insulation would have to be compared to the benefit of increasing the power output to determine whether it is worth installing insulation to such a depth.

While adding insulation to a continuously operating system provided a small benefit, it was found to be essential to the viability of an intermittent system. Initial simulations of intermittent use without insulation were performed, where the fluid was left stagnant during off-peak hours. The findings showed that when the fluid was stagnant, cooling in the upward well lowered the fluid temperature such that when flow was started, the outlet temperatures were below the ideal threshold for power

production. Simulations with insulation added showed significant improvements to the outlet temperature. Temperatures were found to be greater than both the uninsulated intermittent case and the insulated continuous case. Indeed, the Carnot cycle power for the insulated intermittent case was 66% higher than that of the base case, making this a viable option for peak power production.

5.2 Suggestions for Future Work

Future investigations may consider expanding upon this work with the following recommendations.

The modelling employs the assumption that the ground is homogeneous, although this is not the case. A more detailed model could include and accurate layout of the rock layers. Comparing a model that uses detailed rock layer information against a model using homogeneous properties would confirm whether the detailed modelling is necessary. Furthermore, exploring the impact of varying ground composition, with either homogeneous ground properties or an accurate, layered lithology, could lead to improved well selection.

A full model of the power cycle would be helpful in generating power predictions. The methods applied in this thesis were useful for the purposes of prediction and approximation. Modelling the power cycle would advance predictions to give more accurate results.

Bibliography

[1] *World development indicators: electricity production, sources, and access*. The World Bank. [Online]. Available: http://wdi.worldbank.org/table/3.7

[2] O. Edenhofer, "King coal and the queen of subsidies," *Science*, vol. 349, no. 6254, pp. 1286–1287, 2015.

[3] *Total electricity net generation 2014*. U.S. Energy Information Agency. [Online]. Available: http://www.eia.gov/beta/international/data/browser/#/?pa=0000000000000000000000000000fvu&ug=8&tl_id=2-A&vs=INTL.2-12-AFRC-BKWH.A&vo=0&v=H&start=1980&end=2014

[4] J. McKenna, D. Blackwell, C. Moyes, and P. D. Patterson, "Geothermal electric power supply possible from Gulf Coast, Midcontinent oil field waters," *Oil & Gas Journal*, vol. 103, no. 33, pp. 34–40, 2005.

[5] A. Townsend-Small, T. W. Ferrara, D. R. Lyon, A. E. Fries, and B. K. Lamb, "Emissions of coalbed and natural gas methane from abandoned oil and gas wells in the United States," *Geophysical Research Letters*, vol. 43, no. 5, pp. 2283–2290, 2016.

[6] T. Johnson. (2016, June) *Bankrupt energy firms add to Alberta's abandoned*

well problems. Canadian Broadcasting Corporation. [Online]. Available: http://www.cbc.ca/news/canada/calgary/abandoned-oil-wells-in-alberta-1.3613068

[7] *Marcellus shale*. Cabot Oil & Gas Corporation. [Online]. Available: http://www.cabotog.com/operations/marcellus/

[8] E. Barbier, "Geothermal energy technology and current status: an overview," *Renewable and Sustainable Energy Reviews*, vol. 6, no. 1-2, pp. 3–65, 2002.

[9] M. Beerepoot, "Technology roadmap geothermal heat and power," International Energy Association, Tech. Rep., 2011. [Online]. Available: http://www.iea.org/publications/freepublications/publication/Geothermal_roadmap.pdf

[10] *Geothermal technologies compared*. GreenFire Energy Inc. [Online]. Available: http://www.greenfireenergy.com/geothermal-technologies-compared.html

[11] R. Potter, E. Robinson, and M. Smith, "Method of extracting heat from dry geothermal reservoirs," Jan. 22 1974, U.S. Patent 3,786,858.

[12] K. Breede, K. Dzebisashvili, X. Liu, and F. Gioia, "A systematic review of enhanced (or engineered) geothermal systems: past, present and future," *Geothermal Energy*, vol. 1, no. 1, 2013.

[13] M. J. Kaiser and Y. Yu, "Louisiana Haynesville shale-1: characteristics, production potential of Haynesville shale wells described," *Oil and Gas Journal*, 2011.

[14] R. Curtis and D. Dalrymple, "Just the cost of doing business," *World Oil*, vol. 225, no. 10, pp. 77–78, 2004.

[15] L. Johnson and D. L. Simon, "Electrical power from an oil production waste stream," in *Thirty-Fourth Workshop on Geothermal Reservoir Engineering*, Stanford, California, 2009.

[16] W. Gosnold, "Power generation from low to intermediate temperature resources," Tech. Rep., 2015. [Online]. Available: http://www.osti.gov/geothermal/servlets/purl/1186077

[17] (2016, May) *EERE success story—DOE-funded project is first permanent facility to co-produce electricity from geothermal resources at an oil and gas well.* U.S. Department of Energy. [Online]. Available: http://energy.gov/eere/success-stories/articles/eere-success-story-doe-funded-project-first-permanent-facility-co

[18] T. Kujawa, W. Nowak, and A. A. Stachel, "Utilization of existing deep geological wells for acquisitions of geothermal energy," *Energy*, vol. 31, no. 5, pp. 650–664, Apr. 2006.

[19] A. P. Davis and E. E. Michaelides, "Geothermal power production from abandoned oil wells," *Energy*, vol. 34, no. 7, pp. 866–872, Jul. 2009.

[20] X. Bu, W. Ma, and H. Li, "Geothermal energy production utilizing abandoned oil and gas wells," *Renewable Energy*, vol. 41, pp. 80–85, May 2012.

[21] X. Bu, W. Ma, and Y. Gong, "Electricity generation from abandoned oil and gas wells," *Energy Sources, Part A*, vol. 36, no. 9, pp. 999–1006, 2014.

[22] W. Cheng, T. Li, Y. Nian, and C. Wang, "Studies on geothermal power generation using abandoned oil wells," *Energy*, vol. 59, pp. 248–254, Sep. 2013.

[23] W. Cheng, T. Li, Y. Nian, and K. Xie, "Evaluation of working fluids for geothermal power generation from abandoned oil wells," *Applied Energy*, vol. 118, pp. 238–245, Apr. 2014.

[24] W. Cheng, T. Li, Y. Nian, and K. Xie, "An analysis of insulation of abandoned oil wells reused for geothermal power generation," *Energy Procedia*, vol. 61, pp. 607–610, 2014.

[25] Y. Noorollahi, M. Pourarshad, S. Jalilinasrabady, and H. Yousefi, "Numerical simulation of power production from abandoned oil wells in Ahwaz oil field in southern Iran," *Geothermics*, vol. 55, pp. 16–23, May 2015. [Online]. Available: http://www.sciencedirect.com/science/article/pii/S0375650515000127

[26] N. M. Wight and N. S. Bennett, "Geothermal energy from abandoned oil and gas wells using water in combination with a closed wellbore," *Applied Thermal Engineering*, vol. 89, pp. 908–915, 2015. [Online]. Available: http://www.sciencedirect.com/science/article/pii/S1359431115005840

[27] S. A. Ghoreishi-Madiseh, F. P. Hassani, and M. J. Al-Khawaja, "A novel technique for extraction of geothermal energy from abandoned oil wells," in *World Renewable Energy Forum*, 2012.

[28] J. D. Templeton, S. Ghoreishi-Madiseh, F. Hassani, and M. J. Al-Khawaja, "Abandoned petroleum wells as sustainable sources of geothermal energy," *Energy*, vol. 70, pp. 366–373, 2014. [Online]. Available: http://www.sciencedirect.com/science/article/pii/S0360544214004198

[29] S. K. Sanyal and S. J. Butler, "Geothermal power capacity from petroleum

wells–some case histories of assessment," in *World Geothermal Congress*, no. April, 2010. [Online]. Available: https://pangea.stanford.edu/ERE/db/IGAstandard/record_detail.php?id=6797

[30] Y. Noorollahi and R. Itoi, "Production capacity estimation by reservoir numerical simulation of northwest (NW) Sabalan geothermal field, Iran," *Energy*, vol. 36, no. 7, pp. 4552–4569, Jul. 2011.

[31] Y. Noorollahi, S. M. Bina, and H. Yousefi, "Simulation of power production from dry geothermal well using down-hole heat exchanger in Sabalan Field, Northwest Iran," *Natural Resources Research*, 2015.

[32] Y. Noorollahi, H. Yousefi, and M. Pourarshad, "Three dimensional modeling of heat extraction from abandoned oil well for application in sugarcane industry in Ahvaz–Southern Iran," in *World Geothermal Congress 2015*, April 2015, pp. 19–25.

[33] J. Tester, B. J. Anderson, A. S. Batchelor *et al.*, *The Future of Geothermal Energy—Impact of Enhanced Geothermal Systems (EGS) on the United States in the 21st Century*, 2006.

[34] T. S. Dyman and S. M. Condon, "Assessment of undiscovered conventional oil and gas resources: Upper Jurassic-Lower Cretaceous Cotton Valley group, Jurassic Smackover Interior Salt Basins Total Petroleum System, in the East Texas basin and Louisiana-Mississippi salt basins provinces," in *Petroleum Systems and Geologic Assessment of Undiscovered Oil and Gas, Cotton Valley Group and Travis Peak-Hosston Formations, East Texas Basin and Louisiana-Mississippi Salt Basins Provinces of the Northern Gulf Coast Region*, 2006.

[35] H. Ramey Jr., "Wellbore heat transmission," *Journal of Petroleum Technology,*, pp. 427–435, 1962.

[36] I. N. Alves, F. J. S. Alhanati, and O. Shoham, "A unified model for predicting flowing temperature distribution in wellbores and pipelines," *SPE Production Engineering*, vol. 7, no. 4, pp. 363–367, Nov 1992.

[37] Y. Çengel and A. J. Ghajar, *Heat and Mass Transfer: Fundamentals and Applications*, 4th ed. New York: McGraw-Hill Higher Education, 2011.

[38] V. S. Arpaci, *Conduction Heat Transfer*. Addison-Wesley, 1966.

[39] R. Courant, E. Isaacson, and M. Rees, "On the solution of nonlinear hyperbolic differential equations by finite differences," *Communications on Pure and Applied Mathematics*, vol. 5, no. 3, pp. 243–255, 1952.

[40] *GNU Fortran*. [Online]. Available: https://gcc.gnu.org/fortran/

[41] S. Patankar, *Numerical Heat Transfer and Fluid Flow*. CRC press, 1980.

[42] D. W. Peaceman and H. H. Rachford, "The numerical solution of parabolic and elliptic differential equations," *Journal of the Society for Industrial and Applied Mathematics*, vol. 3, no. 1, pp. 28–41, 1955. [Online]. Available: http://www.jstor.org/stable/2098834

[43] B. R. Hutchinson and G. D. Raithby, "A multigrid method based on the additive correction strategy," *Numerical Heat Transfer, Part A: Applications*, vol. 9, no. 5, pp. 511–537, 1986.

[44] J. A. Nunn, "Burial and thermal history of the Haynesville shale: Implications for overpressure, gas generation, and natural hydrofracture," *Gulf Coast Association of Geological Societies Journal*, vol. 1, pp. 81–96, 2012.

[45] Y. A. Çengel and M. A. Boles, *Thermodynamics: An Engineering Approach*, 7th ed. New York: McGraw-Hill, 2011.

[46] P. J. Pritchard, *Fox and McDonald's Introduction to Fluid Mechanics*, 8th ed. Wiley, 2011.

[47] H. S. Carslaw and J. C. Jaeger, *Conduction of Heat in Solids*. Oxford: Clarendon Press, 1959, 2nd ed., 1959.

[48] G. E. Manger, "Porosity and bulk density of sedimentary rocks," U.S. Atomic Energy Commission, Tech. Rep., 1963.

[49] L. Eppelbaum, I. Kutasov, and A. Pilchin, "Thermal Properties of Rocks and Density of Fluids," in *Applied Geothermics*. Springer, 2014, pp. 99–149.

[50] Z. Shengjun, W. Huaixin, and G. Tao, "Performance comparison and parametric optimization of subcritical Organic Rankine Cycle (ORC) and transcritical power cycle system for low-temperature geothermal power generation," *Applied Energy*, vol. 88, no. 8, pp. 2740–2754, Aug 2011. [Online]. Available: http://www.sciencedirect.com/science/article/pii/S0306261911001334

[51] E. Soldo and C. Alimonti, "From an oilfield to a geothermal one: use of a selection matrix to choose between two extraction technologies," *World Geothermal Congress 2015*, no. April, 2015.

[52] "400kW Geothermal Power Plant at Chena Hot Springs, Alaska," Chena Power LLC, Tech. Rep., 2007. [Online]. Available: http://www.akenergyauthority.org/Content/Programs/AEEE/Geothermal/Documents/PDF/FinRepChenaGeoPlant09.pdf

[53] L. A. Burke, S. A. Kinney, and T. B. Kola-Kehinde, "Digital archive of drilling mud weight pressures and wellbore temperatures from 49 regional cross sections of 967 well logs in Louisiana and Texas, onshore Gulf of Mexico basin," U.S. Geological Society, Tech. Rep., 2011.

[54] (2016, July) *FOAMGLAS ONE Insulation*. FOAMGLAS, Pittsburgh Corning. [Online]. Available: http://www.industry.foamglas.com/__/frontend/handler/document.php?id=1064&type=118

[55] (2016, Nov.) *Electricity prices*. Ontario Energy Board. [Online]. Available: http://www.ontarioenergyboard.ca/oeb/Consumers/Electricity/Electricity%20Prices#seasons

[56] J. Stewart, *Calculus Early Trancendentals*. Thompson Brooks/Cole, 2008.

Appendix A

Energy Contained in the Ground Surrounding Oil and Gas Wells

The area of the ground surrounding a well that is disturbed in order to provide 200 kW of power can be computed by examining the thermal energy contained in the ground. 200 kW of electricity over 20 years corresponds roughly to the base case in Chapter 4, where the flow rate is 9 kg/s and the outlet temperature is 75.5°C. In order to provide 200 kW of electricity, a heat extraction rate of 2 MW is required, assuming a power cycle efficiency of 10%. A heat extraction rate of 2 MW over 20 years results in a total of:

$$E = (2.0 \times 10^6)(6.3072 \times 10^8) = 1.26 \times 10^{15}\text{J} \tag{A.1}$$

Consider a well system of length 8,800 m, with an average temperature of 123°C. The length of 8,800 m is chosen since the results in Section 4.2 show that very little net heat transfer occurs in the upward section of the well system. Assume that the

affected radius is brought down to the fluid inlet temperature, 20°C. Therefore, the energy extracted will be a function of the initial average temperature minus the final temperature:

$$E = \rho V c_p(T_{initial,avg} - T_{f,in}) \tag{A.2}$$

Rearranging for the outer radius of the cylinder and solving gives a radius of 15 m. This is smaller than was observed in the results section because the calculation employs the assumption that the ground temperature is brought down to the fluid inlet temperature. In practice, the radius of disturbed ground is larger since it remains at a higher temperature, with temperature increasing as radius is increased.

Appendix B

Model Verification

B.1 Steady State Verification

The numerical model described in Chapter 3 was verified against analytical solutions. Since there is no suitable analytical solution for the coupled fluid-solid domain studied in this thesis, the component domains were verified separately.

B.1.1 Fluid Analytical Verification

The fluid model was checked against steady state analytical solutions for forced convection. In both cases studied, the wall temperature was constant with time.

The first case studied considered a 4000 m long pipe with a constant, uniform wall temperature. The fluid inlet temperature was 85°C and the wall temperature was 87°C. The analytical solution for this problem is:

$$T_f(x) = (T_{f,in} - T_{wall}) \exp\left(\frac{-hP}{\dot{m}c_{p,f}}x\right) + T_{wall} \tag{B.1}$$

Table B.1: Fluid and solid properties used for verification tests

Property	Value
h	1454.6 W/m^2 K
R_{inner}	0.0968375 m
$\dot{m}$	9 kg/s
$c_{p,f}$	4185 J/kgK
k_g	2.769 W/mK

where $T_{f,in}$ is the fluid inlet temperature, T_{wall} is the constant wall temperature, h is the heat transfer coefficient of the fluid, P is the perimeter of the pipe, $\dot{m}$ is the fluid flow rate, and $c_{p,f}$ is the fluid specific heat capacity. Table B.1 includes the fluid properties used in this verification test.

Figure B.1 indicates that the modelled temperature profile matches well with the analytical solution.

The second case considered a wall temperature which was constant with time, but variable with x. The wall temperature was 153°C at the inlet ($T_{wall,max}$) and 21°C at the outlet ($T_{wall,min}$) , which is similar to the scenario where the fluid travels up a vertical well. The analytical solution for this case is:

$$T_f(x) = \frac{(T_{wall,min} - T_{wall,max})}{L}x + T_{wall,max} - \frac{(T_{wall,min} - T_{wall,max})}{L}\left(\frac{\dot{m}c_{p,f}}{hP}\right) + \left\{T_{f,in} - T_{wall,max} + \frac{(T_{wall,min} - T_{wall,max})}{L}\left(\frac{\dot{m}c_{p,f}}{hP}\right)\right\}\exp\left(\frac{-hP}{\dot{m}c_{p,f}}x\right) \quad \text{(B.2)}$$

In Figure B.2, it is clear that the fluid temperature from the model agrees well with the above analytical solution.

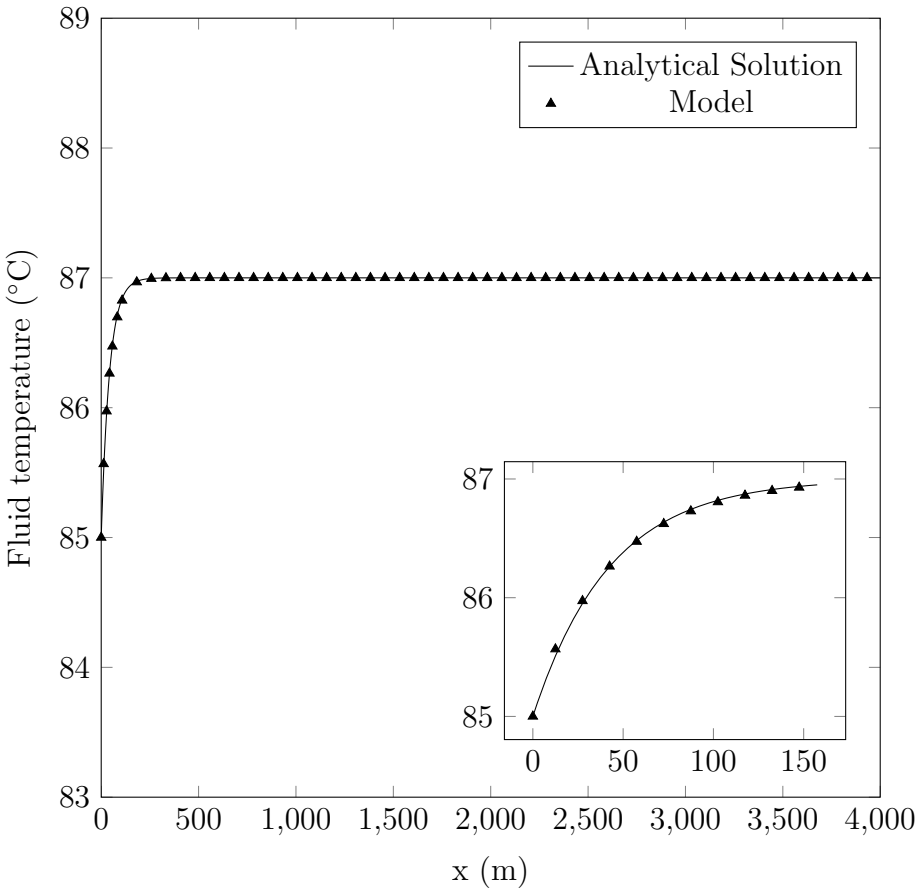

Figure B.1: Verification case: fluid model verification, constant uniform wall temperature, steady state

B.1.2 Solid Analytical Verification

Since the solid domain is two-dimensional, steady state verification was performed for each dimension. To verify the behaviour of radial heat transfer, a convection boundary condition was set on the inner radius, where the fluid temperature was held constant at 85°C. In order to maintain one-dimensional heat transfer, the upper and lower boundaries in the axial direction were set to have zero heat flux. For steady,

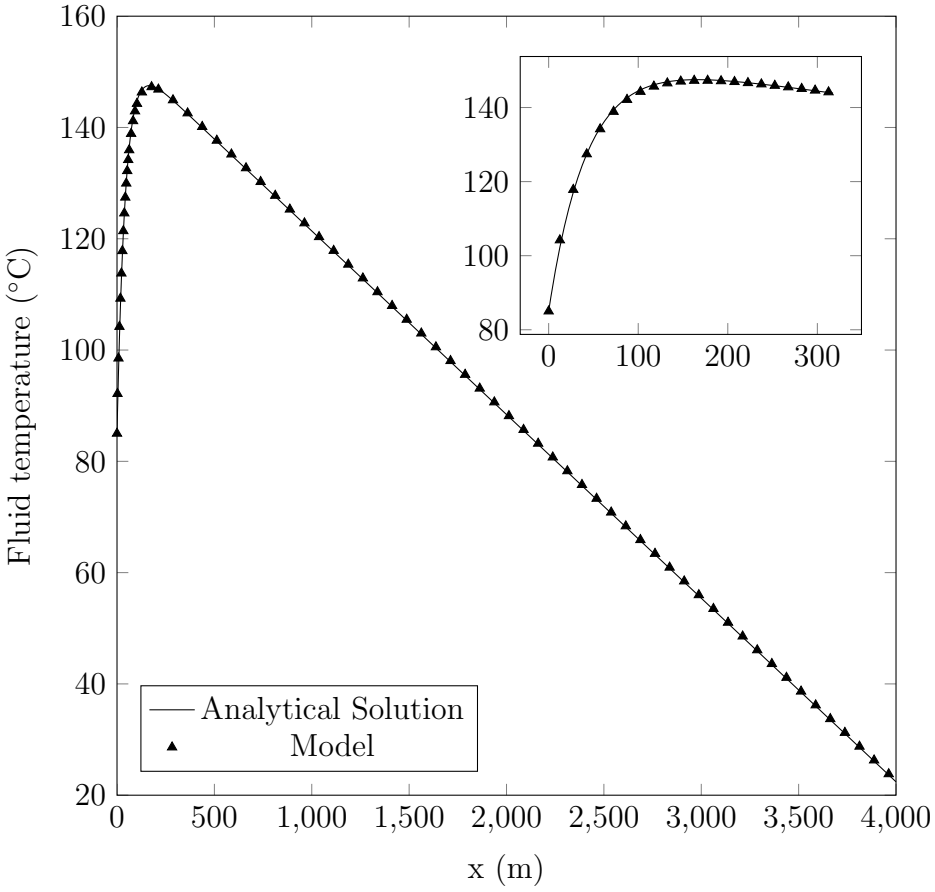

Figure B.2: Verification case: fluid model verification, constant wall temperature, $T_{wall} = -132x + 153$, steady state

radial heat conduction, the general analytical solution is:

$$T(r) = C_1 \ln(r) + C_2 \tag{B.3}$$

The outer radius boundary was set to have a constant temperature of 153°C. These boundary conditions result in a temperature profile of:

$$T_g(r) = \frac{T_{R,outer} - T_f}{\frac{k_g}{hR_{inner}} - ln\left(\frac{R_{inner}}{R_{outer}}\right)} \ln\left(\frac{r}{R_{outer}}\right) + T_{R,outer} \tag{B.4}$$

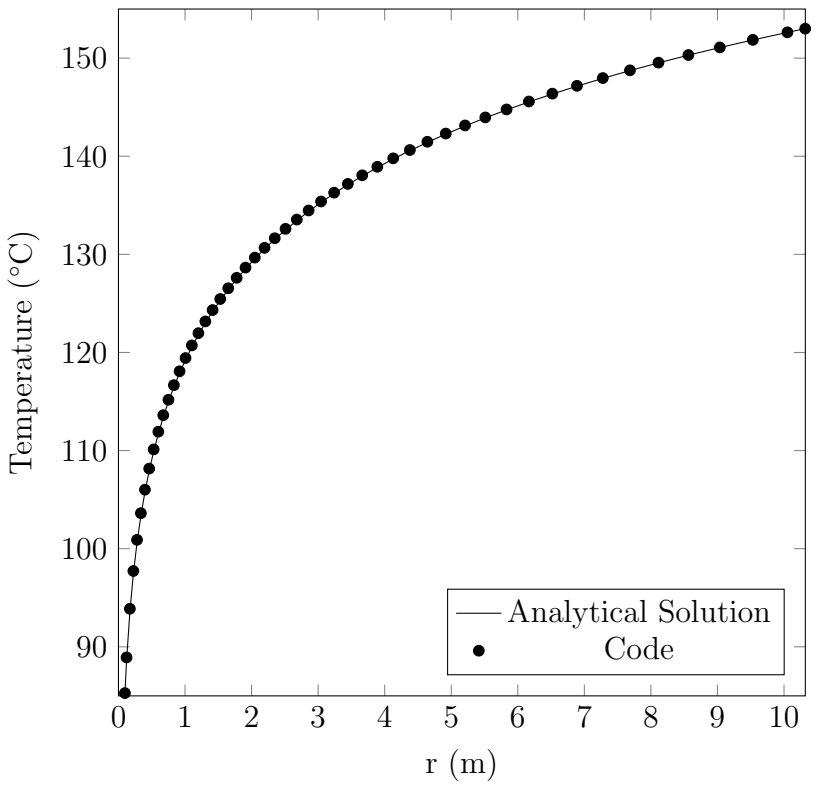

Figure B.3: Verification case: solid model verification, radial heat transfer in a cylindrical tube with a convection boundary condition on the inner radius and a constant temperature condition on the outer radius, steady state

where $T_{R,outer}$ is the constant temperature of the solid domain at the outer radius, k_g is the ground thermal conductivity, and R_{inner} and R_{outer} are the inner and outer radii of the solid domain. Figure B.3 shows that the model results agree well with the steady state solution.

In the axial direction, the model was verified against a case where each axial end was set to a constant temperature. To maintain one-dimensional heat transfer, the inner and outer radius of the system were given zero heat flux boundary conditions. The analytical solution for this case indicates that the axial temperature profile should

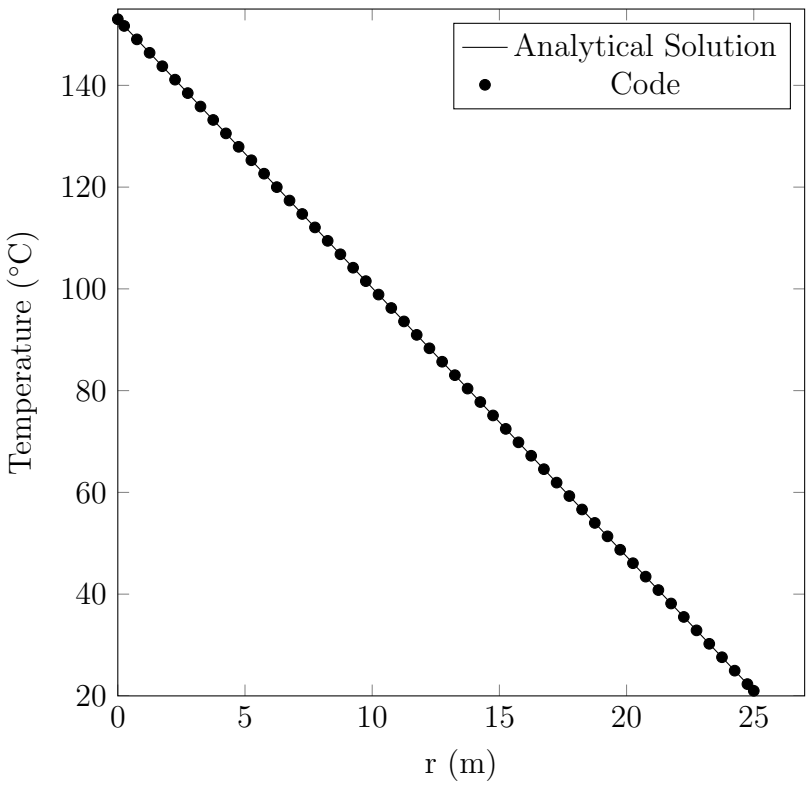

Figure B.4: Verification case: solid model verification, heat flow in the axial direction, steady state

be linear:

$$T_g(x) = \frac{T_g(L) - T_g(0)}{L} x + T_g(0) \tag{B.5}$$

In Figure B.4, one can see that the model conforms with the analytical solution.

B.2 Coupling Analytical Verification

The above verification tests indicate that the separate fluid and solid models produce results that agree with analytical solutions. Verification is still required, however, for the case where the domains are coupled. To establish test cases where the coupled

domain could compare to steady analytical solutions, parameters were set to very large values, simulating the case where those parameters approach infinity. When u approaches infinity while h remains a finite value, the model will behave like a solid conduction case with a convection boundary at the inner radius. When both u and h approach infinity, the model behaves like a solid conduction problem where the inner radius is set to a constant temperature. This coupled verification was performed using the same conditions that were employed in the solid verification testing. The results show that the coupled models produce the same temperature profiles as the models that solved only for the solid temperature profile.

B.2.1 $u \to \infty$: Solid Conduction with Convection at the Inner Radius

The variable u was set to 3.1×10^{25} and h was set to 1454 W/m^{2}K. The fluid temperature was set to a constant 85°C and the outer radius of the solid domain was set to a constant 153°C. As is shown in Figure B.5, the temperature of the solid agrees with the analytical solution for steady conduction in a cylinder with a convection condition at the inner radius.

B.2.2 $u, h \to \infty$: Solid Conduction with a Constant Temperature at the Inner Radius

The variable u was set to 3.1×10^{25} and h was calculated using the Dittus-Boelter relationship, which meant that h also approached a very large value. The fluid temperature was a constant 85°C and the solid outer radius was set to 153°C. As is

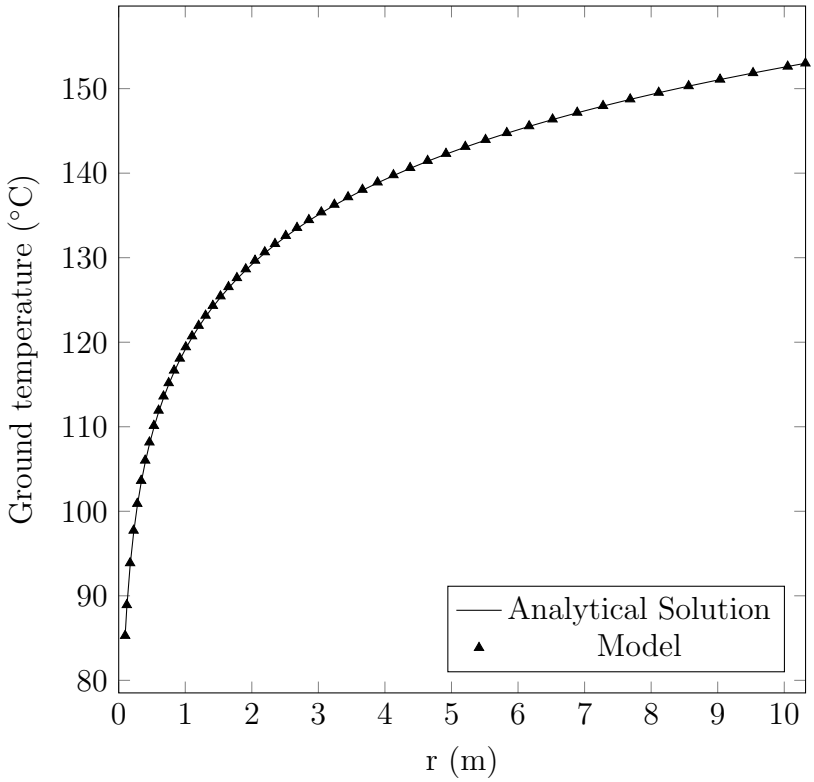

Figure B.5: Coupling verification case: $u \to \infty$

shown in Figure B.6, the temperature of the solid agrees with the analytical solution for steady conduction in a cylinder with a constant temperature condition at the inner radius.

B.3 Transient Analytical Verification

Transient testing on the solid domain was checked using the a solution from Carslaw and Jaeger [47]. Figure B.7 shows the transient non-dimensional temperature at the wall of a semi-infinite domain bounded internally by a cylinder with a constant heat flux of 549 kW applied at the internal cylinder wall. The non-dimensional temperature

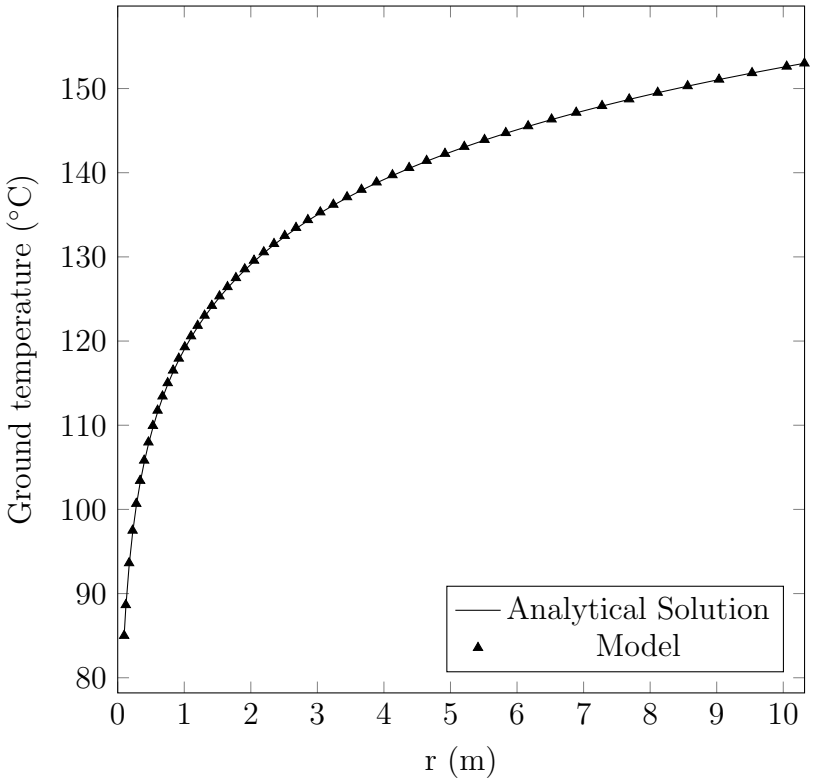

Figure B.6: Coupling verification case: $u, h \to \infty$

at the cylinder wall is defined as:

$$\theta = \frac{kT_{surface}}{RQ} \tag{B.6}$$

where k is the solid conductivity, $T_{surface}$ is the temperature at the surface of the cylinder, R is the radius of the cylinder, and Q is the heat flux at the wall. The simulation considers an initial temperature of 0°C and a constant heat flux at the inside wall. Non-dimensional time is the Fourier number, defined as:

$$\text{Fo} = \frac{\alpha t}{R^2} \tag{B.7}$$

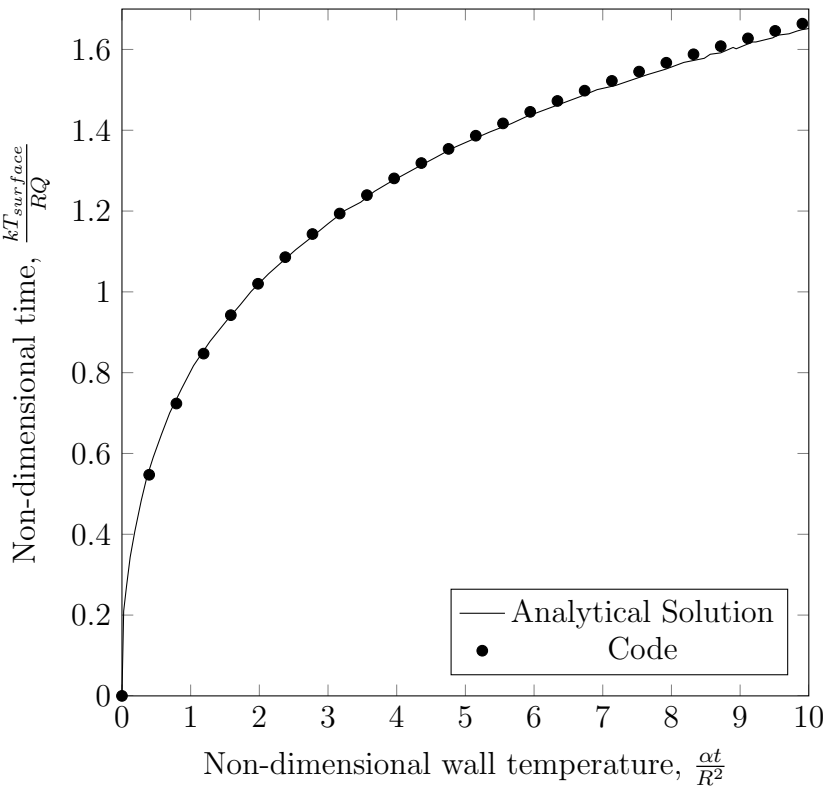

Figure B.7: Verification case: Transient heat conduction in an infinite solid internally bounded by a cylinder [47]

One can see in Figure B.7 that the simulation results match well with the analytical solution determined by Carslaw and Jaeger.

B.4 Intermittent Verification

In the intermittent simulations, the Nusselt number for the stagnant fluid was chosen to be equal to 1. This employs the assumption that the fluid is completely stationary and that conduction is the only heat transfer mechanism. In reality, there will be some natural convection due to the temperature gradients in the wells. To determine if the choice in Nusselt number impacts the results, a simulation was performed where

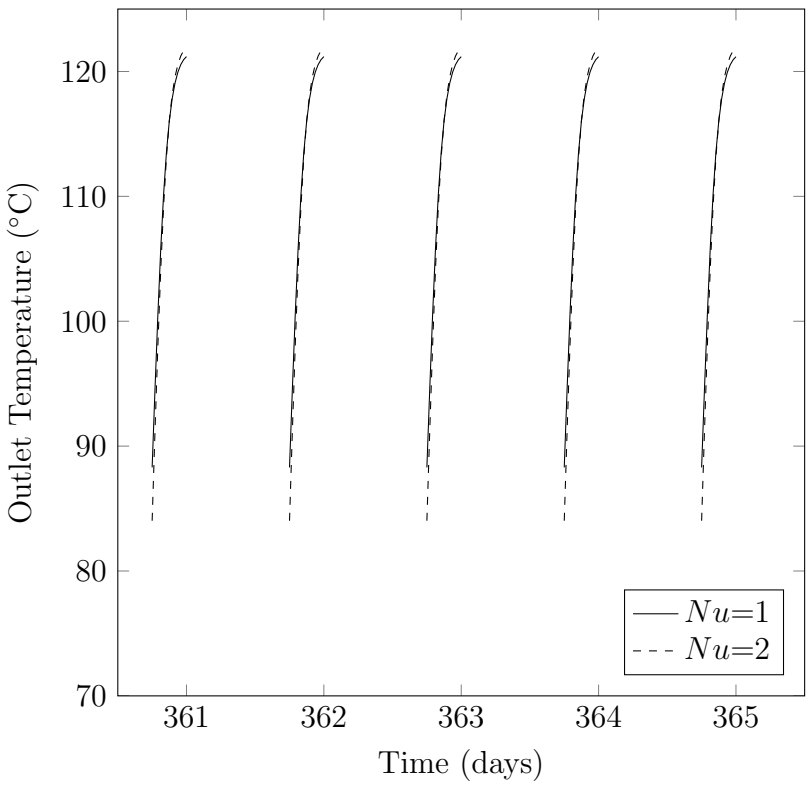

Figure B.8: Verification case: Variation of Nusselt number for stagnant fluid, after 1 year of intermittent operation

Nu was set to 2. The results of this simulation, compared to the Nu=1 case are seen in Figure B.8. The results, taken after one year of intermittent operation, show that there is little difference in the outlet temperature when the Nusselt number is doubled. The higher Nusselt number enhances heat transfer between the fluid and the ground, resulting in a cooler fluid temperature at the end of the stagnant phase. After six hours of fluid flow, however, the difference between the Nu=2 and the Nu=1 outlet temperatures is negligible.

Appendix C

Grid and Time Step Sensitivity Testing

C.1 Grid Independence Testing

Grid independence testing was conducted by progressively decreasing the size of the grid until the fluid and solid temperature solutions no longer changed. The impact of the grid size was assessed for each dimension separately.

In the axial direction, the Δx value was reduced until the solution remained unchanged. Figure C.1 shows that the fluid temperature along the length of the system is not affected when the grid size is reduced from 50 m to 20 m, indicating that a Δx value of 50 m is appropriate. The fluid outlet temperature only changes by 0.05% when the grid is increased from 20 m to 50 m. Figures C.2 and C.3 show that the ground temperatures do not change when the grid is increased in size.

As the grid in the radial direction is an expanding grid (expansion ratio = 1.05), the grid independence study was conducted by halving the size of the radial cell

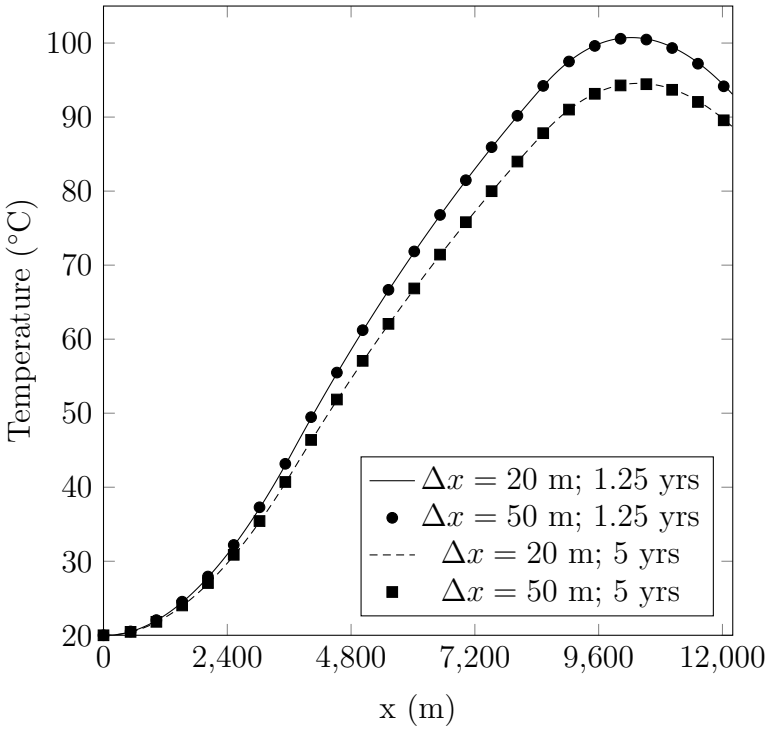

Figure C.1: Fluid temperature after 5 years operation, grid sensitivity testing in x-direction

closest to the wall, Δr_1. The cell size and number of cells had to be carefully chosen through an iterative process in order to maintain a consistent outer radius throughout testing. An initial value for the radial cell size was chosen by dividing the previous value by two. The sum of a geometric series, which gives the domain size, can be used to obtain a first estimate of the number of cells in the radial direction, given the initial Δr_1 value [56]:

$$Cells = \frac{\ln\left(1 - \frac{(1-1.05)(R_{outer}-R_{inner})}{\Delta r_1}\right)}{\ln(1.05)} \tag{C.1}$$

where R_{outer} is the outer radius of the solid domain and R_{inner} is the inner radius of the domain as well as the well radius.

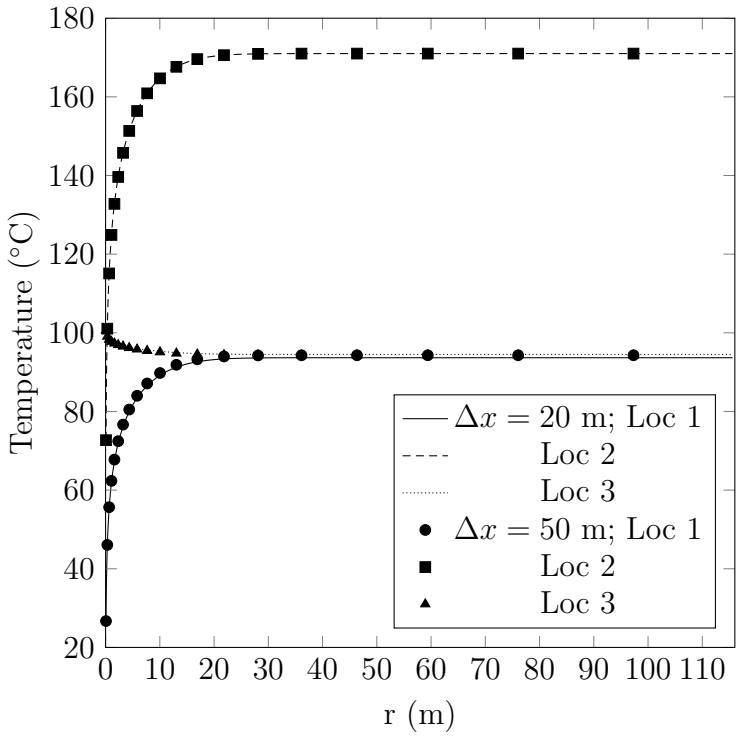

Figure C.2: Ground temperature after 1.25 years of operation, grid sensitivity testing in x-direction

The obtained value for the number of cells was rounded to the nearest integer, and then the equation was rearranged to solve for a new Δr_1 value that would ensure that the outer radius would be maintained. A value of 0.0488 m was chosen for Δr_1 because decreasing the cell size to 0.0244 m showed no change in the solution, with a minimal difference of 0.18% in the outlet temperature. This can be seen in Figure C.4. Figures C.5 and C.6 demonstrate that the ground temperatures are unaffected by the change in grid size.

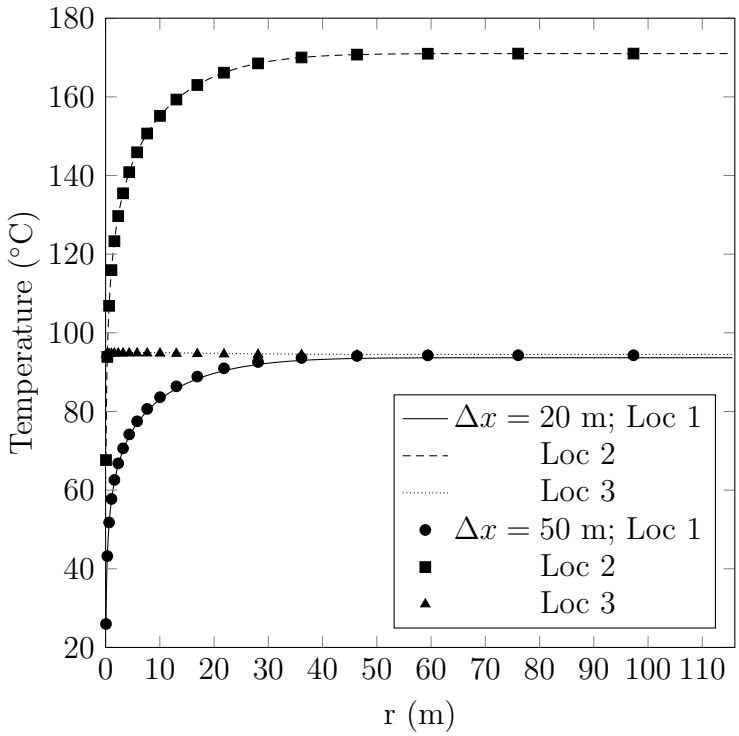

Figure C.3: Ground temperature after 5 years of operation, grid sensitivity testing in x-direction

C.2 Time Step Independence Testing

Time step independence was established similarly to grid independence, by halving the time step until the solution no longer changed. After successively halving the time step, a value of 2700 s was deemed suitable. Reducing the time step to 1350 s resulted in an fluid outlet temperature change of only $6.6\times10^{-6}\%$ compared to the 2700 s time step case. The effect of independence testing on the fluid can be seen in Figure C.7, and the effect on the ground temperatures can be seen in Figures C.8 and C.9.

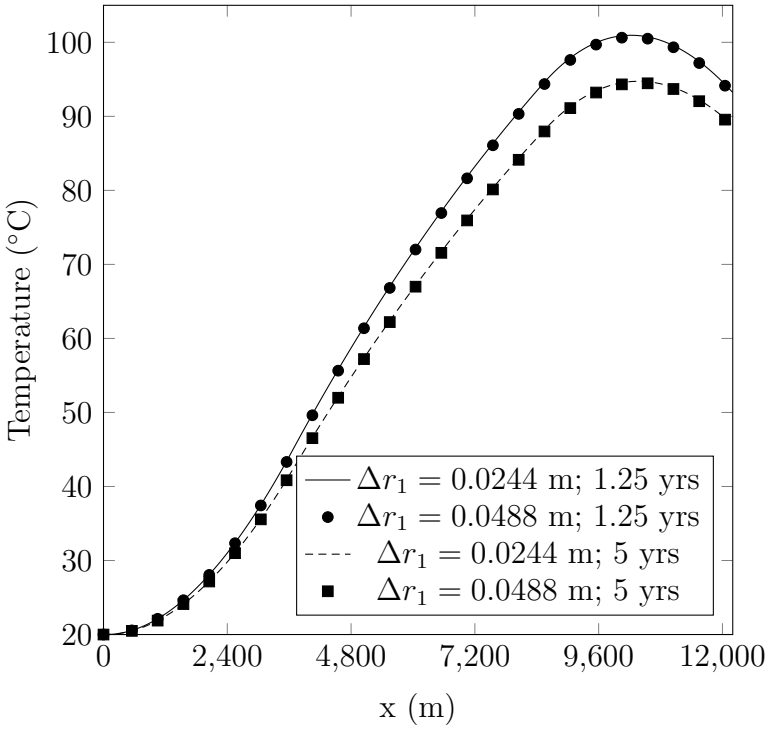

Figure C.4: Fluid temperature after 1.25 and 5 years of operation, grid sensitivity testing in r-direction

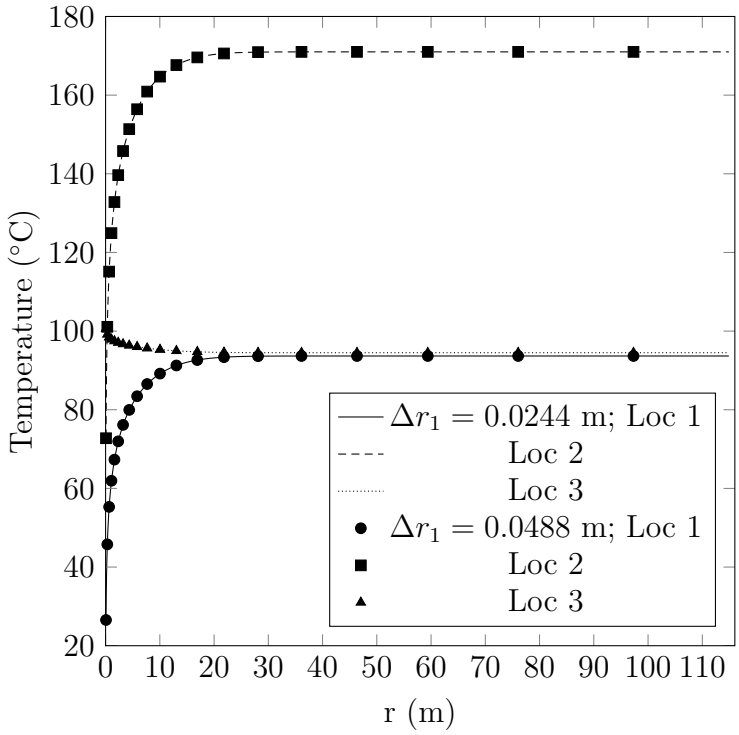

Figure C.5: Ground temperature after 1.25 years of operation, grid sensitivity testing in r-direction

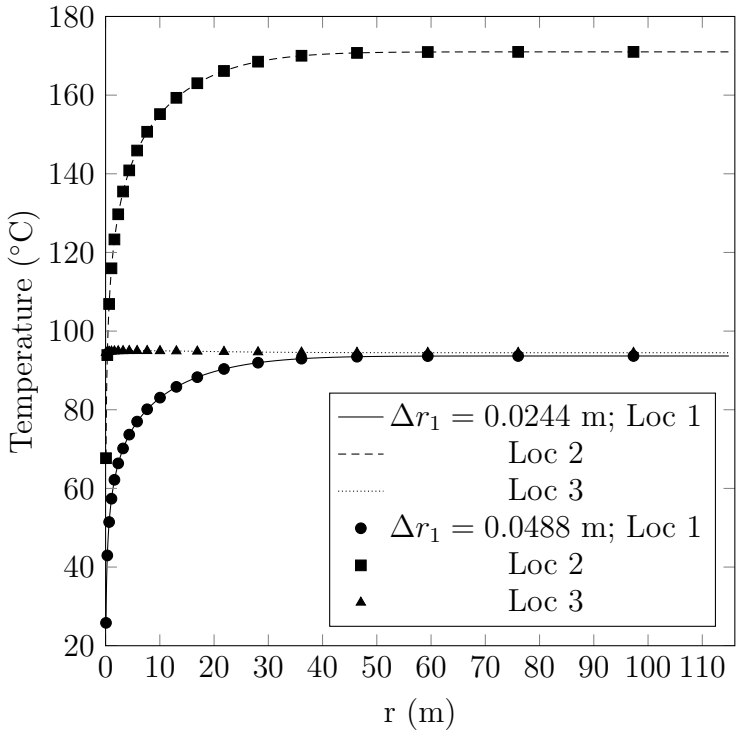

Figure C.6: Ground temperature after 5 years of operation, grid sensitivity testing in r-direction

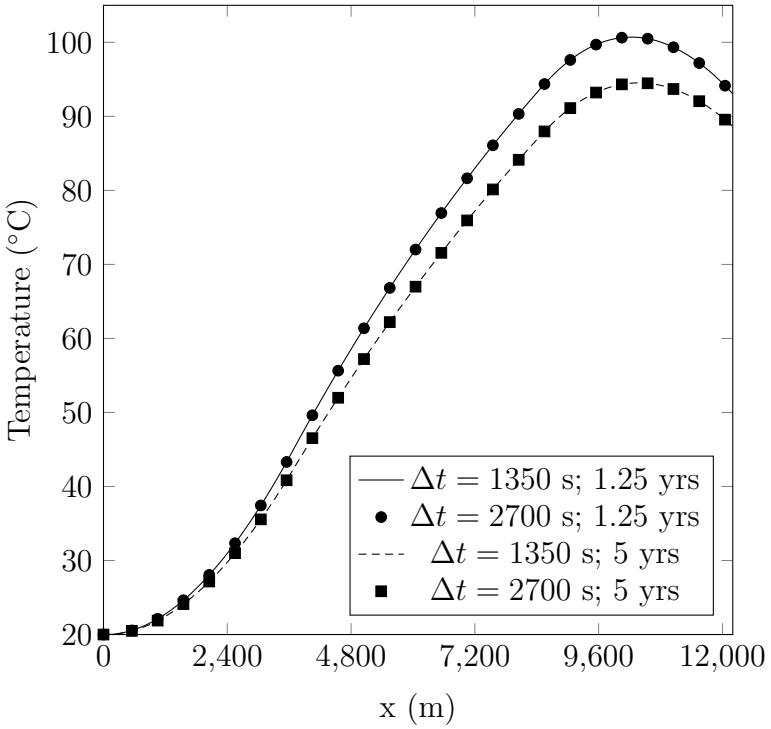

Figure C.7: Fluid temperature after 1.25 and 5 years of operation, time step sensitivity testing

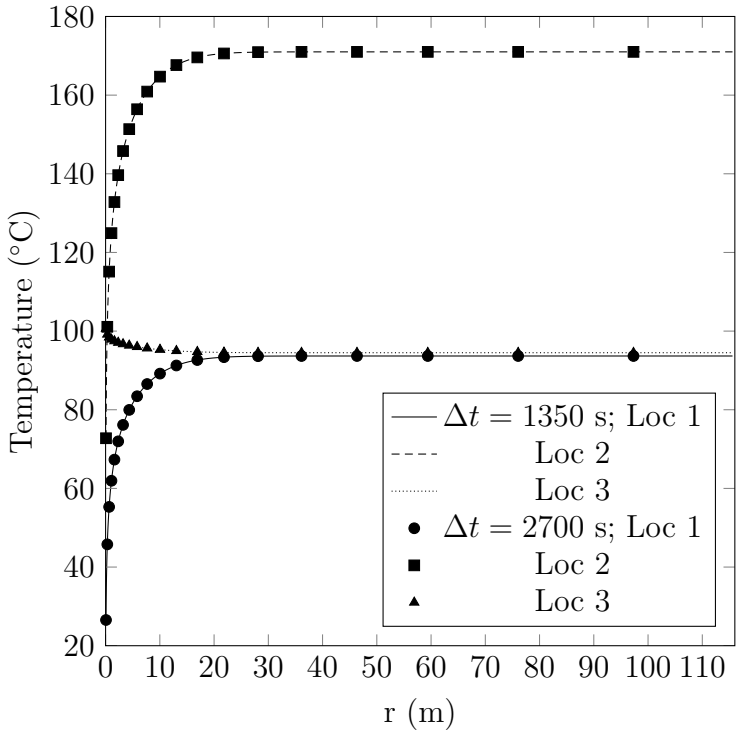

Figure C.8: Ground temperature after 1.25 years of operation, time step sensitivity testing

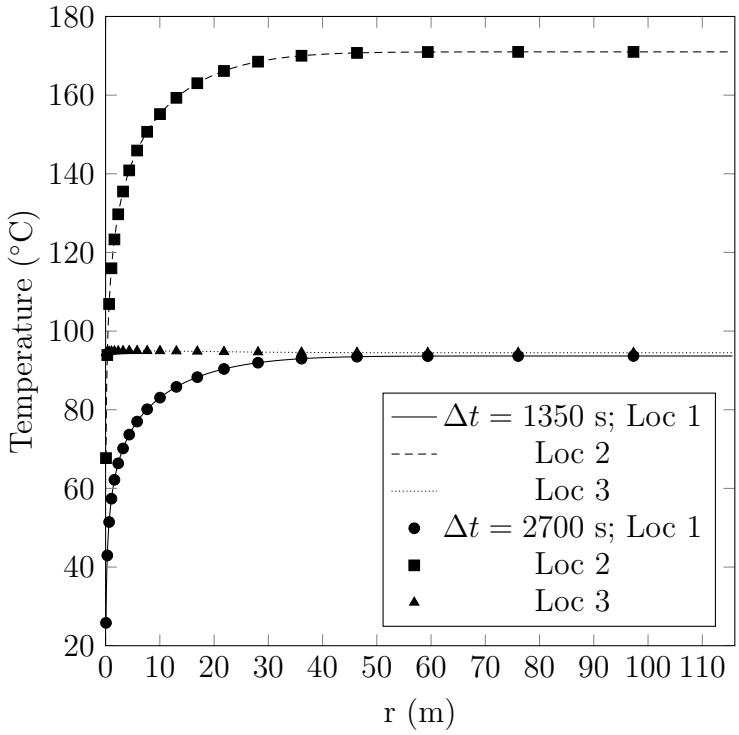

Figure C.9: Ground temperature after 5 years of operation, time step sensitivity testing

Appendix D

Time Scale Analysis

Transient assessment was carried out using time scale analysis. By establishing the transit distance, the distance over which a fluid travels over a given period of time, the early-time simulation results can be verified. Transit distance is:

$$L_{transit} = ut \tag{D.1}$$

where u is the flow velocity and t is the time elapsed. A simulation of only the upward well with a constant inlet temperature was carried out. The axial fluid temperature profiles were examined at various times and compared with the transit distances. The results can be seen in Figure D.1, where the vertical lines representing the transit distances at each time. The expected result was that the fluid at the inlet, which was initially 153°C should be convected only as far as the transit distance for a given time. The position of the fluid temperature peaks should represent, approximately, the location of the slug of fluid that was originally at the inlet. It is clear from the plot that the locations of the peaks in the fluid temperature roughly correspond to

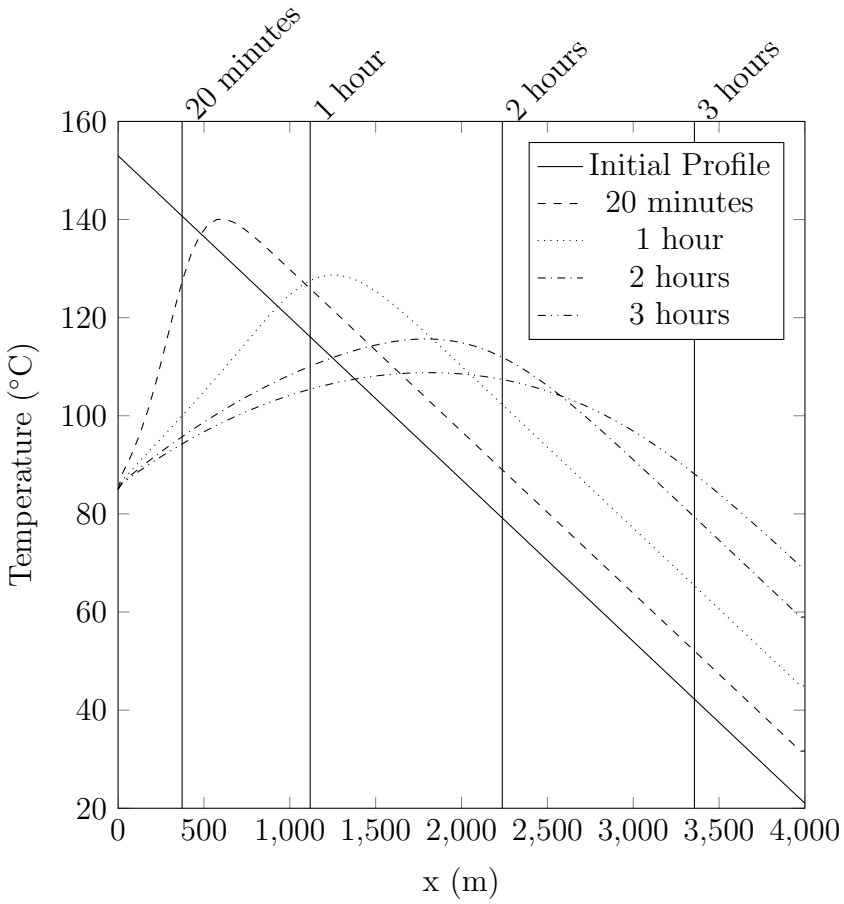

Figure D.1: Fluid temperature over 3 hours, including respective transit distances

the transit distances. At very early times, the peak occurs slightly later than the transit distance line. This can be explained by two effects: convection of other high temperature fluid from just past the inlet and conduction in the soil in the axial direction. Other high temperature fluid near the inlet will have travelled past the transit distance line after 20 minutes. Also, some conduction in the ground near the wall also occurs in the axial direction, acting to warm up the fluid.